Copper Catalysis of Human Hemoglobin Cysβ93 S-Nitrosation and Heme Nitrosylation by S-Nitrosoglutathione

Andrea A. Romeo

A Thesis

In

The Department

Of

Chemistry and Biochemistry

Presented in Partial Fulfillment of the Requirements
for the Degree of Doctor of Philosophy at
Concordia University
Montreal, Quebec, Canada

December 2003

Your file Votre référence
ISBN: 0-612-90400-8
Our file Notre référence
ISBN: 0-612-90400-8

CONCORDIA UNIVERSITY
SCHOOL OF GRADUATE STUDIES

This is to certify that the thesis prepared

By: **Andrea A. Romeo**

Entitled: **Copper Catalysis of Human Hemoglobin Cysβ93 S-Nitrosation and Heme Nitrosylation by S-Nitrosoglutathione**

and submitted in partial fulfillment of the requirements for the degree of

DOCTOR OF PHILOSOPHY (Chemistry)

complies with the regulations of the University and meets the accepted standards with respect to originality and quality.

Signed by the final examining committee:

Dr. M. Von Grunau _____ Chair

Dr. D.S. Bohle _____ External Examiner

Dr. R. Boushel _____ External to Program

Dr. P. Bird _____ Examiner

Dr. J. Powlowski _____ Examiner

Dr. A. English _____ Thesis Co-Supervisor

Dr. J.A. Capobianco _____ Thesis Co-Supervisor

Approved by _____
Chair of Department or Graduate Program Director

December 16 2003

_____
Dean of Faculty

Abstract

Copper catalysis of Human Hemoglobin Cysβ93 S-Nitrosation and Heme Nitrosylation by S-Nitrosoglutathione

Andrea A. Romeo, Ph.D.

Concordia University, 2003

There is evidence that binding of the vasorelaxant, nitric oxide (NO), to Cysβ93 of human adult hemoglobin (Hb) plays a role in blood pressure regulation. S-Nitrosation of Cysβ93 by low-molecular-weight S-nitrosothiols (RSNOs) such as S-nitrosoglutathione (GSNO) was directly probed by FTIR by monitoring the ν(SH) vibrations of Hb and by ESI-MS. The results indicate that Cysβ93 is S-nitrosated when oxyHb ($HbFe^{II}O_2$), but not deoxyHb ($HbFe^{II}$), is exposed to GSNO (1:1 heme/GSNO). No FTIR or ESI-MS evidence was obtained for oxyHb S-nitrosation in the presence of DTPA (a Cu^{II} chelator) and neocuproine (a Cu^{I} chelator). Monitoring the heme Soret and visible bands revealed that oxyHb was converted to metHb ($HbFe^{III}$) in the presence of excess GSNO over Cysβ93 and that this was inhibited on addition of neocuproine. The combined data are consistent with a mechanism involving Cu^{II}-catalysis of Cysβ93 S-nitrosation by *free* NO generated by Cu^{I}-catalysis of GSNO breakdown but not with trans-S-nitrosation (NO^+ transfer between thiols).

Reductive cleavage of GSNO by deoxyHb to release free NO that binds to additional deoxyHb to give nitrosylHb was recently reported [Spencer, N. Y., Zeng, H., Patel, R. P., and Hogg, N. (2000) J. Biol. Chem. 275(47), 36562]. The reaction between

GSNO and deoxyHb was reexamined in the presence of both neocuproine and DTPA using a copper-depleted Hb solution prepared by exhaustive dialysis *vs* EDTA. Direct spectroscopic and mass spectral analyses of the deoxyHb/GSNO incubates show that nitrosylHb formation was significantly decelerated in presence of neocuproine. Deceleration was less in the presence of DTPA and in Hb solutions dialyzed *vs* EDTA.

NitrosylHb formation was almost totally inhibited when neocuproine was added to dialyzed deoxyHb plus GSNO. Extensive GSSG formation was observed by mass spectrometry in deoxyHb/GSNO incubates in the absence of metal chelators where deoxyHb nitrosylation was complete in <5 min. The data presented are *inconsistent* with direct reduction of GSNO by deoxyHb but indicate a mechanism involving *free* NO generated by Cu^{I} catalysis of GSNO breakdown and Cu^{II} reduction by GSH.

The Cu and Zn content in commercial human Hb samples was determined by ICP-MS, and ~20 μM of each metal was present in 5 mM Hb solutions. Superoxide dismutase (CuZnSOD) activity in Hb samples was measured using the pyrogallol method and ~10 μM active CuZnSOD dimer was found, which corresponds to the amount of Cu and Zn determined by ICP-MS. Western blotting with a polyclonal antibody developed against human CuZnSOD showed a CuZnSOD concentration of ~15 μM in 5 mM Hb. From these results, it is proposed that reduced CuZnSOD (Cu^{I} form) catalyzes the release of NO from GSNO, and that oxidized CuZnSOD (Cu^{II} form) catalyzes S-nitrosation of Cysβ93 by free NO.

A possible mechanism of Hb S-nitrosation would be to generate a thiyl radical on Cysβ93, which would react rapidly with NO. Since copper enhanced CO-driven reduction of metHb has been proposed to involve thiyl radical formation via electron

transfer from Cysβ93 to the Fe^{III} β-heme, metHb was incubated with CO in the presence of $CuSO_4$ under various conditions. The formation of carbonylHb ($HbFe^{II}CO$) was confirmed by monitoring the Soret and visible heme absorption. In addition, formation of a peak at 1951 cm^{-1} corresponding to ν(CO) was observed by FTIR. To locate the thiyl radical on Hb, spin scavenging and spin trapping (using $TEMPOL^{\bullet}$ and DBNBS as a spin scavenger and spin trap, respectively), followed by peptide mass mapping of Hb was attempted in the presence of copper ions added as $CuSO_4$, or in the presence of DTPA. Evidence of spin scavenging of a thiyl radical on Cysβ93 was obtained since signals corresponding to the expected TEMPOL-labelled peptide 83-95 were observed in the peptide mass map of β-globin. The results presented in this thesis provide insight into the role and mechanism of Hb S-nitrosation *in vivo*.

Acknowledgements

I would like to begin by thanking my research supervisors. Dr. Ann English for her guidance, support and endless research ideas during my Ph.D. Her enthusiasm and dedication to research are traits I truly admire and I hope I too will have the same energy with my future research endeavors as she has with hers. Dr. John Capobianco for introducing and guiding me to the academic and research environment of the Department of Chemistry and Biochemistry at Concordia University.

I wish to thank the members of my committee, Drs. Justin Powlowski and Peter Bird for some interesting yearly meetings.

I would like to acknowledge everyone at Concordia who played a part in my development as a scientist, especially my friend and colleague Dr. Angelo Filosa who showed me the "ropes" on the mass spectrometer when I started in the lab. Gratitude is also extended to Iolie Bakas, John Wright, and Drs. Susan Aitken, Araz Jakalian and Ashraf Ismail. I would particularly like to thank my friends and colleagues Tyrone Shephard and Christina Esposito who made the first two years of my Ph.D. extremely entertaining and enjoyable.

I am grateful to my parents, my brother and my sister for all the love and support they have given me over the years. Finally, I would like to thank my wife for all her patience, understanding and love. This degree is as much hers as mine.

Dedications

To my mother and father,

Anna Cannizzaro and Giuseppe Romeo,

My grandfather

Andrea Cannizzaro (May 22, 1913 - October 22, 1997),

And my aunt

Orsola Cannizzaro,

For being very close to me always;

To my sons,

Alessandro, Giuseppe Romeo (September 17, 2000),

And

Raphaël, Claude Romeo (May 14, 2003)

For giving me the greatest gift in life;

And to my wife,

For being very supportive and good life companion

Table of Contents

List of Figures

List of Tables

List of Abbreviations

ACN	acetonitrile
CarbonylHb	$HbFe^{II}CO$
CD	circular dichroism
CN^-	cyanide anion
CuZnSOD	copper,zinc-superoxide dismutase
CysSNO	S-nitrosocysteine; S-nitroso-L-cysteinyl
CyanometHb	$HbFe^{III}CN$
DBNBS	3,5-dibromo-4-nitrosobenzenesulfonic acid
DEA/NO	diethylammonium (Z)-1-(N, N-diethylamino)diazen-1-ium-1,2-diolate
DEAE	diethyl aminoethyl
DeoxyHb	$HbFe^{II}$
DMPO	5,5-dimethyl-1-pyrroline N-oxide
DTPA	diethylenetriamine-N,N,N',N",N"-pentaacetic acid
EDTA	ethylenediamine-N,N'-tetraacetic acid
EPR	electron paramagnetic resonance
ESI	electrospray ionization
FSD	Fourier self-deconvolution
FTIR	Fourier transform infrared
FWHM	full-width-at-half-maximum
G25	G-type of Sephadex gel dextran
GSH	glutathione; glycine N-(N-L-γ-glutamyl-L-cysteinyl)

GSNO	S-nitrosoglutathione; glycine N-(N-L-γ-glutamyl-S-nitroso-L-cysteinyl)
GSSG	glutathione disulfide; glycine N-(N-L-γ-glutamyl-L-cysteinyl) disulfide
Hb	human adult hemoglobin
Hb-SNO	Hb S-nitrosated at Cysβ93
HPLC	high-performance liquid chromatography
HWHH	half-width-at-half-height
ICP-MS	inductively coupled plasma mass spectrometry
K factor	enhancement factor
K_d	dissociation constant
LC/MS	liquid chromatography with mass spectrometric detection
Mb	myoglobin
MetHb	$HbFe^{III}$
MS	mass spectrometry
NaPi	sodium phosphate buffer
Neocuproine	2,9-dimethyl-1,10-phenanthroline
NitrosylHb	$HbFe^{II}NO$
NitrosylmetHb	$HbFe^{III}NO$
OxyHb	$HbFe^{II}O_2$
RBC	red blood cell
RSNO	S-nitrosothiol
SNAP	S-nitroso-N-acetyl-D,L-penicillamine
TEMPOL$^{\bullet}$	4-hydroxy-(2,2,6,6-tertamethyl-1-piperidine-N-oxyl)
TFA	triflouroacetic acid

1.0 Introduction

1.1 Nitric oxide (NO)

NO is an important and unique messenger in biological systems. It is synthesized from L-arginine by NO synthase (NOS) and has been variably identified as an endothelial derived relaxation factor (EDRF), antiplatelet substance, neurotransmitter or cytotoxic substance derived from activated macrophages. Its most important biological action is assumed to be the activation of guanylate cyclase (1). The field of NO research has been growing dramatically since the discovery of its biosynthesis. Currently, there are more than 2,000 NO-related reports every year. Despite the growth in research, NO bioaction is still shrouded in mystery and there are many controversial reports on the biological effects of NO. For example, it has been noted that NO causes tissue damage in ischemia-reperfusion systems (2,3), while opposing reports claim that NO is generated to protect tissues from such damage (4).

The purity of NO solutions is very important in investigating its reactions with biologically relevant reagents. However, it is technically very difficult to make pure aqueous solution of NO because of its instability (Section 1.2.1). Also, the high reactivity and volatility of NO makes it difficult to estimate the amount in solution. For these reasons, NO donors are often used for the addition of NO into a system under observation. The commonly used NO donors, nitroglycerin (GTN), sodium nitroprusside (SNP) (5), and S-nitrosothiols (RSNOs) (6) help resolve some of the above problems, but they vary in rate and amount of NO released. For example, RSNOs do not release NO spontaneously, but require heat, light (7), thiols or traces of metal ions as cofactors for the

generation of NO (8). S-Nitrosothiols exhibit vasorelaxant activity just like NO and it was pointed out that the vasorelaxant properties of EDRF are more similar to CysSNO than NO (9). However, this seems not to be the current view since CysSNO does not release NO spontaneously (10).

1.2 Nitric Oxide and S-Nitrosothiols

1.2.1 Physical and Chemical Properties of NO

NO is a highly volatile, hydrophobic, and colorless gaseous material. NO dissolves in water to a maximum of 1.9 mM, and its aqueous solutions are fairly stable under anoxic conditions. The half-life of NO *in vivo* is not well established, but is estimated to be ~100 milliseconds in the blood and a few seconds in tissues (2). In the gas phase it reacts rapidly with O_2 to produce NO_2, a brown gas, and N_2O_3 a colourless gas (Reactions 1.1 and 1.2), which react together to form N_2O_4 a colourless gas (Reaction 1.3):

$$NO + \tfrac{1}{2} O_2 \rightleftharpoons NO_2 \qquad (1.1)$$

$$NO_2 + NO \rightleftharpoons N_2O_3 \qquad (1.2)$$

$$N_2O_3 + NO_2 \rightleftharpoons N_2O_4 + NO \qquad (1.3)$$

Thus, to obtain highly purified NO, the commercial gas is distilled, otherwise NO_x contaminants will be present.

The NO molecule is paramagnetic with the following electronic configuration: $(\sigma_1)^2(\sigma_2^*)^2(\sigma_3)^2(\pi)^4(\pi^*)^1$. The electron in the π^* orbital is relatively easily lost to give the nitrosonium ion, NO^+, which forms many salts. Because an electron is lost from an

antibonding orbital, the NO bond is stronger in NO^+ than in NO. The bond length decreases by 0.09Å and the vibration frequency rises from 1840 cm^{-1} in NO to 2150-2400 cm^{-1} (depending on the environment) in NO^+ (11). A major reaction of NO is coordination to metal ions, such as Fe^{II} in Hb (12). NO^+ can exist in aqueous solution but in most cases NO^+ exists as nitroso compounds or metal nitrosyls and these compounds may behave like NO^+ in aqueous solutions (13). S-Nitrosothiols reportedly play an important role as NO^+ carriers under physiological conditions (14).

NO reacts rapidly ($k = 6.7x10^9\ M^{-1}s^{-1}$) with the superoxide anion to form peroxynitrite (Reaction 1.4), which decomposes ($k = 1.38\ s^{-1}$) to nitrate (Reaction 1.5) (15).

$$NO + O_2^{\bullet -} \rightleftharpoons ONOO^- \qquad (1.4)$$

$$ONOO^- \rightleftharpoons NO_3^- \qquad (1.5)$$

Interestingly, it has also been reported that NO reacts rapidly ($k = 4.1x10^7\ M^{-1}s^{-1}$) at pH = 7.0 with oxymyoglobin or oxyhemoglobin to produce nitrate (Reaction 1.6) *in vitro* (16):

$$NO + MbFe^{II}O_2 \rightleftharpoons MbFe^{III} + NO_3^- \qquad (1.6)$$

The relevance of this reaction *in vivo* is still a matter of debate (see Chapter 4.0).

1.2.2 Physical and Chemical Properties of S-Nitrosothiols

Only a few S-nitrosothiols, including SNAP and GSNO, are stable. SNAP is less soluble in aqueous buffers at neutral pH (~10 mg/mL at pH 7.2) than GSNO and CysSNO (~40 mg/mL at pH 7.2) (17). RSNOs can be characterized by UV-Vis spectroscopy because the *S*-NO group absorbs at ~330 nm (ε ~10^3 $M^{-1}cm^{-1}$) in a manner that varies with the *R*-group (7). In addition, the *S*-NO moiety exhibits NO and NS stretching vibrations at ~1550 and 650 cm^{-1}, respectively (18).

RSNOs are not produced spontaneously on mixing a thiol (RSH) and NO (7,8). The thiol must be first oxidized, and then the resulting thiyl radical reacts with NO (Reactions 1.7 and 1.8) (7):

$$RSH \rightleftharpoons RS^{\bullet} + H^{+} + e^{-} \qquad (1.7)$$

$$RS^{\bullet} + {}^{\bullet}NO \rightleftharpoons RSNO \qquad (1.8)$$

Alternatively, the RSNOs can be prepared by the reaction of RSH with an NO^{+} donor such as HNO_2. RSH in 1 M HCl solution reacts rapidly with HNO_2 (19) following addition of $NaNO_2$ to HCl:

$$HCl + NaNO_2 \rightleftharpoons HNO_2 + NaCl \qquad (1.9)$$

$$RSH + HO\text{-}NO \rightleftharpoons RSNO + H_2O \qquad (1.10)$$

Thiols can also react with NO_2 to form RSNOs as in the following scheme (20):

$$RSH + NO_2 \rightleftharpoons RS\text{-}N(O)OH \qquad (1.11)$$

$$RS\text{-}N(O)OH + RSH \rightleftharpoons RSNO + H_2O + RS^{\bullet} \qquad (1.12)$$

$$RS^{\bullet} + RS^{\bullet} \rightleftharpoons RSSR \qquad (1.13)$$

RSNOs undergo heat and light-induced homolysis to release NO and form disulfides (Reaction 1.14) (21):

$$2\ RSNO \overset{h\nu \text{ or } \Delta}{\rightleftharpoons} RSSR + 2\ NO^{\bullet} \qquad (1.14)$$

For example, homolysis of GSNO is as follows (7):

$$GSNO \rightleftharpoons GS^{\bullet} + NO^{\bullet} \qquad (1.15)$$

$$GS^{\bullet} + GSNO \rightleftharpoons GSSG + NO^{\bullet} \qquad (1.16)$$

$$GS^{\bullet} + GS^{\bullet} \rightleftharpoons GSSG \qquad (1.17)$$

The thiyl radicals generated on homolysis react with GSNO (Reaction 1.16) to give GSSG and a second NO, or dimerizes to yield GSSG (Reaction 1.17). Autocatalysis of RSNO breakdown (Reaction 1.16) was reported to be significant at RSNO concentrations >1 mM (22).

In the dark, the first-order rate constant for Reaction 1.15 is $\sim 10^{-5}$ s^{-1} (23). However, it has been observed that metal ions, such as Cu^{I} (24), catalyze Reaction 1.15. In the presence of metal-ion chelators, such as ethylenediamine-N,N'-tetraacetic acid

(EDTA) or diethylenetriamine-N,N,N',N",N"-pentaacetic acid (DTPA), the rate of GSNO decomposition (Reaction 1.15) is on the order of the uncatalyzed reaction (25).

Another reported reaction of RSNOs is *trans*-S-nitrosation (7):

$$R\text{-}SNO + R'\text{-}S^- \rightleftharpoons R\text{-}S^- + R'\text{-}SNO \quad (1.18)$$

This reaction is reportedly 10^3-fold faster (k_{obs} ~10^{-2} s^{-1} under pseudo-first-order conditions) than the thermal decomposition of RSNO, and proceeds readily at physiological pH (23). The reaction rate constant depends on the pK_a of R'-SH since R'-S^- is the nucleophile that attacks RSNO (26).

RSNOs exhibit a wide range of physiological functions. These include immune functions (27), inhibition of oxidant-response enzymes (28), modulation of ion-channel conductivity (29), and antimicrobial effects (30). Additionally, *S*-nitrosothiols have been proposed to play a role in bronchodilation (31) and vasodilation (32). RSNOs have also been shown to be neuroprotective (33) and GSNO appears to be concentrated in the central nervous system on the order of 6-8 μM (34). One potential mechanism of neuroprotection by RSNOs involves S-nitrosation of free thiols at the redox modulatory site of the N-methyl-D-asparatate receptor by CysSNO (29). Additionally, recent studies have implicated S-nitrosation of the active-site cysteine of caspases 1, 3, and 8 in the inhibition of apoptosis (35).

1.2.2.1 CysSNO

S-nitroso-L-cysteinyl (CysSNO, Figure 1.1a) can be synthesized by combining L-

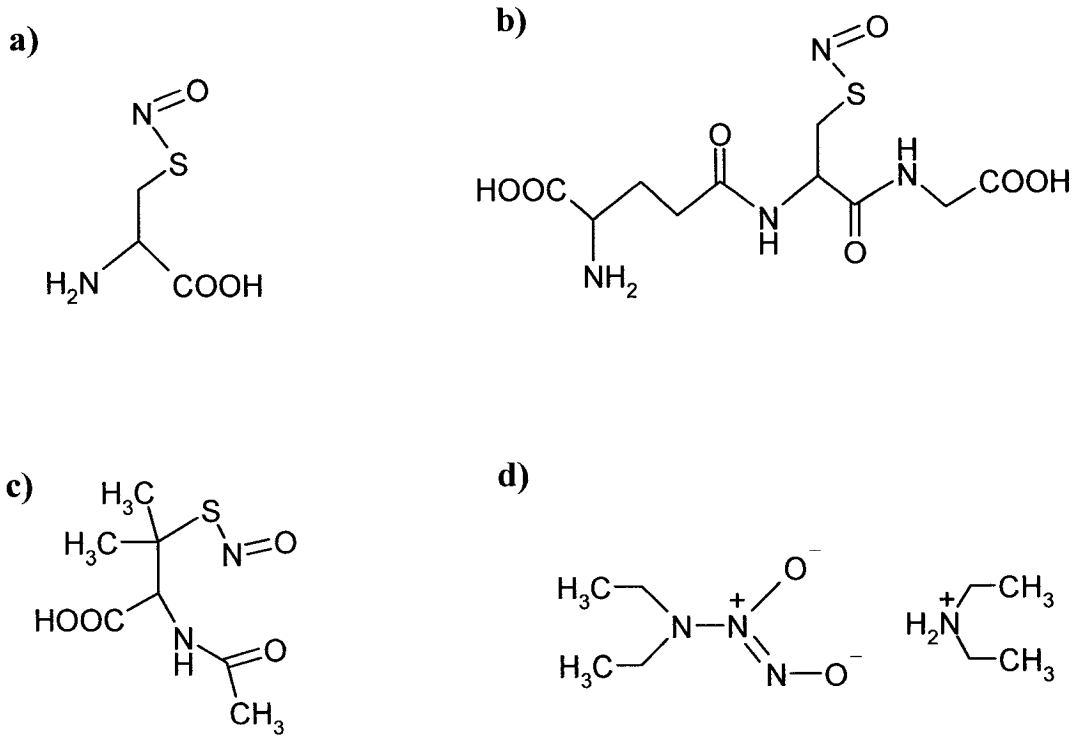

Figure 1.1. NO donors commonly used in S-nitrosation studies: (a) CysSNO (10), **(b)** GSNO (10), **(c)** SNAP (37), **(d)** DEA/NO (38).

cysteine with sodium nitrite in 1 M HCl (36) as shown in Reactions 1.9 and 1.10. CysSNO is relatively stable in the absence of free Cys and transition metal ions (e.g., Cu^{I}) (24), and its stability can be monitored by UV/Vis using $\varepsilon_{335\ nm} = 8000\ M^{-1}cm^{-1}$ (39). In the dark and in the absence of metal ions, its reported half-life is 9 h at 37°C (23,36). CysSNO is very soluble in sodium phosphate buffer (NaPi) at pH 7.2, and has been used as a vasodilator as have GSNO and SNAP (40).

1.2.2.2 GSNO

Glycine N-(N-L-γ-glutamyl-S-nitroso-L-cysteinyl) (GSNO, Figure 1.1b) is a stable S-nitrosothiol derivative that is widely used as an NO donor. It can also be prepared by Reactions 1.9 and 1.10, and its solubility in NaPi (pH 7.2) is ~35 mg/mL. GSNO has a $\lambda_{max} = 333$ nm ($\varepsilon = 8500\ M^{-1}cm^{-1}$). On incubation at 37°C in the dark, GSNO does not spontaneously release NO (41), and its half-life when shielded from light in 200 mM NaPi (pH 7.2), in the presence of DTPA at 25°C, is ≥ 10 h (Section 2.5.1). GSNO is a potent smooth muscle relaxer and inhibitor of platelet aggregation (26,42). It is more potent than SNAP at inhibiting collagen-induced platelet aggregation (26). Studies regarding GSNO conflict as to whether its effects are due to NO release or to the action of the intact compound (43).

1.2.2.3 SNAP

S-Nitroso-N-acetyl-D,L-penicillamine (SNAP, Figure 1.1c) is a stable S-nitrosothiol and NO donor. It can be stored as the crystalline solid at -20°C for at least one year. A stock solution can be prepared in organic solvents such as ethanol, dimethyl

sulfoxide (DMSO), or dimethylformamide. The solubility of SNAP in these solvents is ≥ 25 mg/mL, and the SNAP solutions are stable for at least six months if stored at -20°C. Its concentration can be determined in water solutions using $\varepsilon_{338\ nm}$ = 7400 $M^{-1}cm^{-1}$. Dilutions of the stock solution into aqueous buffers or isotonic saline should be made prior to use. Organic-solvent-free aqueous solutions of SNAP can be prepared by directly dissolving the crystalline compound in neutral or acidic aqueous buffers. The solubility of SNAP in NaPi (pH 7.2) is ≥ 10 mg/mL, and its half-life is ~12 h at pH 6-8 and 37°C in the presence of metal chelators (8,24,39). SNAP is a potent vasodilator, and again it is a matter of debate as to whether the vasodilator effect is due to the release of NO or to the direct effects of the compound on vascular smooth muscle (8,42). The x-ray structure of SNAP (Figure 1.10) has been reported (37) and reveals that C-S-N-O moiety adopts an *anti* conformation with a C-S-N-O dihedral angle close to 180° (18).

1.2.2.4 DEA/NO

Another widely used NO donor is diethylammonium (Z)-1-(N, N-diethylamino) diazen-1-ium-1, 2-diolate (DEA/NO, Figure 1.1d) Its chemistry as a NO donor is quite different from that of the RSNOs (38). DEA/NO spontaneously releases NO in the absence of an electron donor (Reaction 1.19):

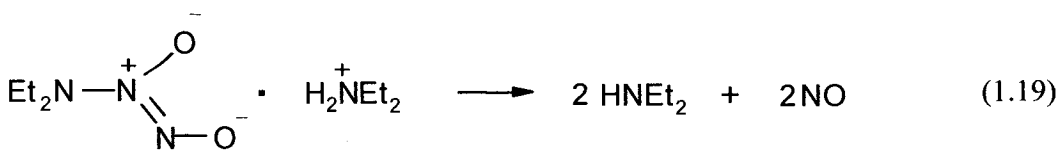

(1.19)

One molecule of DEA/NO dissociates to give 2 molecules of NO and of the amine in a pH-dependent manner following first-order kinetics (Reaction 1.19). Its alkaline solutions (0.01 M NaOH) are very stable and can be stored at 0°C for 24 h. DEA/NO is highly soluble in water and relatively concentrated solutions can be prepared for further dilution. To initiate the release of NO, a portion of an alkaline stock solution of DEA/NO is added to excess buffer at pH 7.0-7.4. Its half-life is 2.1 min at 37°C (8 min at 22°C) in 100 mM phosphate buffer (pH 7.4) but its decomposition is nearly instantaneous at pH 5 (44). Intact DEA/NO has a characteristic UV absorbance at 250 nm (ε = 9,180 $M^{-1}cm^{-1}$), permitting quantitation in aqueous solutions (44).

1.3 Hemoglobin Structure

Adult hemoglobin A (Hb) is a tetrameric protein (~64 kDa) consisting mainly of α-helical secondary structure (Figure 1.2), and is found in red blood cells (RBCs) at a concentration of ~5 mM (45). Its main function is to transport oxygen from the lungs to tissues. In its native form, Hb is composed of two α- (141 amino acid residues) and two β-subunits (146 amino acid residues) (Table 1.1). Each subunit contains one non-covalently bound heme group.

Hb exhibits positive cooperativity in O_2 binding, where the binding of O_2 to one heme site of Hb increases the affinity of the other heme sites (46). Thus, a sigmoidal relationship is observed between degree of binding and the free O_2 concentration. X-ray crystallographic studies have demonstrated the existence of two quaternary structures for Hb, the T- (tense) deoxygenated, and the R- (relaxed) oxygenated structures. Cooperative

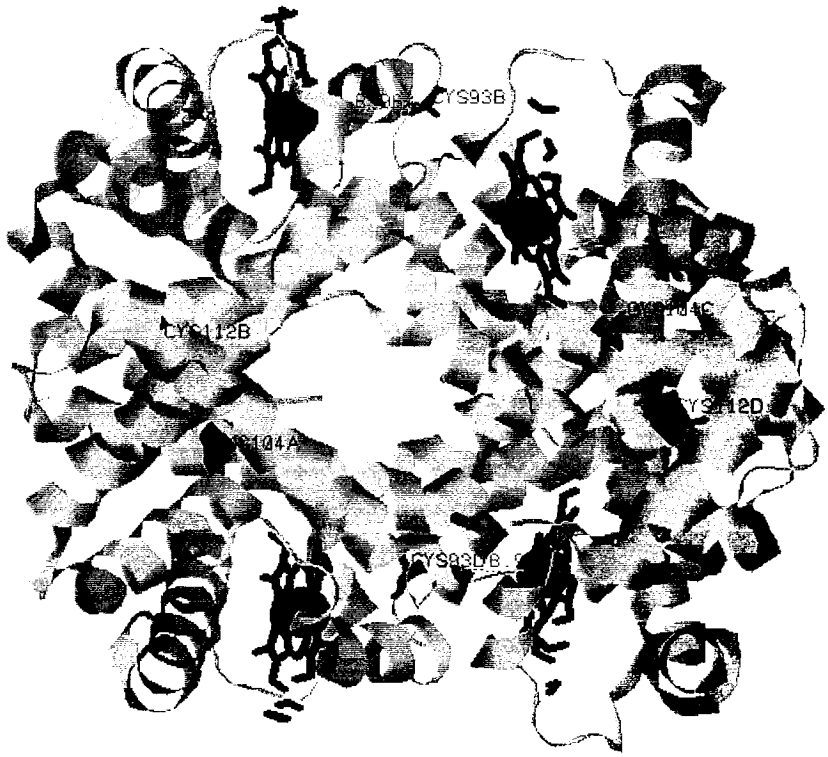

Figure 1.2. X-ray structure of human oxyHb. The structure is mainly α-helical. The 4 heme groups (black with iron in red), and 6 cysteine residues (blue) are indicated (structure from PDB file 2HHB).

α-chain 141 amino acid residues

1	VLSPADKTNV	KAAWGKVGAH	AGEYGAEALE
31	RMFLSFPTTK	TYFPHFDLSH	GSAQVKGHGK
61	KVADALTNAV	AHVDDMPNAL	SALSDLHAHK
91	LRVDPVNFKL	LSHCLLVTLA	AHLPAEFTPA
121	VHASLDKFLA	SVSTVLTSKY	R

β–chain 146 amino acid residues

1	VHLTPEEKNA	VTTLWGKVNV	DEVGGEALGR
31	LLVVYPWTQR	FFESFGDLSS	PDAVMGNPKV
61	KAHGKKVLGA	FSDGLNHLDN	LKGTFAQLSE
91	LHCDKLHVDP	ENFKLLGNVL	VCVLAHHFGK
121	EFTPQVQAAY	QKVVAGVANA	LAHKYH

Table 1.1. Amino acid sequence of α- (P01922) and β-chains (P02023) of adult human hemoglobin. The three cysteine residues are underlined.

O_2 binding by Hb is explained in terms of a reversible transition between these two quaternary structures upon partial ligation of the four hemes (46). The main difference between the T- and the R- structures, revealed by X-ray analysis, is that the $\alpha^2\beta^2$ dimer is rotated and translated relative to the $\alpha^1\beta^1$ dimer. The two β-subunits are ~5 Å farther apart in the T quaternary structure than in the R structure. Large structural differences occur in the $\alpha^1\beta^2$ subunit interface, where breaking and formation of hydrogen bonds and salt-bridges take place upon O_2 ligation to Hb (47). The ^{1}H NMR signal of Tyrα42, which forms a hydrogen bond with Aspβ99 in the T-state but is free in the R-state, has served as a diagnostic marker for the quaternary structure (46).

Allosteric effectors preferentially stabilize Hb in one quaternary state. For example, 2,3-diphosphoglycerate (DPG) and inositol hexaphosphate (IHP) lower the O_2 affinity of Hb *in vivo* by binding tightly to the T-structure close to Hisβ2 (47). Both bind at the same site on $\alpha_2\beta_2$ tetramer, and this site straddles the two β subunits across a 2-fold symmetry axis. This binding site is destroyed when the quaternary structure changes to the R-state because the β-globins move closer together. Consequently, the T-state has much higher affinity for these effectors than the R-state. DPG is present at high concentration (~5 mM) in most mammalian RBCs. The O_2 affinity of Hb is also physiologically coupled to the CO_2 content of blood, with increased CO_2 causing release of O_2 from oxyHb. CO_2 binds as the carbamate to the free α-amino groups (N-termini) of both α- and β- chains in the T-state:

$$Hb{\sim}NH_2 + CO_2 \rightleftharpoons Hb{\sim}NH\text{-}CO_2^- + H^+$$

Binding of CO_2 to the T-structure is favored because the ionized carbamate forms a salt-bridge with Argα141 from each α-subunit. These positively charged residues are not in the same position in the R-state so the salt-bridges are broken (47). The total number of cysteine resides in human Hb is six, two Cysβ93, two Cysβ112 and two Cysα104 (Figure 1.2). Although the Cysβ93 residues are conserved in all mammalian and avian Hbs, the function of these two highly reactive SH groups (48) has not been established.

1.4 NO Binding to Cysβ93 of Hemoglobin

NO is continuously synthesized in endothelial cells and is a critical endogenous vasodilator (25,49,50). Although it is generally believed that endothelium-derived NO is the primary determinant of NO-mediated control of basal blood flow in humans (51), considerable recent controversy has focused on the role of intravascular NO-derivatized molecules that could stabilize NO bioactivity and contribute to blood flow and oxygen delivery. Such molecules include high- and low-molecular-weight RSNOs in plasma (6,52-55). NO donors and NO can nitrosate the surface thiol on Cysβ93 to form *S*-nitrosohemoglobin (Hb-SNO). Hence, it has been proposed recently that Hb can carry out a second cycle, in addition to the O_2/CO_2 cycle, in which it binds NO in the lungs and releases it in the blood vessels. Since NO is a vasodilator (9,40), this O_2/NO cycle could potentially help stabilize blood pressure (56). The binding of O_2 to the heme-iron promotes the binding of NO to the SH group of Cysβ93, forming Hb-SNO (57). Deoxygenation is accompanied by the R$\rightarrow$T allosteric transition in Hb-SNO that facilitates NO release from Cysβ93. Thus, Hb-SNO formation contracts blood vessels in the R-structure, while NO release relaxes vessels to improve blood flow in the T-

structure. Thus, by sensing the physiological O_2 gradient in tissues, Hb reportedly exploits conformation-associated changes in the position of Cysβ93-SNO to bring local blood flow in line with oxygen requirements (56). Stamler and coworkers also suggest that the RBC has evolved a way to counteract platelet activation in small vessels and the aggregatory effects of oxidative stress by forming Hb-SNO (58).

Examining the X-ray structures of R- and T-state Hb it would appear that Cysβ93 adopts positions in deoxyHb and oxyHb that control the reactivity of the thiol. In deoxyHb (T-state), Cysβ93 points out toward the protein surface, up above the external Hisβ146-Aspβ94 salt-bridge. The γ-sulfur of Cysβ93 is deactivated by the salt-bridge that shields it and the acidic environment of Aspβ94 and Gluβ90 promotes its protonation (Figure 1.3a). Therefore, in the T-structure, the reactivity of Cysβ93 toward NO is low. In R-state Hb, the Hisβ146-Aspβ94 salt-bridge breaks and Cysβ93 points in and away from the solvent. Cysβ93 is brought into proximity with Hisβ92 (the proximal heme Fe^{II} ligand), which facilitates deprotonation of the γ-sulfur and enhances its nucleophilicity (Figure 3.1b) (56). Examining the recently published X-ray structure of nitrosylHb-SNO (59), it is evident that Hb is in the R-state, since the Hisβ146-Aspβ94 salt-bridge is broken and the SNO moiety of Cysβ93 points in and away from the solvent. Therefore, the binding of NO to Cysβ93 is facilitated in the R-structure.

It has been proposed (56) that NO transfer from a low-molecular-weight RSNO, such as CysSNO or GSNO, to Cysβ93 of Hb could occur via a *trans*-S-nitrosation mechanism as follows:

$$\text{CysSNO} + \text{Hb-SH} \rightleftharpoons \text{CysSH} + \text{Hb-SNO} \qquad (1.20)$$

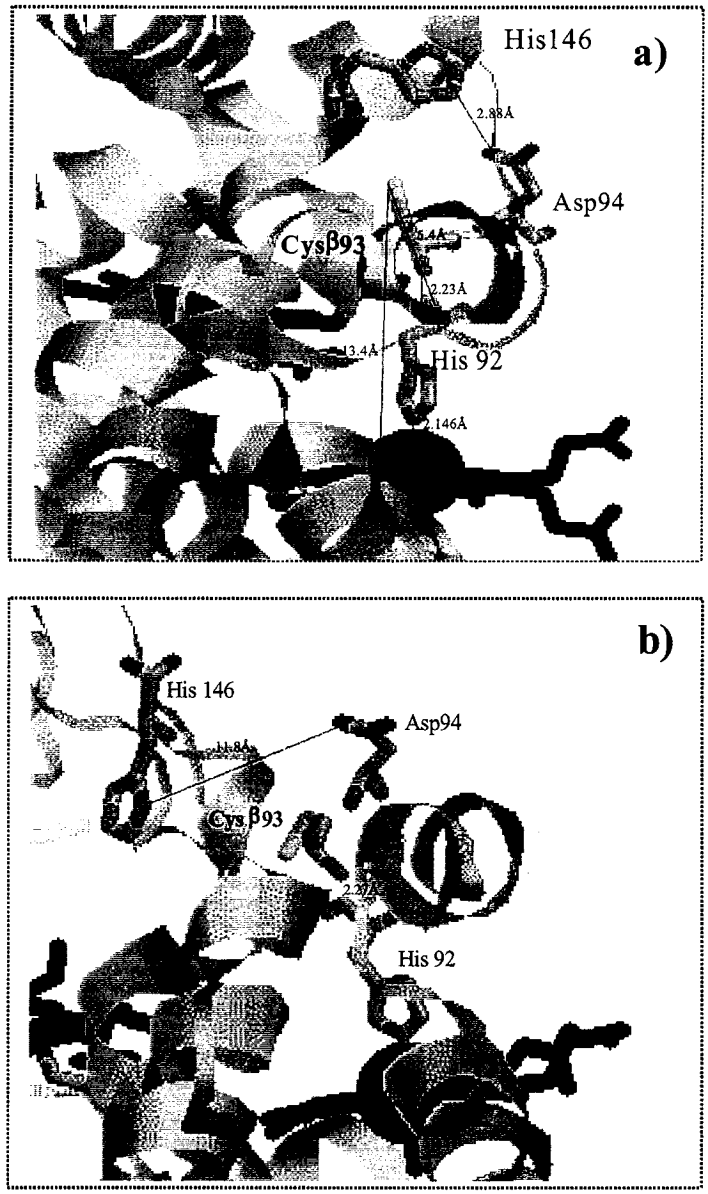

Figure 1.3. Structural environment of Cysβ93 in deoxyHb and oxyHb. (**a**) In deoxyHb, Cysβ93 points toward the protein surface, up above the external Hisβ146-Aspβ94 salt-bridge. The γ-sulfur of Cysβ93 (yellow) is deactivated by the salt-bridge that shields it. (**b**) In oxyHb, the salt-bridge breaks and the γ-sulfur (yellow) points in and away from the solvent [structures from PDB files 2HHB (for a) and 1HHO (for b)].

It is believed that S-nitrosation of Hb occurs by direct nucleophilic attack of the thiolate anion (RS^-) of Cysβ93 on the nitrogen atom of CysSNO or GSNO leading to NO^+ transfer to Cysβ93. NO also reacts reversibly with deoxyHb to form an NO-heme adduct, nitrosylHb ($HbFe^{II}NO$). The assumption of high-affinity NO binding to Fe^{II} heme of deoxyHb has dominated the view of deoxyHb/NO interactions. NO binds rapidly to Fe^{II} in deoxyHb (k_{on} ~10^7 $M^{-1}s^{-1}$) and once bound, the NO is largely irretrievable (k_{off} ~10^{-5} s^{-1}). In fact, the binding is so tight that is unaffected by O_2 (12). However, as pointed out by Stamler and coworkers, these kinetic data refer to fully heme nitrosylated Hb, while Hb is only partially nitrosylated *in vivo*. Using difference spectroscopy, Gow and Stamler (56) have shown that O_2 drives the conversion of partially nitrosylated Hb in the T-structure to oxyHb-SNO in the R-structure. That is, NO is transferred from the Fe^{II} heme to Cysβ93 by an undefined mechanism.

A model that depicts the physiologically relevant reactions of NO with Hb during the respiratory cycle in RBCs (Figure 1.4) has been proposed by Stamler (56) and others (60). In this model, NO from a low-molecular-weight RSNO binds oxyHb in the lungs to form oxyHb-SNO, where Cysβ93 is S-nitrosated. In the arteriole, oxyHb-SNO delivers O_2 thereby releasing NO. In the capillaries, NO binds to the heme of the α-globin of deoxyHb, which has a higher NO affinity than the β-globin heme (61). In the proximity of the lungs, the pO_2 increases and O_2 displaces NO from the heme of α-globin, which then binds to heme of β-globin. Once in the lungs, Hb is fully oxygenated and the released NO binds to a free thiol such as GSH (60) forming RSNO or to Cysβ93 of Hb and re-enters the cycle.

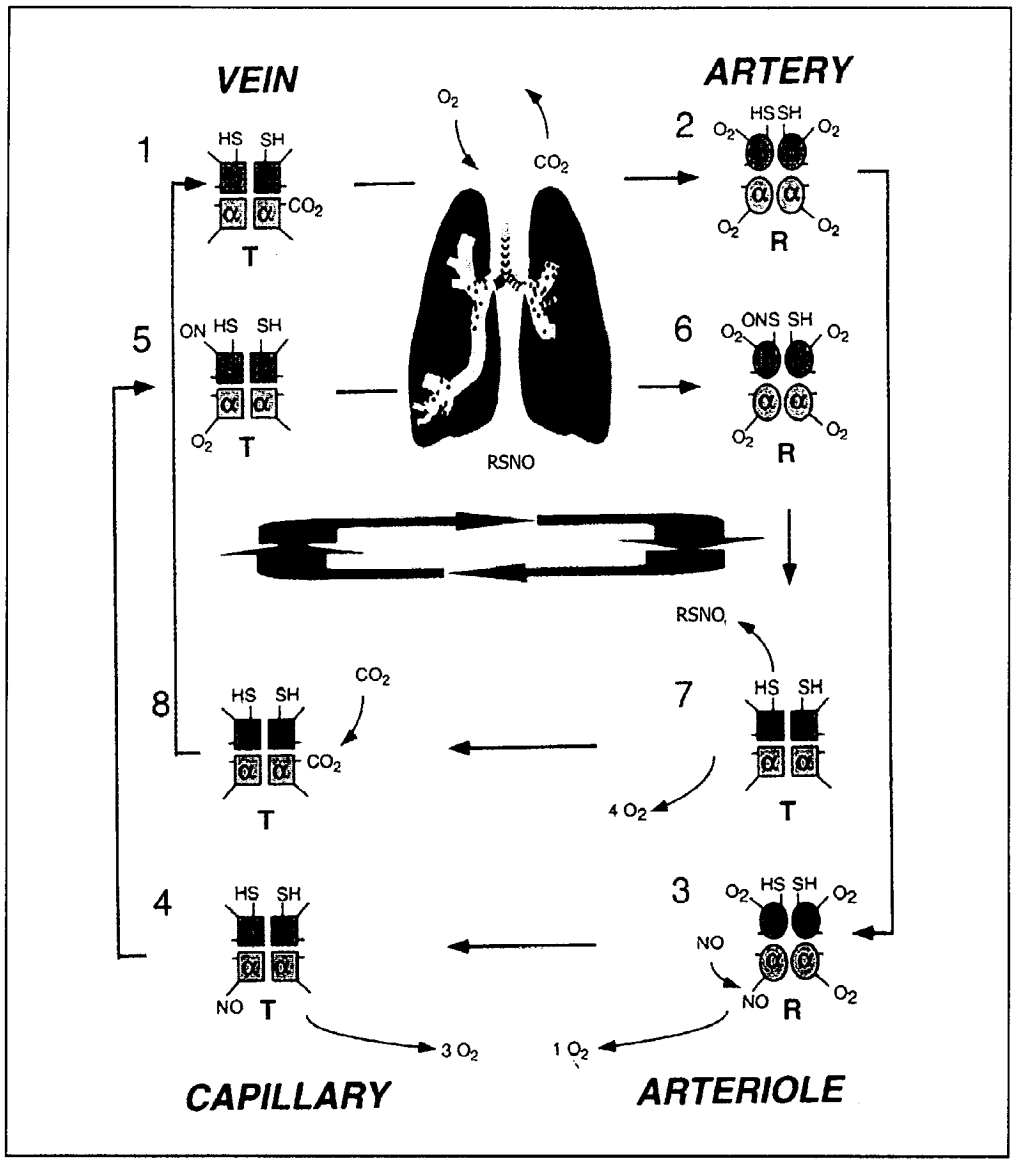

Figure 1.4. The proposed physiologically relevant reactions of NO with Hb during the respiratory cycle in RBCs (60).

Two observations had supported the role of Hb-SNO as an NO transporter. These were reports of observed arterial-venous gradients of Hb-SNO in the rat suggesting a dynamic cycle, and evidence that delivery of O_2 and NO are allosterically coupled events (12,56,58). In rats, a major fraction of NO in the blood (~300 nM) is bound to the thiols of Hb, forming Hb-SNO, which releases NO on deoxygenation in the microcirculation (19). Hb-SNO is found in the systemic circulation of rats at concentrations approximately 10 times higher in arterial (~300 nM) than venous (~30 nM) blood (57). However, evidence for a dynamic cycle is brought into question by the absence of arterial-venous Hb-SNO gradients in humans (55). Also, widely varying reports of the levels of intracellular Hb-SNO in arterial and venous blood have appeared in the recent literature. The reported levels vary from 200 nM to 5 μM and were determined using a variety of different assays, mostly based on photolysis or chemically mediated release of NO gas and subsequent detection by the ozone-based chemiluminescence analyzer (6,55,58,62,63). In addition, although both kinetic and thermodynamic arguments have been made to support the allosterically mediated release of NO from Hb-SNO (12,58,64), the physiological relevance of this process has been challenged. For example, the very high O_2 affinity of Hb-SNO would potentially limit its role in basal regulation of O_2/NO delivery (57,65,66).

1.5 Superoxide Dismutase

Cu,Zn-superoxide dismutase (CuZnSOD) catalyses the dismutation reaction of the superoxide radical to molecular oxygen and hydrogen peroxide:

$$2O_2^- + 2H^+ \rightleftharpoons O_2 + H_2O_2 \qquad (1.21)$$

CuZnSOD forms a crucial part of the cellular antioxidant defence mechanism by protecting oxygen-metabolizing cells against the harmful effects of superoxide radicals (67-70). SOD enzymes are widespread in nature. They are present in all oxygen-metabolizing cells (71), and have been also found in anaerobic bacteria (72). They have been purified from diverse sources such as *Streptococcus mutans*, *E. coli*, *Saccharomyces cerevisiae*, *Neurospora crassa* and wheat germ (73-76). Three superoxide dismutases are characterized by different metal content. A blue-green Cu^{II},Zn enzyme is the main copper protein in RBCs; a wine-red Mn^{III} protein is found in *E. coli* and in mitochondria (77,78), and a yellow Fe^{III} enzyme has been isolated from *E. coli* (79).

Bovine erythrocyte CuZnSOD has been extensively studied. It is highly homologous to the enzyme from human erythrocytes and beef heart (80,81). CuZnSODs, which are extremely stable enzymes are located in the cytosol, lysosomes, peroxisomes, the nucleus, and in the intermembrance space of mitochondria (82). The molecular weight of the bovine enzyme is 32,500 Da and there are two Cu and two Zn atoms per molecule (83). It has been found that Zn has a structural, stabilizing role, while Cu is directly involved in the catalytic activity (84). CuZnSOD consists of two subunits of identical molecular weight held together by non-covalent interactions. Each subunit is composed of a flattened cylindrical barrel of β-pleated sheet from which three external loops of irregular structure extend. One Cu and one Zn atom, bridged by the imidazolate ring of a histidyl side chain, are present in each subunit. The Cu lies at the bottom of a narrow channel that is large enough to admit only water, small anions and small ligands. In addition to the positively charged $Cu^{I/II}$ ion at the bottom of the channel, the positively charged side chain of Arg141 is part of the walls of the channel, which directs the superoxide anion toward the

copper. In addition, two positively charged lysine side chains (Lys120, Lys134) are close to the mouth of the channel. A disruption in the structure of the enzyme and of the channel would decrease the efficiency of the enzyme to direct anions toward the copper, thus leading to a diminution in the enzyme activity.

SODs have medical relevance as potential therapeutic agents in diseases related to oxidative stress and moderating the ageing process. Furthermore, it has been recently demonstrated that bovine CuZnSOD catalyzes the reductive elimination of NO from GSNO and other low-molecular-weight S-nitrosothiols (85). Thus, CuZnSOD can be considered a GSNO reductase.

1.6 Overview of the Techniques Used in this Thesis

1.6.1 Fourier Transform Infrared Spectroscopy

Fourier transform infrared (FTIR) spectroscopy is used to probe the ν(SH) stretching vibration of cysteine thiols in proteins. The ν(SH) bands provide a unique opportunity to probe changes in protein structure around thiol groups that may result from changes in amino acid sequence, oxidation state, ligand binding, pH and temperature. Variations in the ν(SH) band parameters reflect differences in local environment and hydrogen bonding experienced by the S-H groups. The frequency of the ν(SH) band is expected to increase with increasing S-H bond strength. Band intensity will increase as the strength of the dipole associated with the SH bond increases. Strong hydrogen bonding with the SH group serving as proton donor will lower the frequency and increase the intensity of the ν(SH) band (86). The bandwidth is related to the

mobility of the environment around the SH group, with more mobile environments giving rise to increased bandwidths due to inhomogeneous broadening.

Three ν(SH) bands were identified in the IR spectrum of oxyHb (87). The ν(SH) bands of the three types of cysteine are readily distinguished from each other. The SH group of Cysα104, located at the $\alpha^1\beta^1$ interface and strongly hydrogen bonded to the peptide carbonyl of Leuα100 (86), absorbs at the lowest frequency (2553 cm^{-1}) with the highest intensity. The Cysα104 band is expected to provide a sensitive probe of the tertiary structure of the α-subunit G helix at the $\alpha^1\beta^1$ interface and the quaternary structure of the Hb tetramer. Cysβ112 is located at the nonpolar $\alpha^1\beta^1$ interface (86,88), but its environment is less hydrophobic than of Cysα104, and it absorbs at a higher frequency (2566 cm^{-1}) with lower intensity, indicating weaker hydrogen bonding. Cysβ93 is located in the F-H α-helical pocket near the surface of the Hb molecule. Its environment is the most polar of the three cysteine residues and it absorbs at the highest frequency (2589 cm^{-1}) with the lowest intensity, indicative of weak hydrogen bonding (89).

Fourier self-deconvolution (FSD) was used to enhance the resolution of the ν(SH) bands. FDS is applied to spectral data to separate overlapping features that cannot be resolved by collecting data at a higher resolution setting. By setting the bandwidth, which is an estimate of the widths of the overlapped bands, and the enhancement, which is a measure of the degree to which the data are resolved experimentally, the FSD process can be controlled to optimize the resolving power applied to the data (90,91).

1.6.2 Spin Scavenging Coupled with LC/MS

Protein-based radicals (such as $R^{\bullet}$ discussed in Chapter 6) are often difficult to detect because they are short-lived and highly reactive. As a result, the technique of spin trapping has been frequently used in EPR investigations (92). Spin traps (ST) are diamagnetic compounds that react with $R^{\bullet}$ to form more stable paramagnetic adducts (R-$ST^{\bullet}$). EPR analyses have been successfully used to provide information on the radical centers of R-$ST^{\bullet}$ species and their environments (92,93). One shortcoming of this technique is that the *specific sites* of radical formation in proteins are often difficult to identify. For example, horse cytochrome c contains four tyrosine residues (Tyr48, 67, 74 and 97) (94); hence, EPR analysis alone cannot unambiguously identify on which tyrosine R-$ST^{\bullet}$ is formed. Given that the formation of R-$ST^{\bullet}$ results in an increased mass of the compound of interest, high-performance liquid chromatography (HPLC) with mass spectrometric (MS) detection (LC/MS) has been successfully used to identify spin adducts of various small molecules (95,96).

Our research group has extended this use of LC/MS to proteins to overcome the inherent limitations of EPR. We have found that reduction of R-$ST^{\bullet}$ gives rise to a more stable diamagnetic mass adduct (R-MA) and permits the assignment of $X^{\bullet}$ to a *specific amino acid* residue when spin trapping and on-line peptide mass mapping by LC/MS are coupled (97). In addition to increased specificity, LC/MS offers enhanced sensitivity over EPR since considerably smaller quantities (picomole vs nanomole) of sample can be analyzed (98). Moreover, since MS detects mass changes, and not unpaired spins, conversion of radicals to stable diamagnetic adducts is possible. Hence, stable nitroxide radicals, such as 2,2,6,6-tetramethylpiperidinyl-1-oxy (TEMPO$^{\bullet}$), have recently been used in our group to scavange protein-based radicals leading to diamagnetic TEMPO-

adducts (99). As with any technique, adduct formation coupled with LC/MS possesses certain limitations. For example, accessibility of spin scavengers or spin traps to buried radicals will be limited. For studies on proteins, it is important to use spin scavengers and traps that are water soluble, stable at room temperature and photostable (92,100).

1.7 Hypotheses, Scope and Organization of Thesis

The hypotheses are (i) that Hb S-nitrosation occurs via a copper-catalyzed mechanism and that (ii) NO binds preferentially to Cysβ93 of oxyHb and not to deoxyHb. The scope of the work presented here is to clarify the mechanism of Hb S-nitrosation to understand the possible role of NO/Hb interactions in vasodilation. Experiments to determine whether NO binds to Cysβ93 of both oxyHb and deoxyHb were performed. FTIR was extensively used to monitor NO binding to Cysβ93 by examining the ν(SH) stretching vibrations (~2500 cm^{-1}). LC/MS was used to localize the NO adduct in the β-globin of Hb. The role of copper in NO release from NO donors and NO binding to Hb was investigated. The Hb R→T allosteric transition was found to be important in regulating S-nitrosation of Cysβ93 of Hb. This is attributed here to the requirement for copper for NO binding to Cysβ93 *in vitro* (Chapter 3). A key step for Hb S-nitrosation by RSNO is the formation of a thiyl radical on Cysβ93, and CuZnSOD-catalysis of reductive elimination of NO from RSNO is essential for thiyl radical formation as demonstrated in Chapter 4.

1.8 Contributions of Colleagues

Chapters 3, 4 and 5 are published manuscripts. Chapters 2 and 6 are currently being prepared for publication. All abbreviations, citations, figures and table numbering systems in the published works were changed to the format of this thesis.

Chapter 3 was published in the *Journal of American Chemical Society* [Romeo, A. A., Filosa, A., Capobianco J. A. and English, A. M. (2001) *J. Am. Chem. Soc.* 123, 1782] and is reproduced with the permission of the journal. I carried out all the work reported in this publication and prepared the manuscript. A. Filosa provided instruction on the use of LC/MC instrumentation and on data analysis. Both A. M. English and J. A. Capobianco provided intellectual support, and A. M. English edited the manuscript.

Chapter 5 was published in the *Journal of Biological Chemistry* [Romeo, A. A., Capobianco, J. A. and English, A. M. (2002) *J. Biol. Chem.* 227(27), 24153] and is reproduced with the permission of the journal. I carried out all the work reported in this publication and prepared the manuscript. Both A. M. English and J. A. Capobianco provided intellectual support, and A. M. English edited the manuscript.

Chapter 4 is in press in the *Journal of American Chemical Society* [Romeo, A. A., Capobianco, J. A. and English, A. M. (2003) *J. Am. Chem. Soc.* 125(47), 14370] and is reproduced with the permission of the journal. I carried out all the work reported in this publication and prepared the manuscript. A. M. English and J. A. Capobianco provided intellectual support, and A. M. English edited the manuscript.

2.0 Control of S-Nitrosothiol Stability

2.1 Abstract

The effects of trace metal ions on the stability in the dark of three RSNOs, CysSNO, GSNO and SNAP, and non-thiol NO donor DEA/NO were studied under anaerobic conditions. UV-Vis spectroscopy was used to monitor the decomposition of the NO donors in solution as a function of time. By following the decrease in absorption maxima of the *S*-NO group, the half-lives in solution were determined. Decomposition was investigated in 200 mM NaPi (pH 7.2) at 25°C in the dark in both the presence and in the absence of 200 μM DTPA and 100 μM neocuproine. The half-lives obtained reveal that the NO donors have varying stability (SNAP > GSNO > CysSNO ≥ DEA/NO). RSNOs are more stable in the presence of DTPA and neocuproine, while DEA/NO stability is not affected by the presence of the metal chelators. In addition, CD spectroscopy was used to monitor RSSR formation with and without metal chelators and 5,5'-dithiobis(2-nitrobenzoic acid) (DTNB) was used to determine the free thiol concentration. The results confirm that metal ions (e.g., Cu^{I}) are required for NO release from RSNO.

2.2 Introduction

RSNOs are believed to play an important role in storing, transporting, and releasing NO *in vivo* (7,101). Numerous biological functions of RSNOs continue to be uncovered. For example, blood flow may be regulated by Hb-SNO (Chapter 1) *via* the release of NO (24). S-nitrosation of certain thiol groups on calcium-release channels may

regulate channel function (102), and S-nitrosation may control calcium binding to proteins (103).

Interestingly, many S-nitrosoproteins, such as S-nitrosoalbumin that contain a primary cysteine residue, are significantly more stable than small RSNOs molecules. Tertiary low-molecular-weight RSNOs are normally more stable than primary RSNOs. However, GSNO, a primary RSNO, has comparable stability to the tertiary RSNO, SNAP. The reasons for the stability of GSNO, SNAP and some S-nitrosoproteins are not yet fully understood. *Ab initio* calculations have been attempted in order to account for the stability of SNAP (104). It is reported that decomposition of RSNOs (Chapter 1) occurs thermally and photochemically to give the disulfide (RSSR) and NO (8,24). In solution, trace metal ions such as copper catalyze the decomposition of RSNOs (105), and calculations have shown that Cu^{I} complexation promotes degradation of RSNOs (106). In this work DTPA and neocuproine were used as specific Cu^{II} and Cu^{I} chelators, respectively (Figure 2.1). The use of metal chelators prevents redox turnover of copper, inhibiting its catalytic effect. In addition, reducing agents such thiols can stimulate decomposition of RSNOs by reduction of metal ions (10,24,107). The goal of this study was to determine the stability in the dark of commonly used NO donors in 200 mM NaPi buffer (pH 7.2) with or without metal chelators. These are the experimental conditions used in the studies in Chapters 3, 4, and 5 of this thesis. MetHb ($HbFe^{III}$) was added to probe its effect on NO-donor stability.

2.3 Experimental Procedures

2.3.1 Materials

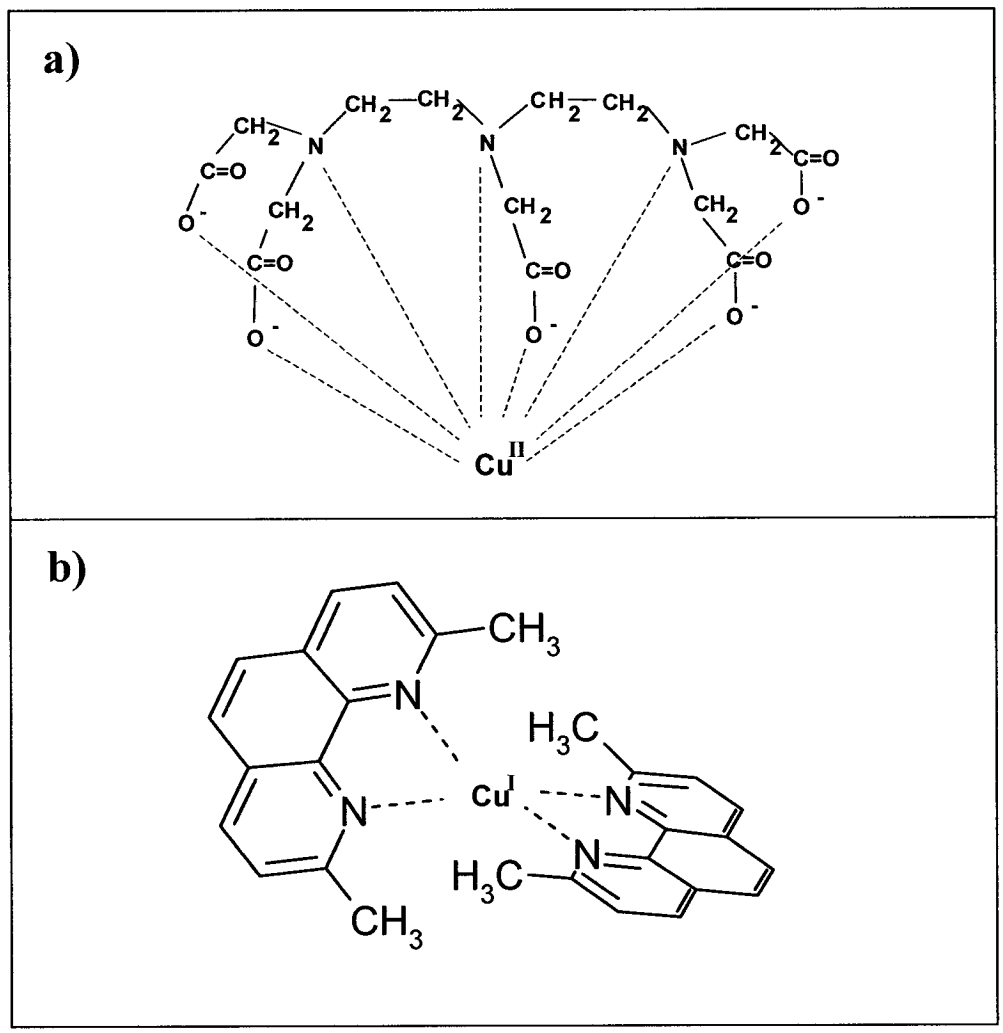

Figure 2.1. Coordinating atoms in DTPA and neocuproine. **(a)** One molecule of DTPA can provide up to 8 lone pairs of electrons to a Cu^{II} ion. **(b)** Two molecules of neocuproine provide 4 lone pairs of electrons to a Cu^{I} ion.

Human Hb A (Sigma) was used without further purification. A stock solution of metHb was prepared at a concentration of 32 mM (heme) in 200 mM NaPi (pH 7.2). The Hb concentration was determined spectrophotometrically ($\varepsilon_{500\ nm}$ = 10 and $\varepsilon_{630\ nm}$ = 4.4 $mM^{-1}\ cm^{-1}$ per heme).

All reagents were of the highest quality available and were obtained from the following suppliers: sodium phosphate salts (Na_2HPO_4, NaH_2PO_4) from Anachemia and Fisher, GSNO [glycine, N-(N-L-γ-glutamyl-S-nitroso-L-cysteinyl)], SNAP (S-nitroso-N-acetyl-D-penicillamine) and DEA/NO [diethylammonium (Z)-1-(N,N-diethylamino) diazen-1-ium-1,2-diolate] from Cayman; DTPA (diethylenetriamine-N,N,N',N",N"-pentaacetic acid) and L-cysteine from Sigma, $NaNO_2$ from Anachemia and DTNB [5, 5 - dithiobis(2-nitrobenzoic acid)] from ICN Biochemicals Inc. Nanopure water (specific resistance 18 MΩ-cm), obtained from a Millipore Simplicity water purification system and treated with Chelex-100 (Sigma) to remove trace metal ions, was used to prepare all buffers and H_2O solutions.

2.3.2 Synthesis of CysSNO

CysSNO was synthesized in the dark under nitrogen by mixing 500 μL of 200 mM free cysteine in 1 M HCl with 500 μL of 200 mM $NaNO_2$ in water at 25°C (Reactions 1.9 and 1.10, Chapter 1) (36). After completion of the reaction (~1 min), the intense red solution was adjusted to pH 7.2 with 1 M NaOH. Formation and concentration of CysSNO were verified spectrophotometrically using ε_{335} = 8000 $M^{-1}\ cm^{-1}$ (Figure 2.2). Previous studies have established that essentially no nitrite remains in the nitrosothiol solutions using this synthetic method (17). CysSNO was always prepared

under nitrogen just before use, and diluted in the dark into 200 mM NaPi buffer (pH 7.2). To minimize metal-ion impurities the distilled-deionized water used was passed through a Chelex-100 column. CysSNO is relatively stable in absence of free cysteine, light, heat, and transition metal ions. It has been reported that its half-life is 9 h at 37°C (23,108).

2.4 Methods

2.4.1 UV-Vis experiments

The decomposition of CysSNO, GSNO, SNAP and DEA/NO was followed spectrophotometrically as a function of time. A Beckman DU 650 UV-Vis spectrophotometer was used to follow the decrease in absorbance in a 1-cm cuvette at the λ_{max} of 335, 333, 338 and 250 nm for CysSNO, GSNO, SNAP and DEA/NO, respectively, in 200 mM NaPi (pH 7.2), under nitrogen in the dark at 25°C in both the presence and absence of 200 μM DTPA and 100 μM neocuproine or metHb. Aliquots (200 μL) of fresh stock solutions of the NO donors were immediately diluted in cuvettes containing NaPi under nitrogen and mixed using a cuvette stirrer (Hellma Model 333). Absorbances were measured every min over 30 min. For each NO donor, plots of ln A *vs* time decreased linearly indicating first-order decomposition. This was confirmed by the independence of the half-life (ln2/k) on the NO-donor concentration within the range examined (50 μM to 500 μM).

2.4.2 Near UV-CD Experiments

Near-UV-CD spectroscopy allows the observation of disulfide bond formation.

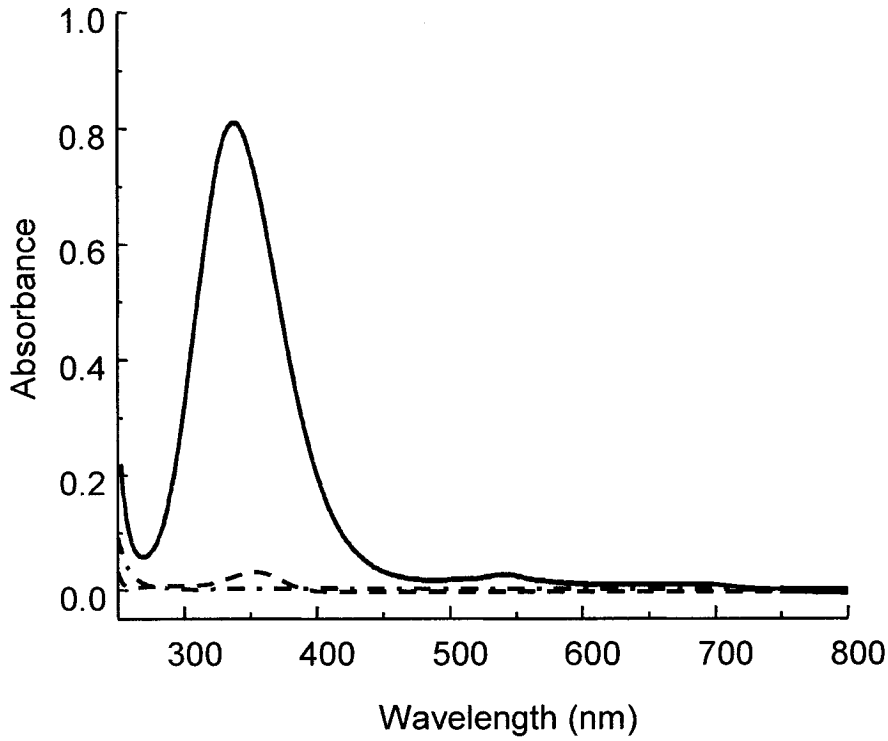

Figure 2.2. UV-Vis spectra of CysSNO, free cysteine and $NaNO_2$. 100 μM CysSNO, ε_{335} = 8000 $M^{-1}cm^{-1}$ (—); 1 mM $NaNO_2$, ε_{355} = 22.5 $M^{-1}cm^{-1}$ (- - -); and 1 mM cysteine, ε_{208} = 21.5 $M^{-1}cm^{-1}$ (- . - . -). Absorption spectra were recorded under nitrogen in 200 mM NaPi (pH 7.2) in the dark at 25°C in a 1-cm quartz cuvette at a scan rate of 1200 nm/min.

This results in a CD signal due to the n $\rightarrow$ σ^* transition of the S-S bond (109). To investigate the rate of NO release from CysSNO in the presence and absence of metal chelators, different CysSNO incubates were monitored by UV-CD spectroscopy. Chelators were employed since NO release from CysSNO and formation of cystine (CysS-SCys) can occur via a Cu^{I}-catalyzed mechanism (23,24,26,36).

A Jasco 710 spectropolarimeter was flushed with N_2 for 15 min (flow rate of 5 L/min) before use. The following parameters were used for all experiments: scan range 400 to 200 nm; a step resolution 0.2 nm; scan speed 50 nm/min for the accumulation of 5 scans; response, 0.5 s; bandwidth, 1.0 nm; and sensitivity, 100 mdeg. CysSNO was prepared fresh under nitrogen just before use and diluted into 10 mM NaPi (pH 7.2) in a 1-cm quartz cuvette. The concentration of CysSNO and buffer salts used were those recommended for near UV-CD measurements (110,111).

2.4.3 Free thiol determination using Ellman's reagent

Ellman's reagent [5,5'-dithiobis(2-nitrobenzoic acid), DTNB], is a sensitive probe of free thiols (112). The sensitivity is due to the intense absorption of the 5-thiol-2-nitrobenzoate anion (TNB) ($\varepsilon_{412\,nm}$ = 14,150 M^{-1} cm^{-1} in NaPi) produced together with the mixed disulfide from the reaction of the thiolate anion (RS^-) with DTNB (Reaction 2.1).

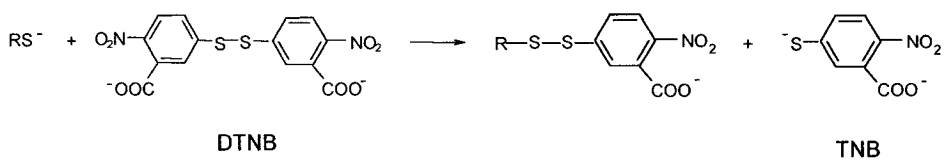

(2.1)

The TNB produced in Reaction 2.1 can also react with NO and NO donors (20), which bleaches the yellow color at 412 nm. However, this does not occur under anaerobic

conditions (20), which were used in the present studies. A 1 mM DTNB stock solution was freshly prepared in 200 mM NaPi (pH 7.2) and added to a 50 μM cysteine solution that was also freshly prepared to monitor TNB formation at 412 nm *vs* time. This reaction was also investigated under the different conditions used to investigate RSNO stability (presence of chelators, etc.).

2.5 Results

2.5.1 UV-Vis experiments

Changes in the UV-Vis spectra (Figure 2.3) showed that the decomposition of the NO donors studied here follows first-order kinetics over 0.2 to 1 half-life (Figure 2.4) (113). The half-life of each donor was independent of concentration in the range used in these experiments (50 μM – 1 mM) indicating that autocatalysis (Reaction 1.16) did not contribute to RSNO breakdown as reported at higher (61 mM) RSNO concentrations (22). The half-lives listed in Table 2.1 reveal that the NO donors have varying stability in NaPi (SNAP > GSNO > CysSNO ≥ DEA/NO). When the RSNOs were incubated with the metal chelators their half-lives increased dramatically (Table 2.1). Surprisingly, the presence of metHb also increased RSNO stability. This may be due to the fact that 2 copper binding sites are present in human Hb (114). Therefore, Hb may act as a copper chelator preventing its catalytic action. DEA/NO stability is not affected by the presence of the metal chelators or metHb. These results indicate that metal ions catalyze the release of NO from RSNOs but not DEA/NO.

2.5.2 Near UV-CD Experiments

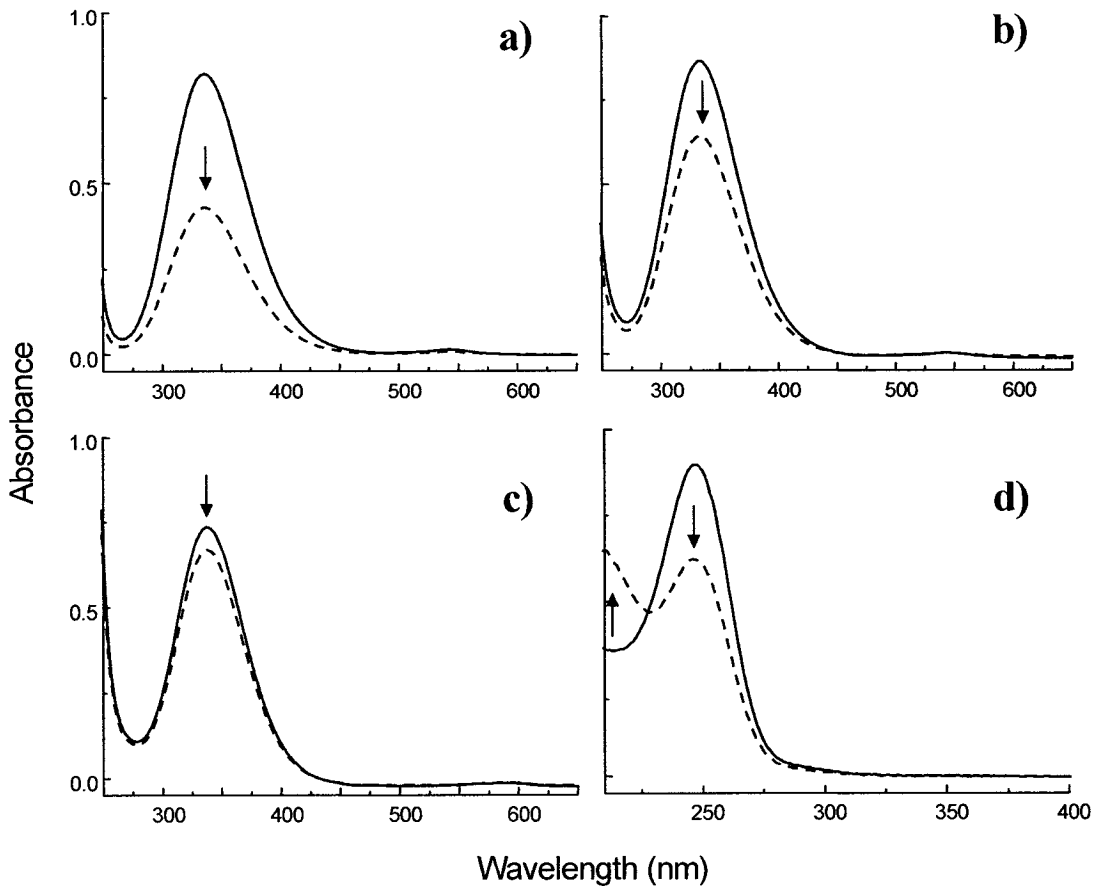

Figure 2.3. UV-Vis spectra of 100 μM NO donor solutions after 5 min. (**a**) CysSNO; (**b**) GSNO; (**c**) SNAP; (**d**) DEA/NO. Spectra of the NO donors in 200 mM NaPi (pH 7.2) at 25°C under nitrogen in the dark were recorded every min in a 1-cm quartz cuvette. Spectra at t = 0 min (—) and t = 5 min (----) are shown here.

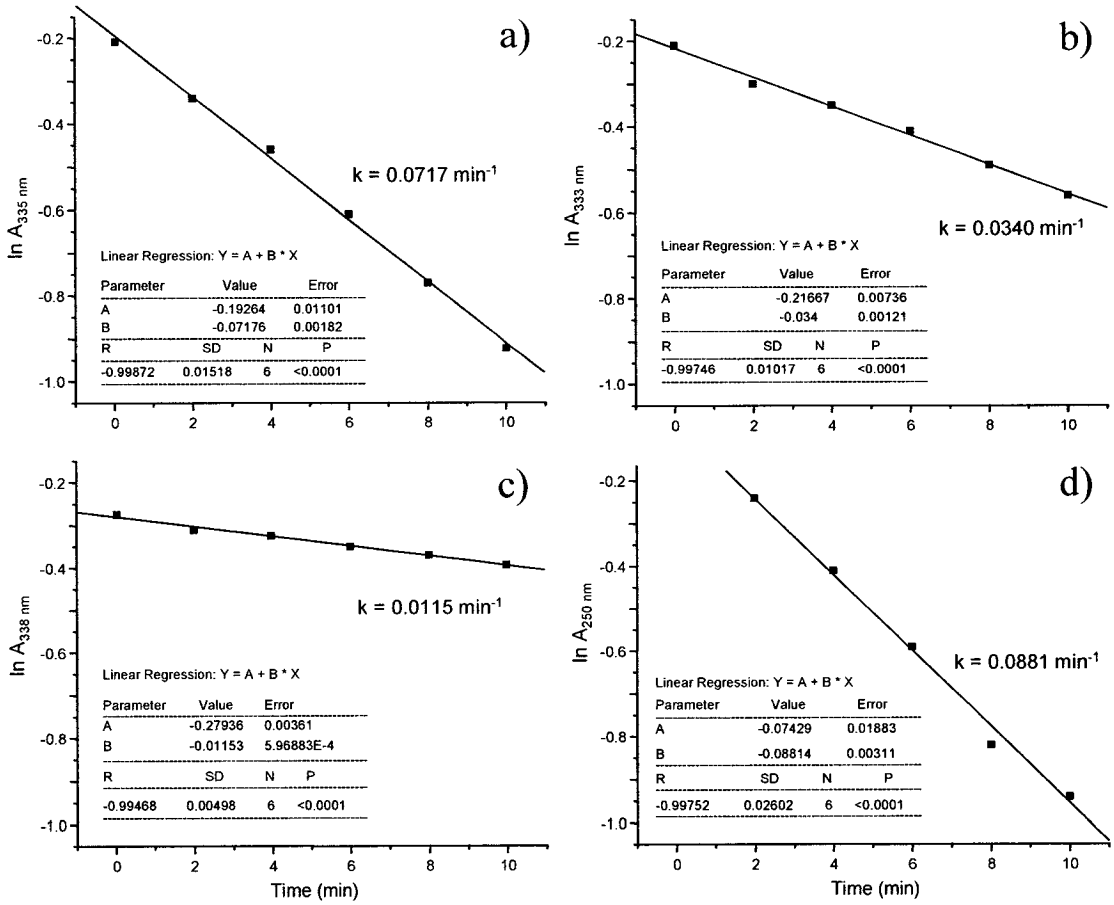

Figure 2.4. Fit to first-order kinetics of NO donor decomposition. (**a**) 100 μM CysSNO; (**b**) 100 μM GSNO; (**c**) 100 μM SNAP; (**d**) 100 μM DEA/NO. Absorbance changes were recorded in 200 mM NaPi (pH 7.2) under nitrogen in the dark at 25°C in a 1-cm quartz cuvette.

The near UV-CD spectra of 15 mM cysteine and 15 mM CysSNO after 20-min incubation in the dark under anaerobic conditions are shown in Figure 2.5. The spectra of CysSNO, and of the CysSNO/DTPA/neocuproine/$CuSO_4$ incubate show an intense negative peak at 270 nm, and a weak negative peak at ~325 nm that is assigned to the disulfide, CysS-SCys (23). In these CysSNO incubates with free copper, metal-catalyzed CysSNO reductive cleavage is follow by disulfide formation (Reactions 2.2 and 2.3) (7):

$$CysSNO + Cu^{I} \rightleftharpoons CysS^{-} + Cu^{II} + NO \qquad (2.2)$$

$$2CysS^{-} + 2Cu^{II} \rightleftharpoons CysS\text{-}SCys + 2Cu^{I} \qquad (2.3)$$

The free cysteine and the CysSNO/DTPA/neocuproine incubates absorbs minimally at 265 nm and do not shown any disulfide CD absorption at ~325 nm.

2.5.3 Free Thiol Determination

When excess DTNB was added to 50 μM free cysteine, formation of ~50 μM TNB was observed immediately as monitored by the absorbance at 412 nm (Figure 2.6 and Table 2.2). Also, when excess DTNB was added to a Cys/CysSNO/DTPA/neocuproine incubate formation of ~50 μM TNB was observed. As expected, DTNB addition to CysSNO or CysSNO/DTPA/neocuproine incubates revealed the presence of no free thiols in solution (Table 2.2). When excess DTNB was added to the Cys/CysSNO incubate, initially ~50 μM TNB was observed, which decreased to half its initial concentration in ~15 min (Table 2.2). Since metal chelators were not present in

Table 2.1. Half-lives of RSNOs and DEA/NO in anaerobic solutions in the dark

NO Donor	Concentration (μM)	$t_{1/2}$ (min) NaPi [a]	$t_{1/2}$ (min) NaPi + DTPA + neo [b]	$t_{1/2}$ (min) NaPi + metHb [c]
CysSNO	50	10.3	416	205
	100	9.7	420	210
	500	9.5	412	201
	1000	9.2	409	204
GSNO	50	17	588	279
	100	20	600	285
	500	21	583	281
	1000	18.5	591	273
SNAP	50	57	701	392
	100	60	720	400
	500	58	710	395
	1000	61	703	387
DEA/NO	50	8.8	8.9	8.2
	100	7.9	9.0	8.5
	500	9.8	10.2	8.9
	1000	8.6	9.5	9.1

[a] 200 mM sodium phosphate buffer (pH 7.2) under 1 atm N_2 at 25°C in the dark

[b] 200 mM sodium phosphate buffer (pH 7.2) + 200 μM DTPA + 100 μM neocuproine under 1 atm N_2 at 25°C in the dark

[c] 200 mM sodium phosphate buffer (pH 7.2) + 500 μM human metHb under 1 atm N_2 at 25°C in the dark

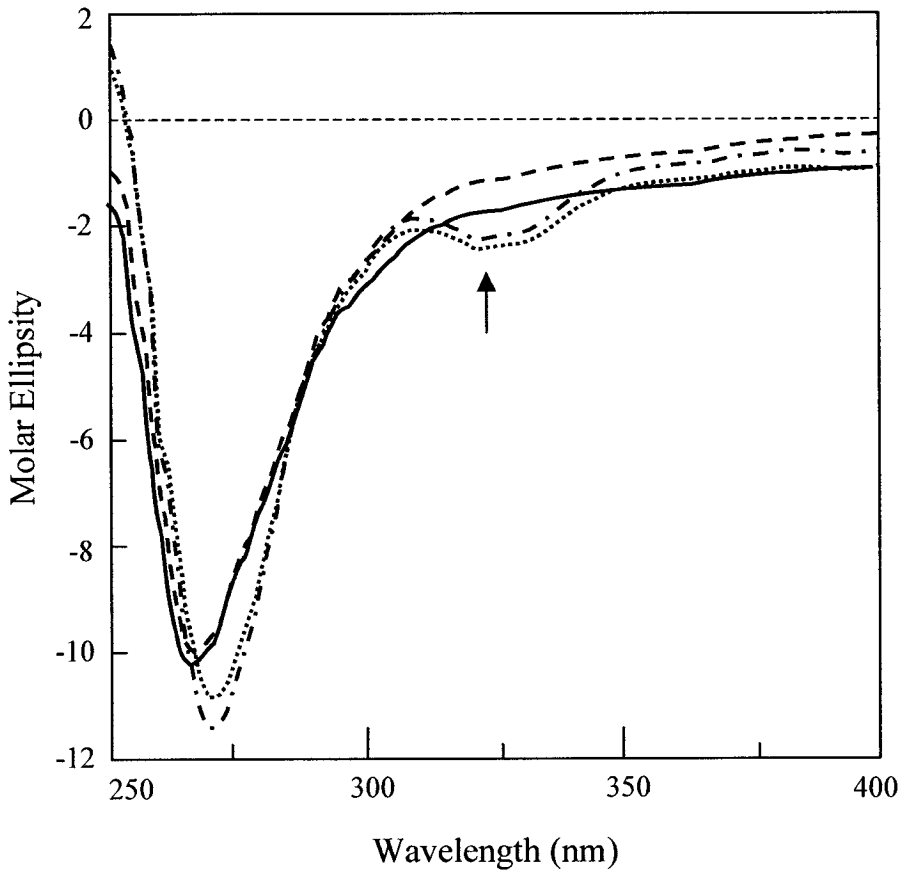

Figure 2.5. Near UV-CD spectra of 20-min incubates of cysteine and CysSNO. 15 mM CysSNO + 200 μM DTPA + 100 μM neocuproine (—); 15 mM CysSNO (···); 15 mM cysteine (– – –); 15 mM CysSNO + 200 μM DTPA + 100 μM neocuproine + 300 μM $CuSO_4$ (–·–·–). Spectra were obtained under nitrogen in 10 mM NaPi (pH 7.2) at 25°C in a 1-cm quartz cuvette with a step resolution of 0.2 nm, a speed of 50 nm/min, an accumulations of 5 scans, a response of 0.5 s, a bandwidth of 1.0 nm and a sensitivity of 100 mdeg. Exposure to room light was minimized. Buffer absorption was subtracted from all spectra.

this incubate, NO was released from CysSNO by Reaction 2.2, and the decrease in TNB absorbance (Figure 2.6) was presumably due to the metal-catalyzed TNB S-nitrosation (Reactions 2.4, 2.2 and 2.5) (20):

$$TNB\text{-}S^- + Cu^{II} \rightleftharpoons TNB\text{-}S^\bullet + Cu^{I} \qquad (2.4)$$

$$CysSNO + Cu^{I} \rightleftharpoons CysS^- + Cu^{II} + NO \qquad (2.2)$$

$$NO^\bullet + TNB\text{-}S^\bullet \rightleftharpoons TNB\text{-}SNO \qquad (2.5)$$

When the Cys/CysSNO incubate was first placed in the spectrophotometer (0 min) negligible S-nitrosation of TNB had occurred. In fact, the decrease in TNB concentration in the Cys/CysSNO incubate (Figure 2.6 and Table 2.2), occurs on a similar time scale to that of CysSNO decomposition (Table 2.1).

2.6 Discussion

There are extensive literature data on NO-donor stability in different buffer systems under various conditions (7,8,115-119). The goal of this work was to characterize the stability of the NO donors in the buffer (200 mM NaPi, pH 7.2) and temperature (25°C) used in the experiments presented in this thesis both in the presence and absence of 200 μM DTPA and 100 μM neocuproine. The half-lives obtained from the UV-Vis experiments (Table 2.1) corroborate the values reported for NO donors in similar buffer systems (7,8,119,120). As expected from the literature, the stabilities in NaPi vary as SNAP > GSNO > CysSNO ≥ DEA/NO (Table 2.1). The RSNOs are ~10- to 40-fold more stable in the presence of DTPA and neocuproine, while DEA/NO's

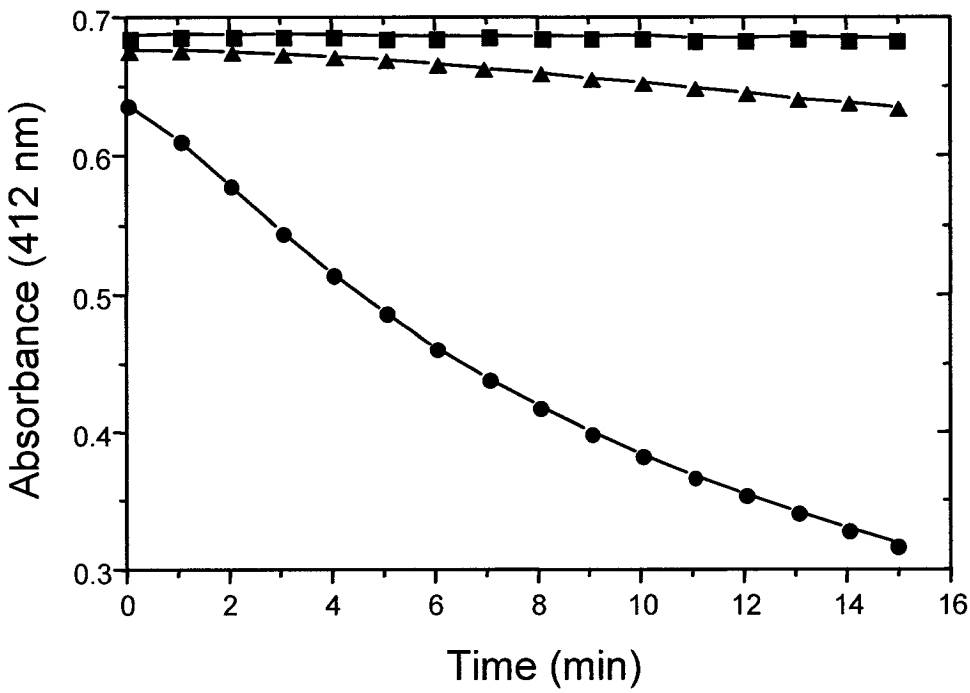

Figure 2.6. DTNB determination of free thiol concentration *vs* time. Squares (■): 50 μM Cys; triangles (▲): 50 μM Cys + 50 μM CysSNO + 100 μM neocuproine + 200 μM DTPA; and circles (●): 50 μM Cys + 50 μM CysSNO. Measurements were performed under N_2 in 200 mM NaPi (pH 7.2). The absorbance at 412 nm was measured in a 1-cm quartz cuvette at 25°C using a Beckman DU 650 UV-Vis spectrophotometer.

Table 2.2. Reactivity of DTNB with 50 μM Cys and 50 μM CysSNO

Incubate[a]	Time (min)[b]	Absorbance at 412 nm	Free thiol (μM)[c]
Cys	0	0.689	48.7
Cys	15	0.688	48.6
CysSNO	0	0.000	0
CysSNO	15	0.000	0
CysSNO/DTPA/neo	0	0.000	0
CysSNO/DTPA/neo	15	0.000	0
Cys/CysSNO	0	0.642	45.4
Cys/CysSNO	15	0.324	22.9
Cys/CysSNO/DTPA/neo	0	0.678	47.9
Cys/CysSNO/DTPA/neo	15	0.644	45.5

[a] Solutions containing 50 μM free cysteine, 50 μM CysSNO, 200 μM DTPA and 100 μM neocuproine were prepared in 200 mM sodium phosphate buffer (pH 7.2), under N_2 in the dark at 25°C, and their spectra immediately recorded in a 1-cm quartz cuvette

[b] The absorbance at 412 nm was recorded following 0 or 15 min incubation

[c] Concentrations were calculated using $\varepsilon_{412\ nm}$ = 14,150 M^{-1} cm^{-1} for the TNB anion (Reaction 2.1)

stability is not affected by the presence of the metal chelators. It is known that metal ions, particularly copper ions, catalyze the breakdown and formation of RSNOs (7,10). Incubation of RSNOs with 500 μM metHb significantly decreased their decomposition rates (Table 2.1). This can be explained by the fact that Hb possesses two copper binding sites (114), which may act as copper chelators preventing the catalytic action of the metal.

The near UV-CD spectra of CysSNO incubates were used to monitor CysS-SCys formation (Reaction 2.3). Disulfide formation occurred in the CysSNO incubates containing free copper ions (CysSNO or CysSNO/DTPA/neo/$CuSO_4$, Figure 2.5) confirming the requirement of such ions for prompt CysSNO breakdown (7). Addition of DTNB to the incubates (Table 2.2) also showed that copper is required for NO release from CysSNO. Release of free NO in the Cys/CysSNO incubate resulted in bleaching of the yellow colour due to TNB absorbance at 412 nm. Direct reaction between NO and TNB does not occur under anaerobic conditions (20). Therefore, loss of TNB absorption in the Cys/CysSNO incubate (Figure 2.6, circles) can be explained by the metal-catalyzed S-nitrosation of TNB (Reactions 2.4, 2.3 and 2.5). In contrast, negligible loss of absorption is seen in the Cys/CysSNO/DTPA/neo incubate over 15 min suggesting that the chelators inhibit CysSNO breakdown and TNB-SNO formation.

However, the TNB-SNO formed appears to be unstable since addition of NO to aerobic solutions of preformed TNB gives rise to DTNB absorption (20). Therefore, determination of SH groups by Ellman's reagent in the presence of NO donors is complicated since TNB can be reoxidized back to DTNB in the presence of NO and O_2 or metal ions with loss of absorbance at 412 nm (20). Nonetheless, in anaerobic solutions in

the presence of chelators, DTNB can indicate the free-thiol concentration (Table 2.2), as well as signaling the release of NO in the absence of chelators.

2.7 Conclusions

The experiments presented here are consistent with prompt metal-catalyzed NO release from RSNOs (Reactions 2.2 and 2.3). The stability of RSNOs in anaerobic solutions in the dark is clearly a function of the presence or absence of trace metal ions (e.g., Cu^{I}, Chapter 4). Sufficient metal-ion impurities are present in the buffer used (see Table 4.1, Chapter 4) here to shorten the half-lives of the RSNOs to ~10 min (CysSNO) to ~60 min (SNAP) in the dark in the absence of oxygen.

The observation of first-order RSNO decay (Figure 2.4) for a scheme involving Reactions 2.2 and 2.3 suggests that the rate-determining step may be Reaction 2.2. The mechanism could involve a rapid pre-equilibrium (Reaction 2.2a) followed by slow cleavage of the complex (Reaction 2.2b):

$$\text{CysSNO} + \text{Cu}^{\text{I}} \overset{\text{Rapid}}{\rightleftharpoons} [\text{CuCysSNO}]^{+} \qquad (2.2a)$$

$$[\text{CuCysSNO}]^{+} \overset{\text{Slow}}{\rightarrow} \text{Cu}^{\text{II}} + \text{CysS}^{-} + \text{NO} \qquad (2.2b)$$

The nature of the $[CuCysSNO]^{+}$ complex formed in 2.2a has been examined *in silico* (106). The calculated bond lengths suggest that the formation of $[CuRSNO]^{+}$ intermediates results in weakening of the S-N bond and strengthening of the N-O bond, which would promote S-N bond breaking and NO release from RSNO (106).

3.0 Metal Chelators Inhibit S-Nitrosation of Cysβ93 in Oxyhemoglobin

3.1 Abstract

There is evidence that binding of the vasorelaxant, nitric oxide (NO), to Cysβ93 of hemoglobin (Hb) plays a role in blood pressure regulation. NO reportedly equilibrated between Hb and low-molecular-weight nitrosothiols such as nitrosoglutathione (GSNO) via *trans*-S-nitrosation (NO^+ transfer between thiols). S-Nitrosation of Cysβ93 was directly probed by FTIR by monitoring the ν(SH) vibrations of Hb and by ESI-MS. The results indicate that Cysβ93 is S-nitrosated when oxyHb (but not deoxyHb) is exposed to GSNO (1:1 heme/GSNO). No FTIR or ESI-MS evidence was obtained for oxyHb S-nitrosation in the presence of DTPA, a Cu^{II} chelator. Monitoring the heme Soret and visible bands revealed that oxyHb was converted to metHb in the presence of GSNO and that this was inhibited on addition of neocuproine, a Cu^{I} chelator. The combined data are consistent with a mechanism involving Cu^{II}-catalysis of Cysβ93 S-nitrosation by *free* NO generated by Cu^{I}-catalysis of GSNO breakdown. The results are inconsistent with simple *trans*-S-nitrosation which is *not* metal catalyzed.

3.2 Results and Discussion

The role in blood flow of S-nitrosohemoglobin (Hb-SNO), where Hb is S-nitrosated at Cysβ93, is currently the subject of intense debate (57,58,63,64,66,121). Hb-SNO presumably controls delivery of the vasorelaxant nitric oxide (NO) to hypoxic

tissues in an oxygen-sensitive manner (63,64). In support of a role for Hb in NO transport, a significant fraction of NO in the blood is in the form of Hb-SNO, with concentrations ~10 times higher in arterial (~300 nM) *vs* venous (~30 nM) blood (58), although more recent studies did not detect arterial-venous Hb-SNO gradients (121). Hb-SNO formation may also provide red blood cells (RBCs) with a mechanism to counteract platelet activation (52). Despite its potential physiological importance, the mechanism of Hb-SNO formation *in vivo* remains unknown, but a *trans*-S-nitrosation equilibrium with low-molecular-weight nitrosothiols, such as nitrosoglutathione (GSNO), is a central postulate (57,58,63,64,66,121):

$$\text{GSNO} + \text{Hb-SH} \rightleftharpoons \text{GSH} + \text{Hb-SNO} \qquad (3.1)$$

We have *directly* probed spectrometrically the protein products formed on mixing Hb and GSNO. Cysβ93 S-nitrosation was detected only in oxyHb and, unlike *trans*-S-nitrosation (7), *requires* the presence of metal ions.

Fourier transform infrared spectroscopy (FTIR) is a valuable probe of protein thiols (90,122,123). The SH stretching vibration ν(SH) falls in a spectral window (~2500 cm^{-1}) with minimum H_2O and protein absorption (90,122,123). The FTIR spectra of human oxy and deoxyHb were recorded alone and in the presence of GSNO, the nitroso form of the dominant thiol in RBCs (120). Although ~6 mM Hb is necessary to observe the weak IR ν(SH) absorption (90,122,123), comparable Hb concentrations are found in RBCs (~5 mM). The FTIR spectrum of oxyHb in Figure 3.1a exhibits the three ν(SH) peaks at 2586, 2566 and 2556 cm^{-1} assigned previously to Cysβ93, Cysβ112 and

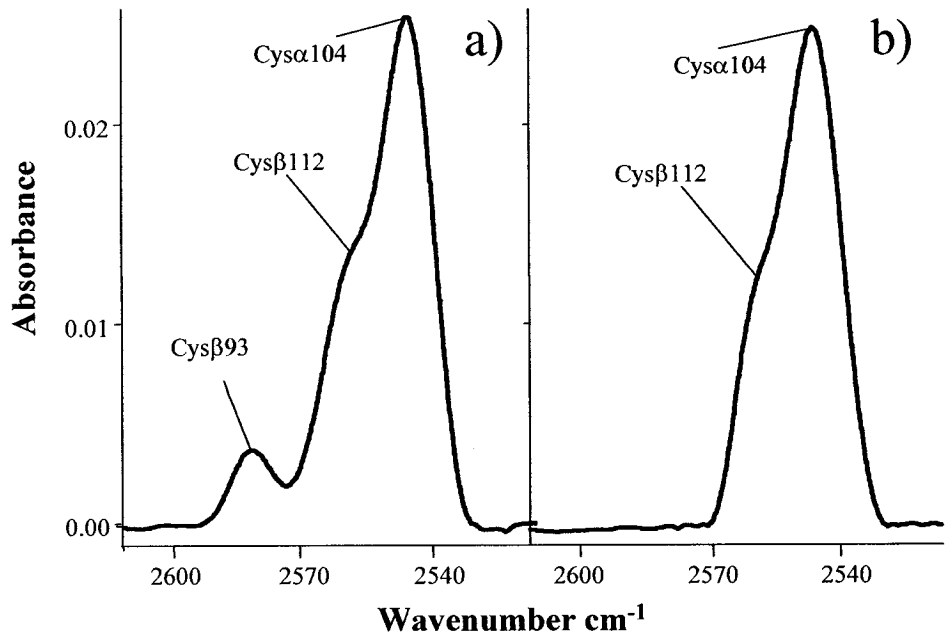

Figure 3.1. FTIR spectra in the ν(SH) region of (a) 30 mM (heme) oxyHb, and (b) 28 mM (heme) oxyHb with 28 mM GSNO. Experimental procedures: oxyHb was prepared from human metHb (Sigma) as described previously (124). The Hb samples (20 μL) in 200 mM sodium phosphate buffer (pH 7.2) were added by syringe onto a 13-mm CaF_2 window with 250-μm Teflon spacer. The cell was immediately assembled and the spectra were recorded at 25°C on a Nicolet Magna-IR 550 spectrometer with a MCT detector cooled to 77 K and purged with dry air from a Whatman FTIR Purge (Model 75-52). Each spectrum is the average of 500 scans recorded in 6 min [starting at t = 2 min following mixing of oxyHb and GSNO (Cayman) for sample b] at 2-cm^{-1} resolution with an aperture of 32. Omnic (Nicolet) software was used for subtraction, baseline correction, smoothing, and Fourier self deconvolution (HWHH 8.2 cm^{-1}, K factor 1) of the spectra.

Cysα104, respectively (90,123). The oxyHb/GSNO spectrum does not exhibit a 2586-cm^{-1} peak (Figure 3.1b), consistent with S-nitrosation of the Cysβ93 residues, which are the two reactive thiols in Hb (63). This was confirmed by mass spectrometry; the deconvolved mass spectra of the heme-free subunits from oxyHb reveal a new peak corresponding to β-globin plus NO (+ 29 Da for CysH → CysSNO) on GSNO exposure whereas the mass of α-globin remains unaltered (Figure 3.2a). DeoxyHb also exhibits three ν(SH) peaks but Cysβ93 ν(SH) absorption is observed in the oxyHb/GSNO spectrum and no β-globin nitrosation was detected in the mass spectra of either deoxyHb sample (data not shown). Thus, our FTIR and mass spectral data support the findings, obtained by indirect measurements by Stamler and coworkers, that Cysβ93 readily undergoes S-nitrosation in oxyHb (R-state) but not in deoxyHb (T-state) (58). This presumably allows Hb to act as an allosterically controlled NO buffer (58,63,64).

The UV-Vis spectra provide further insight into the mechanism of Hb-SNO formation. Evidence for partial heme-iron nitrosylation is seen in the Soret and visible bands of the deoxyHb/GSNO sample and in its blue-shifted (2584 cm^{-1}) Cysβ93 ν(SH) (data not shown), which falls between that of nitrosylHb (2585 cm^{-1}) and deoxyHb (2578 cm^{-1}) (90,123). GSNO reduction by deoxyHb, which would release the free NO required for heme nitrosylation, has been reported (125):

$$\text{deoxyHb} + \text{GSNO} \rightleftharpoons \text{metHb} + \text{GS}^- + \text{NO} \qquad (3.2)$$

NitrosylHb formation under the present conditions (heme:GSNO = 1:1) would require GSH oxidation by nitrosylmetHb ($HbFe^{III}NO$), and GSSG was detected by mass

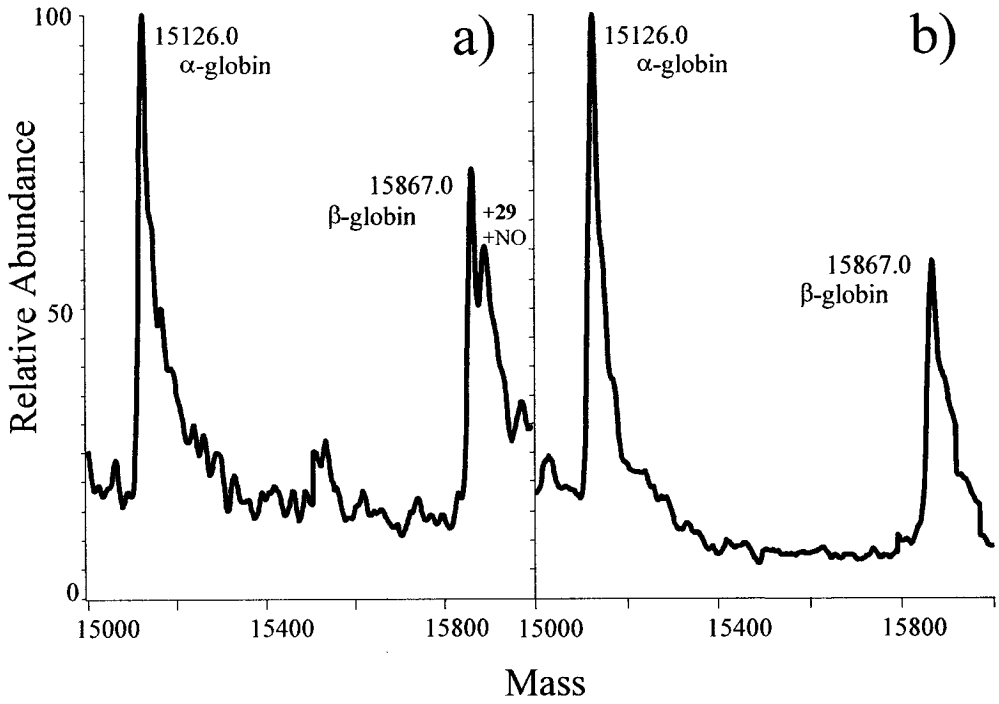

Figure 3.2. Deconvolved electrospray mass spectra of the heme-free Hb subunits from the reactions of (a) oxyHb with GSNO, and (b) oxyHb with GSNO and DTPA. Experimental procedures: Samples prepared as in Figure 3.1 (500 μM DTPA was added to b) were diluted 10^3-fold with H_2O to give ~0.5 μg/μL Hb. Aliquots (100 μL) were infused into the electrospray source of the mass spectrometer (Finnigan SSQ7000) by flow injection from the HPLC (HP1090) at 50 μL/min using 75% CH_3CN (0.05% TFA) isocratic elution. Under these conditions, Hb dissociates into free heme, and α- and β-subunits. The unresolved shoulders on the subunit peaks at high mass are due to sodium adducts.

spectrometry (data not shown). A blue-shift in the Soret of the oxyHb/GSNO sample (Figure 3.3a) is evidence of metHb formation, which has a Soret maximum at 405 nm (124). Reaction 3.3 has not been reported but, since GSNO is known to oxidize free O_2^- (126), it may also oxidize the $Fe^{III}O_2^-$ center of oxyHb:

$$\text{oxyHb} + \text{GSNO} \rightleftharpoons \text{metHb} + \text{GS}^- + \text{O}_2 + \text{NO} \qquad (3.3)$$

Additional metHb would be produced by Reaction 3.4, which is well documented (16,127):

$$\text{oxyHb} + \text{NO} \rightleftharpoons \text{metHb} + \text{NO}_3^- \qquad (3.4)$$

NO release from GSNO could also be catalyzed by ubiquitous copper impurities (7,10,125,128):

$$\text{RSNO} + \text{Cu}^{\text{I}} \rightleftharpoons \text{RS}^- + \text{NO} + \text{Cu}^{\text{II}} \qquad (3.5)$$

Surprisingly, in the presence of 200 μM DTPA no significant loss of Cysβ93 ν(SH) intensity was observed in the oxyHb/GSNO FTIR spectrum, which resembled that in Figure 3.1a. Mass spectral analysis confirmed that β-globin S-nitrosation was inhibited by DTPA (Figure 3.2b). Consistent with these results, amperometric measurements of NO consumption indicated that Cu^{II} induces rapid Hb-SNO formation in the presence of *free* NO (21). Thus, we propose that in the *absence* of chelators, GSNO decomposes to

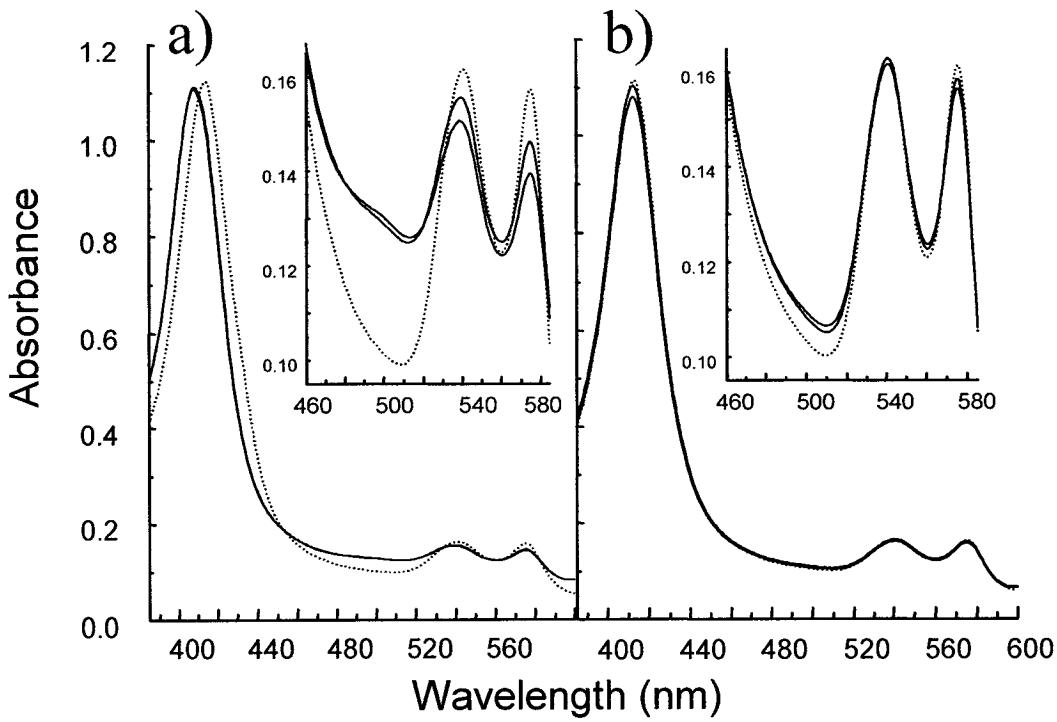

Figure 3.3. UV-Vis absorption spectra of 15 mM (heme) oxyHb, and 15 mM (heme) oxyHb with 15 mM GSNO. (a) No metal chelators present; **(b)** 200 μM DTPA (diethylene-triamine-N,N,N',N",N''-pentaacetic acid; ICN) and 120 μM neocuproine (2,9-dimethyl-1,10-phenanthroline; Sigma) present. Experimental procedures: Samples (10 μL) in 200 mM sodium phosphate buffer (pH 7.2) were added to the FTIR cell (6-μm teflon spacer) as described in Figure 3.1, and the cell was placed in a custom-made bracket in the spectrophotometer (Beckman DU 650). Spectra were recorded (1200 nm/min) at 25°C for oxyHb (---), and for oxyHb with GSNO (—) at t = 2 min and 15 min.

give free NO (Reaction 3.5) which rapidly S-nitrosates Cysβ93 of oxyHb by Reaction –3.5. Cysβ93 is S-nitrosated rather than GSH since Cu^{II}-catalyzed RSNO formation is not kinetically competitive with RSSR formation ($RS^- + Cu^{II} \rightleftharpoons ½\ RSSR + Cu^{I}$) for low-molecular-weight thiols (7,10,21,128). If all the Cu^{II} present is chelated by DTPA, NO generated by Reaction 3.5 is consumed by Reaction 3.4, thus converting oxyHb to metHb with no Hb-SNO formation. A copper-catalysed mechanism for Hb-SNO formation *in vivo* is plausible since RBCs contain ~20 μM copper (129). Intriguingly, two copper-binding sites (114) have been identified in Hb *in vitro*, but their Cu-loading in RBCs has not been reported. We detected ~50 μM Cu in 5 mM human Hb (Sigma) by atomic absorption analysis (data not shown). Thus, the products observed here reflect competition between Hb (114), GSH and GSSG (128) for copper in the absence of added chelators. To distinguish between NO generation by Reactions 3.3 and 3.5, the experiments were repeated in the presence of chelators. The Cu^{II}-chelator, DTPA, did not inhibit formation of metHb, but in the presence of the Cu^{I}-chelator, neocuproine, the growth of metHb absorption in the oxyHb/GSNO sample was negligible (Figure 3.3b), indicating that NO is generated mainly *via* Reaction 3.5.

3.3 Conclusions

In summary, the data presented are *inconsistent* with Hb-SNO formation *via* simple *trans*-S-nitrosation (NO^+ transfer; Reaction 3.1) and with the putative *trans*-S-nitrosation equilibrium and rate constants derived from experimental data where Hb-SNO formation was only inferred, not observed (66,130,131). Our results strongly point to a mechanism involving Cu^{II}-catalysis of Cysβ93 S-nitrosation (Reaction –3.5) by *free* NO

generated by Cu^{I}-catalysis of RSNO breakdown (Reaction 3.5). The crux of this hypothesis is the identification of the Cu catalysts *in vivo*.

Appendix 1.0 Supplementary Experimental Data to Chapter 3.0

A1.1 Introduction

Supplementary experimental data to Chapter 3.0 are presented here. Since CysSNO is a RSNO with similar characteristic to GSNO (Chapter 2), the products of deoxyHb and oxyHb incubations with CysSNO were investigated and compared to those from incubations with GSNO. The ν(SH) bands of Cysβ93 in the Hb/CysSNO incubates were examined by FTIR, and visible spectroscopy was used to characterize the different redox and ligation states of Hb. The absorption spectra reveal that, as observed in the Hb/GSNO incubates, Cysβ93 S-nitrosation occurs when the heme group has a bound O_2:

$$\text{CysSNO} + \text{oxyHb-SH} \rightleftharpoons \text{CysSH} + \text{oxyHb-SNO} \qquad \text{(A1.1)}$$

Additional data reported in this appendix include: (i) the results of an examination of Hb ν(SH) bands by Raman spectroscopy and (ii) LC/MS analysis of oxyHb/GSNO incubates to confirm the site of NO-adduct formation on the β-globin. Further experimental details are also provided.

A1.2 Preparation and Characterization of Hb Samples

Agilent 8451a diode-array and Beckman DU650 UV-Vis spectrophotometers were used to obtain Hb spectra in quartz cuvettes (1-cm pathlength) and the FTIR cell (6-μm pathlength). A solution of human metHb from the bottle (Sigma) was prepared at a concentration of ~32 mM (heme) in 200 mM NaPi (pH 7.2) as described in Section

5.3.2.1. Soret absorption readily differentiates between metHb, deoxyHb and oxyHb since the reported maxima are 405, 430 and 415, respectively (Figure A1.1) (125). The visible bands between 500 and 600 nm are diagnostic of the spin state of iron. Low-spin hemes (oxyHb) exhibit two characteristic bands with maxima at ~540 and ~575 nm while high-spin hemes (deoxyHb) have a single maximum at ~556 nm (Figure A1.1, inset) (132,133).

The Soret spectrum of a 5-min incubate of 16 mM (heme) deoxyHb with 24 mM CysSNO shows a maximum at 418 nm which corresponds to the value reported for nitrosylHb ($HbFe^{II}NO$) (Figure A1.1). The visible spectrum of this incubate (Figure A1.1, inset) is charactersistic of low-spin heme and confirms the formation of nitrosylHb. The Soret spectrum of a 5-min incubate of 16 mM (heme) oxyHb with 24 mM CysSNO shows a maximum at 409 nm (Figure A1.1), which is due to metHb formation. The visible spectrum of this incubate (Figure A1.1, inset) also shows the spectral changes due to metHb formation. The excess NO (over Cysβ93) produced in this incubate reacted with the $Fe^{II}O_2$ heme to give Fe^{III} heme and NO_3^- (Reaction 3.4). Presumably, Cysβ93 was first S-nitrosated by the released NO, as observed for oxyHb in the presence of GSNO (Figures 4.3 and 4.6), followed by reaction of the excess NO with the $Fe^{II}O_2$ heme.

A1.3 FTIR Experiments

FTIR spectra were recorded between 4000-400 cm^{-1} on a Nicolet–Magna-IR 550 series II spectrometer as described in Section 5.3.2.4. The ν(SH) falls in a spectral window (~2500 cm^{-1}) with minimum H_2O and protein absorption as shown in Figure

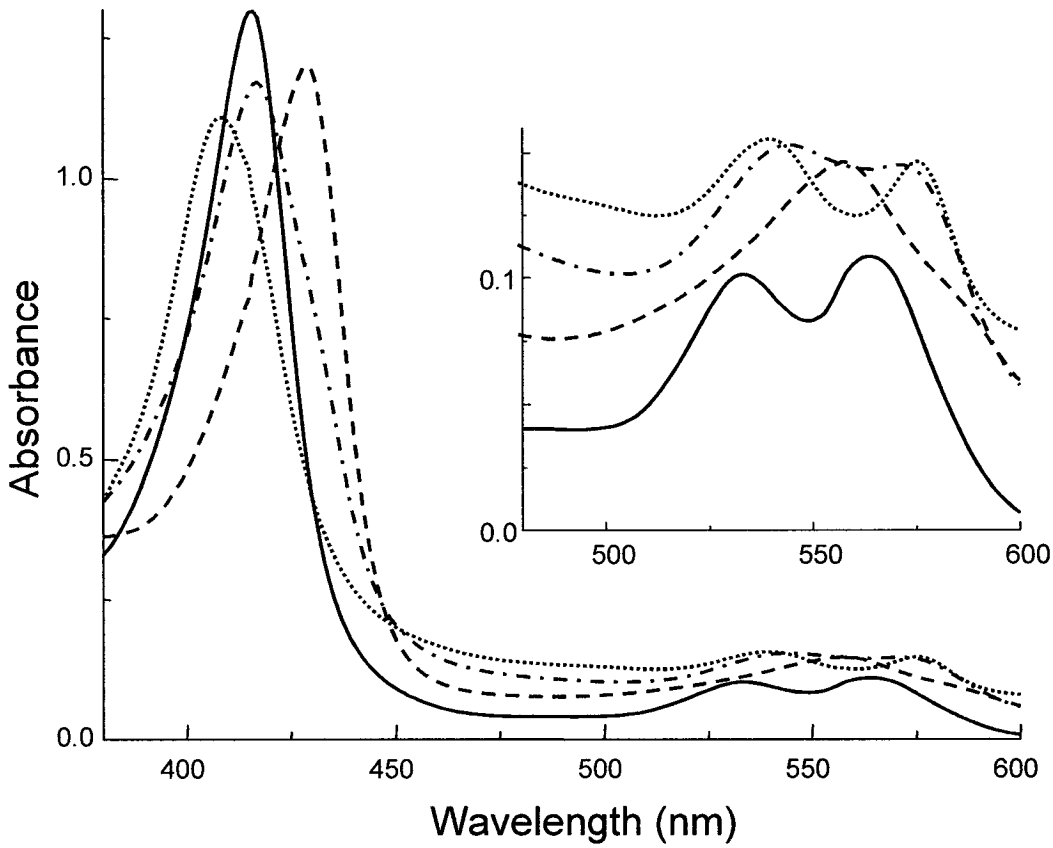

Figure A1.1. Soret and visible spectra of 4 mM (16 mM heme) deoxyHb, oxyHb, deoxyHb/CysSNO and oxyHb/CysSNO in 200 mM NaPi (pH 7.2). Soret and visible spectra of deoxyHb [(- - -) ε_{430} = 133 and ε_{555} = 12.5 $mM^{-1}cm^{-1}$)], oxyHb [(—) ε_{415} = 131, ε_{541} = 13.5 and ε_{576} 14.6 mM^{-1} cm^{-1})], deoxyHb + 24 mM CysSNO (-·-), oxyHb + 24 mM CysSNO (· · ·). All spectra were recorded using a 6-μm spacer in the FTIR cell as described in Section 5.3.2.1.

A1.2. Variations in the ν(SH) band parameters reflect the differences in local environment and hydrogen bonding experienced by the SH groups in the three cysteines of Hb. The frequency of the ν(SH) vibration is expected to increase with increasing SH bond strength, and band intensity will increase as the strength of the dipole associated with the SH bond increases (90). The differences, in terms of frequency and intensity, between the oxyHb and deoxyHb FTIR ν(SH) spectra are due to the quaternary structural changes between R- (oxyHb) and T-state (deoxyHb) of Hb (Section 1.3). The FTIR spectra of 24 mM (heme) oxyHb and deoxyHb are shown in Figures A1.3c and d and the spectra of 24 mM (heme) oxyHb and deoxyHb following 5-min incubation with 36 mM CysSNO are shown in Figure A1.3f. A CysSNO to heme ratio of 1.5 corresponds to a CysSNO to Cysβ93 ratio of 3.0. Excess CysSNO was present because of its instability (Section 1.2.2.1). It can be seen that the ν(SH) assigned to Cysβ93 at 2588 cm^{-1} disappears in the spectrum of oxyHb/CysSNO incubate, while in the spectrum of the deoxyHb/CysSNO incubate, the ν(SH) peak assigned to Cysβ93 has blue-shifted to 2580 cm^{-1} (Figure A1.3f).

The loss of Cysβ93 absorption when oxyHb is treated with CysSNO or GSNO supports the proposal of Stamler and coworkers that *trans*-S-nitrosation from low-molecular-weight thiols to Cysβ93 occurs only in deoxyHb (R-state) (56). The 5-cm^{-1} blue-shift observed for ν(SH) peak of Cysβ93 in deoxyHb/CysSNO (Table A1.1) and deoxy/GSNO can be explained by the formation of nitrosylHb (Figure A1.3f and Chapter 5). In the FTIR experiments reported by Caughey *et al.* (123), a ~7-cm^{-1} blue-shift in the ν(SH) peak of Cysβ93 (2578→2585 cm^{-1}) was observed for nitrosylHb compared to that

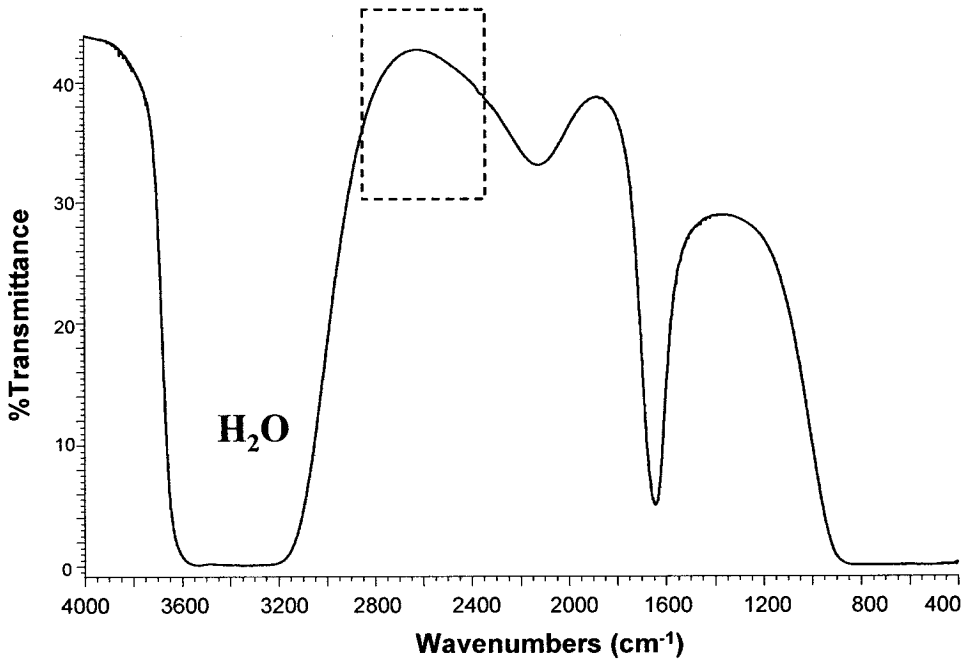

Figure A1.2. Spectral window in H_2O (---) for the SH stretching vibration ν(SH) centered at ~2500 cm^{-1}. FTIR spectrum of H_2O was recorded in a 250-μm pathlength FTIR cell at 25°C, and is the average of 500 scans at 2-cm^{-1} resolution. These were the conditions used to record the FTIR ν(SH) spectra of Hb.

Figure A1.3. FTIR spectra in the ν(SH) region of 24 mM (heme) metHb, nitrosylHb, oxyHb, deoxyHb/CysSNO and oxyHb/CysSNO in 200 mM NaPi (pH 7.2). (a) nitrosylHb; **(b)** metHb; **(c)** oxyHb; **(d)** deoxyHb; **(e)** oxyHb + 36 mM CysSNO; **(f)** deoxyHb + 36 mM CysSNO. Spectra were recorded in a 250-μm pathlength FTIR cell at 25°C, and are the average of 500 scans at 2-cm^{-1} resolution. Background subtraction, baseline correction, smoothing and Fourier transform self-deconvolution were performed as outlined in Section 5.3.2.4. The observed ν(SH) frequencies for Cysβ93, Cysβ112 and Cysα104 in the six Hb samples are given in Table A1.1

Table A1.1. Comparison of FTIR data from Figure A1.3 with literature data.

	ν(SH) (cm^{-1}) [a]		
Hb sample [b]	Cysβ93	Cysβ112	Cysα104
NitrosylHb	2582 (2585)	2563 (2566)	2552 (2552)
MetHb	2589 (2590)	2566 (2566)	2552 (2553)
OxyHb	2588 (2589)	2566 (2566)	2553 (2553)
DeoxyHb	2577 (2578)	2563 (2563)	2554 (2556)
OxyHb/CysSNO	not observed	2566	2553
DeoxyHb/CysSNO	2582	2562	2552

[a] Data in brackets are from Refs 90,123

[b] Hb samples and incubates were prepared as described in Section 5.3.2.4

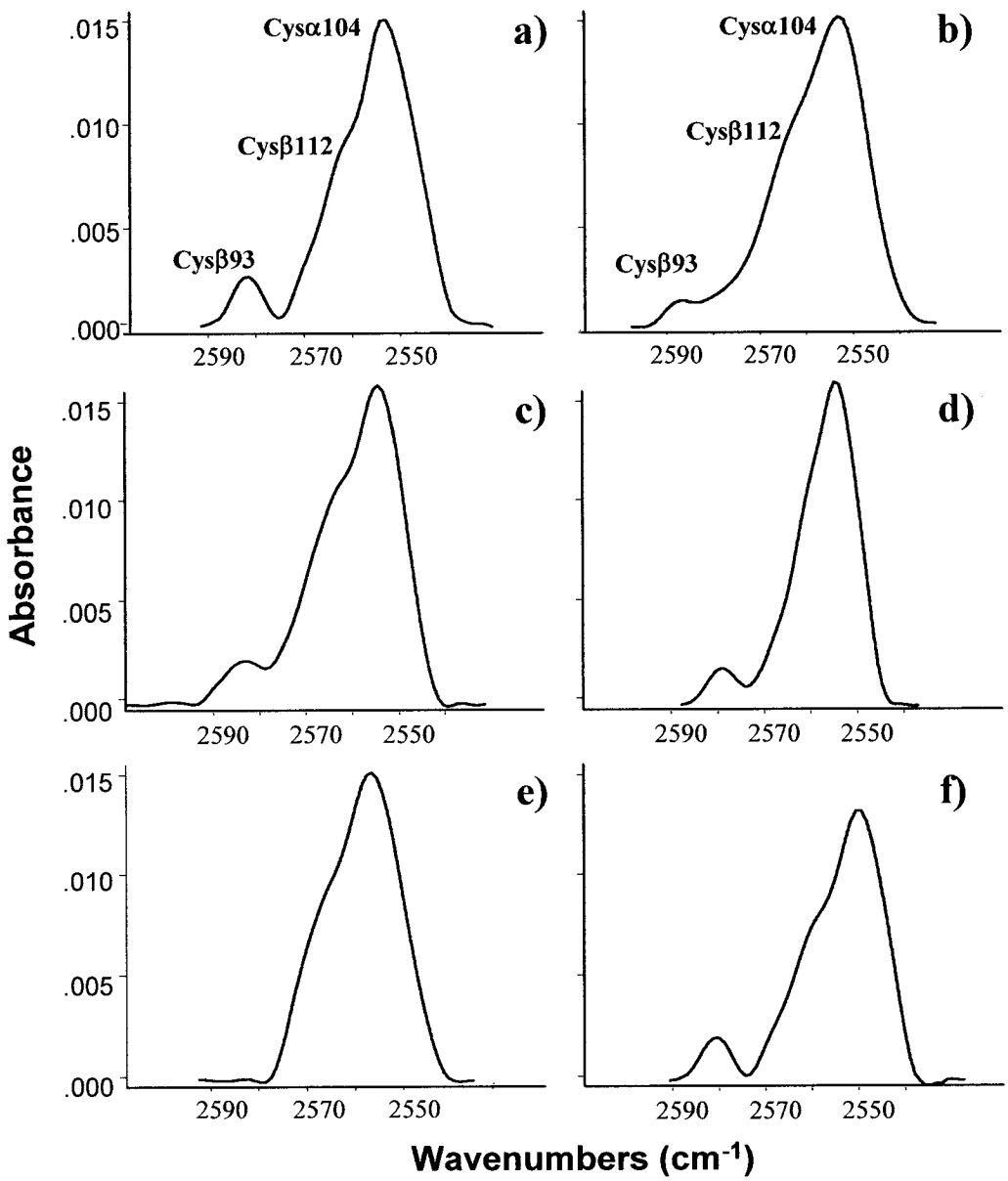
a)
b)
c)
d)
e)
f)
Cysα104
Cysβ112
Cysβ93
.015
.010
.005
.000
2590
2570
2550
Absorbance
Wavenumbers (cm-1)

Figure A1.3

of deoxyHb. Figure A1.3a shows FTIR spectrum of authentic nitrosylHb with a maximum for the Cysβ93 peak at 2582 cm^{-1}, which differs by ~3 cm^{-1} from the value reported (123). This frequency difference is attributed to errors in determing the peak maxima of the weak overlapping ν(SH) bands. Peak maxima obtained for the Cysβ93, Cysβ112 and Cysα104 ν(SH) bands shown in Figure A1.3 are similar to the ones reported (123) with differences of 1 or 2 cm^{-1} (Table A1.1).

Trapping of NO at the heme suggests decomposition of CysSNO by a metal-catalyzed reaction (Chapter 2). Therefore, the experiments were repeated in the presence of a metal chelator. Surprisingly, no loss of Cysβ93 ν(SH) intensity was observed when either deoxyHb or oxyHb was treated with CysSNO in the presence of 500 μM DTPA (data not shown). The fact that *trans*-S-nitrosation from CysSNO does not occur when a chelator is added indicates that this process, like that involving GSNO (Chapter 3), is catalyzed by trace metal ions in solution. Since *trans*-S-nitrosation reactions occurring *via* direct NO^+ transfer reportedly do not require metal-ion catalysis (19,57,58), S-nitrosation of Hb by neither CysSNO nor GSNO occurs by the direct NO^+ transfer mechanism proposed for low-molecular-weight R'SH/RSNO *trans*-S-nitrosation reactions (7,66,130,131).

A1.4 Examination of Hb ν(SH) by Raman Spectroscopy

Since molecular vibrations can be Raman and/or IR active, the two spectroscopic techniques are complementary. It was hoped that lower protein concentrations could be used to detect the ν(SH) vibrations of Hb by Raman spectroscopy due to the relatively high polarizability of bonds to sulfur. To verify the results obtained by FTIR, the ν(SH)

peaks of metHb were examined by Raman spectroscopy. A 20-W argon ion laser (Coherent CR-18) was used as source, and a Jarrell-Ash 1-m Czerny-Turner monochromator with 240-μm slits and RCA-C 31034-02 photomultiplier were used as the detector system. The laser excitation wavelength was 488 nm with 200 mW power (at the source), which was reduced to ~20 mW (at the sample) using a neutral density filter and samples were held in a 3-mm glass tube at room temperature. Stanford SR 465 software was used for data acquisition. Unfortunately, Raman spectroscopy with visible excitation suffers from strong interference from the heme in Hb. Therefore, the signal-to-noise ratio observed was very low. Nonetheless, ν(SH) bands at 2585 (Cysβ93), 2573 (Cysβ112) and 2562 cm^{-1} (Cysα104) were observed (Figure A1.4) for 1 mM metHb in 200 mM NaPi (pH 7.2). The 11-cm^{-1} blue-shift observed in the Raman band for Cysα104 compared to the FTIR band (Table A1.1) is likely due to the lack of calibration since the Raman shift was obtained simply by subtracting the excitation frequency from the monochromator readout. The intensities of the other ν(SH) Raman bands are too low to obtain accurate frequencies. In summary, absorption of the laser beam by the heme prevents analysis of the ν(SH) bands of Hb by laser Raman using visible excitation.

A1.5 Tryptic Digestion and Peptide Mass Mapping of Hb-SNO by LC/ESI/MS

To locate the NO adduct on the S-nitrosated oxyHb obtained from the 5-min incubate of 28 mM (heme) oxyHb with 28 mM GSNO (Figure 3.2a), peptide mass mapping was carried out. The α-globin and β-globin subunit derived from oxyHb-SNO were subjected to tryptic digestion and the peptides analyzed by LC/MS. A 20-μL aliquot (~190 μg) of oxyHb-SNO was loaded on a Vydac reversed-phase C_{18} column

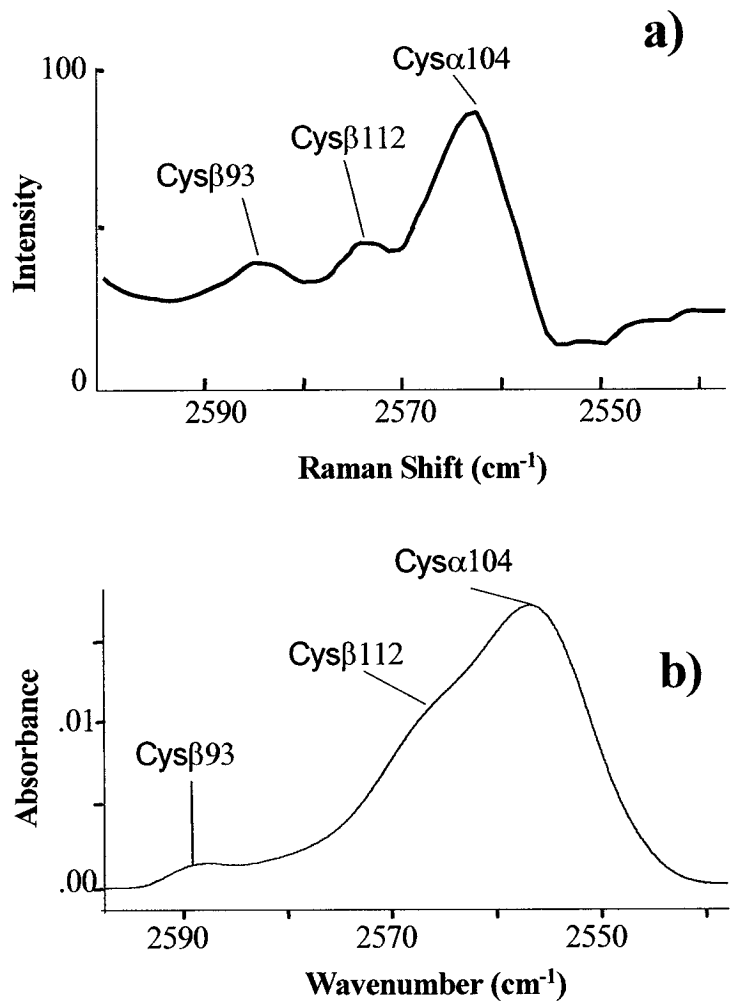

Figure A1.4. Raman and FTIR spectra of metHb in 200 mM NaPi (pH 7.2). (a) Raman spectrum of 4 mM (heme) metHb. Laser excitation was at 488 nm with 20 mW power at the sample. The spectrum was recorded with 240-μm slits in a stationary 3-mm glass tube at room temperature. The ν(SH) Raman peaks (cm^{-1}) are assigned as follow: 2585 (Cysβ93), 2573 (Cysβ112) and 2562 (Cysα104). **(b)** FTIR spectrum of 28 mM (heme) metHb. The spectrum was recorded in a 250-μm pathlength FTIR cell at 25°C, and is the average of 500 scans at 2-cm^{-1} resolution. Background subtraction, baseline correction, smoothing and Fourier transform self-deconvolution of the FTIR spectrum were performed.

(4.6x250 mm) and the protein was separated from the buffer salts and excess reactants with a 20-55% CH_3CN gradient in 0.05% TFA at 1 mL/min over 20 min on an HPLC system (Agilent Model 1090). The HPLC trace (Figure A1.5) shows that the order of elution from column is: NaPi buffer salts (2.5 min), GSH (11 min), β-globin (17 min), α-globin (18 min) and heme (19 min).

The HPLC eluate was split, 20% directed into the ESI source, and the remainder collected (~1 mL) and lyophilized. The masses of the eluting species in Figure A1.5 were confirmed by MS on the SSQ7000. The lyophilised α- and β-globin HPLC-fractions were dissolved and digested with 1:50 (w/w) trypsin/protein at 40°C for 20 h in 200 mM NaPi buffer (pH 7.2). Aliquots of the digests (20 µL) were loaded on a Vydac microbore C_{18} column (1x300 mm) and the peptides eluted with a 5-60% CH_3CN gradient in 0.05% TFA at 40 µL/min over 100 min. Online analysis by ESI-MS was performed to detect the NO-modified tryptic peptides (Figure A1.6). An NO-modified peptide eluted at 54.75 min (Figure A1.6) with a mass corresponding to residues 83-95+NO. Peptide 31-40, and unmodified peptide 83-95 were co-eluted with NO-modified 83-95 (Figure A1.6b).

Figure A1.7 shows the ESI mass spectrum of the 54.75-min peak from Figure A1.6. Peaks corresponding to MH^+ and MH_2^{2+} ions of peptide 31-41 (m/z 1274.5 and m/z 637.6), peptide 83-95 (m/z 1422.2 and m/z 711.6) and peptide 83-95+NO (m/z 1451.9 and m/z 726.4) are labeled with their amino acid sequences. The identification of NO-labelled peptide 83-95 of β-globin provides strong support for S-nitrosation of oxyHb at Cysβ93. Sequencing of the NO-modified peptide 83-95 on the single quadrupole mass spectrometer used for these experiments (SSQ7000) was not feasible due to the presence of unmodified peptide 83-95 and peptide 31-40 in the same peak (Figure A1.6).

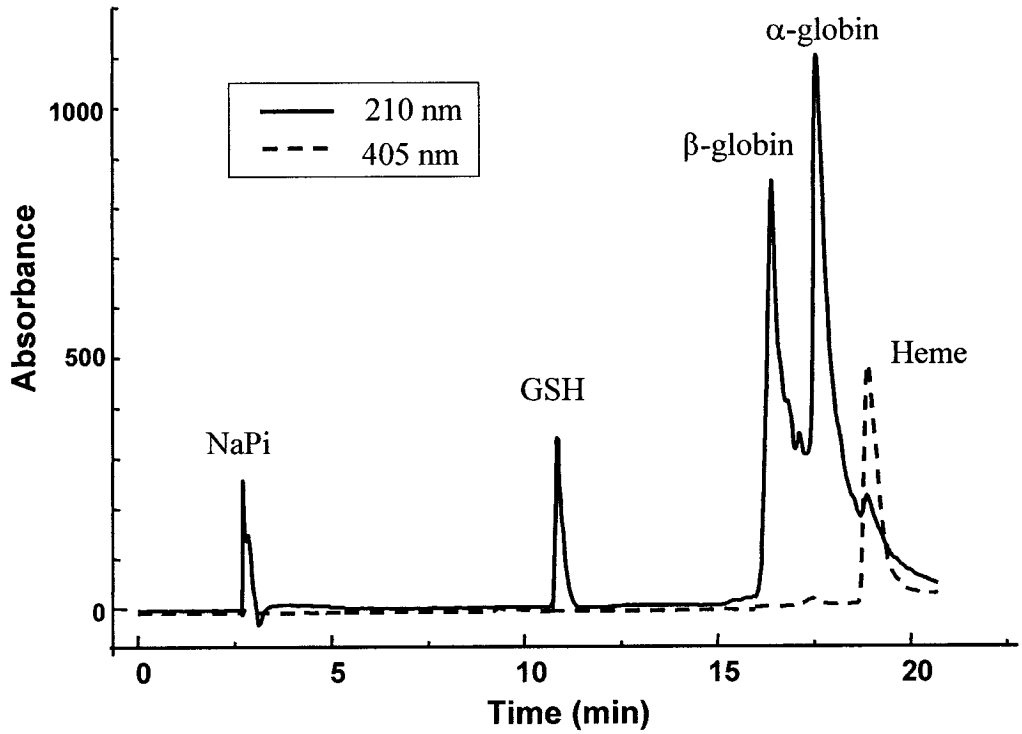

Figure A1.5. HPLC separation of α- and β-globins of Hb from heme, GSH and NaPi. The separation was performed on a Vydac reversed-phase C_{18} column (4.6x250 mm) with a 20-55% CH_3CN gradient in 0.05% TFA at 1 mL/min over 20 min. A 20-μL aliquot of Hb solution (~190 μg protein) was loaded on the column.

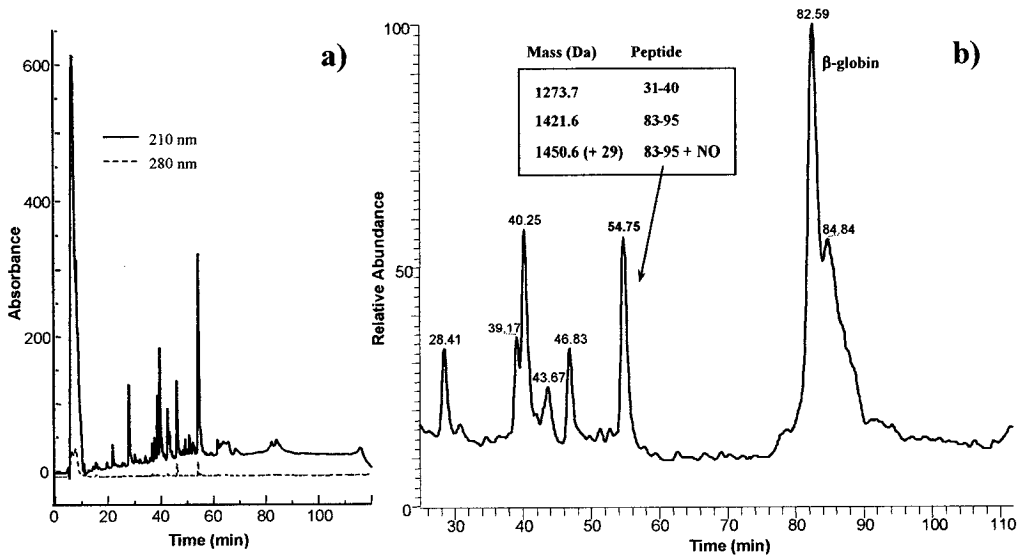

Figure A1.6. HPLC separation of the tryptic digest of β-globin from human oxyHb-SNO. The tryptic peptides (~100 μg) were separated on a Vydac microbore reversed-phase C_{18} column (1x300 mm) with a 5-60% CH_3CN gradient in 0.05% TFA at 40 μL/min over 100 min. (**a**) Peptide absorbance *vs* time using the HPLC diode-ray UV detector; (**b**) TIC *vs* time using the ESI-MS detector. The 54.75-min peak contains unmodified peptides 31-40 (1273.7 Da) and 83-95 (1421.6 Da), and modified peptide 83-95 + NO (1450.6 Da).

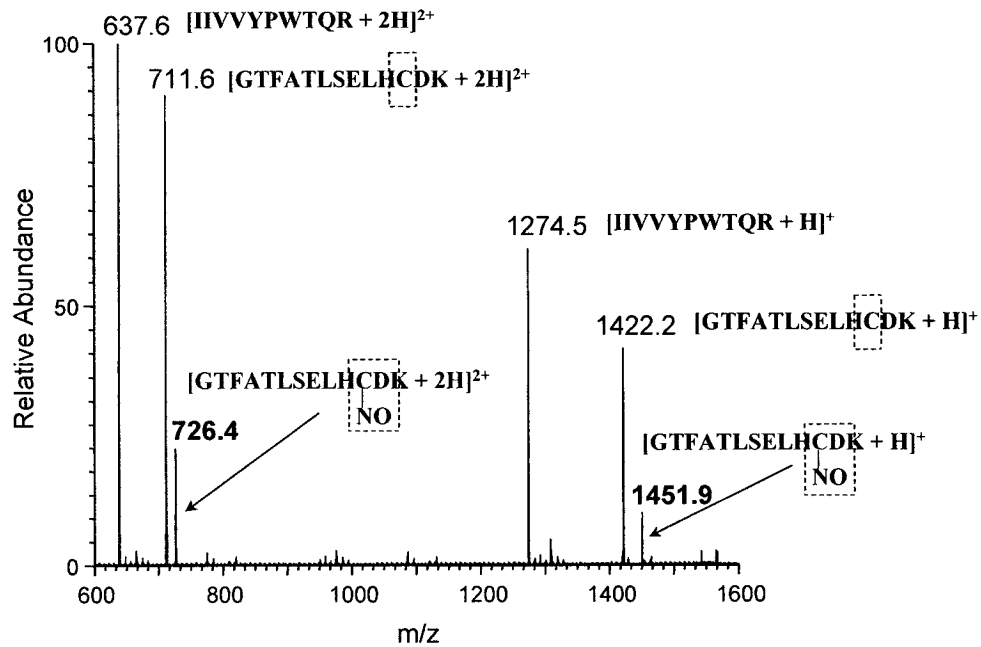

Figure A1.7. ESI mass spectrum of the 54.75-min peak from Figure A1.6. Peaks corresponding to MH^+ and MH_2^{2+} ions of peptides 31-41 (m/z 1274.5 and m/z 637.6), peptide 83-95 (m/z 1422.2 and m/z 711.6) and peptide 83-95+NO (m/z 1451.9 and m/z 726.4) are labeled with their amino acid sequences. Modification of peptide 83-95 by NO is assumed to accur on Cysβ93.

However, the absence of ν(SH) of Cysβ93 in oxyHb-SNO FTIR spectrum (Figure 3.1b) coupled with the present results provides confirmation of Cysβ93 S-nitrosation.

4.0 Superoxide Dismutase Targets NO from GSNO to Cysβ93 of Oxyhemoglobin in Concentrated but not Dilute Solutions of the Protein

4.1 Abstract

The role of hemoglobin (Hb) in transmitting the vasodilatory property of NO throughout the vascular system is of much current interest. NO exchange between Hb and low-molecular-weight nitrosothiols such as S-nitrosoglutathione (GSNO) has been speculated and reported *in vitro*. Previously, we reported that NO delivery from GSNO to Cysβ93 of human oxyHb is prevented in the presence of the Cu chelators, neocuproine and DTPA (134). In the present work, 5 mM solutions of commercial human Hb were found by ICP-MS to contain ~20 μM Cu and Zn, suggesting the presence of Cu,Zn-superoxide dismutase (CuZnSOD), which was confirmed by Western blotting. SOD activity measurements were consistent with the presence of ~20 μM CuZnSOD monomer in 5 mM Hb solutions, which are the physiological concentrations of these proteins in the red blood cell. Incubation of 3.75 mM oxyHb (15 mM heme; 7.5 mM Cysβ93) with 3.75 or 7.5 mM GSNO gave rise to 50% or 100% S-nitrosation, respectively, of Cysβ93 as monitored by FTIR ν(SH) absorption, whereas excess GSNO over Cysβ93 converted oxyHb to metHb due to the reaction, oxyHb + NO ⇌ metHb + NO_3^-. Removal of CuZnSOD by anion-exchange chromatography yielded a oxyHb sample that was *unreactive* towards GSNO, and replacement with bovine CuZnSOD restored reactivity. Addition of 1 μM GSNO (Cysβ93/GSNO = 1) to solutions diluted 10^4-fold from

physiological concentrations of oxyHb and CuZnSOD resulted largely in metHb formation. Thus, this work reports the following key findings: CuZnSOD is an efficient catalyst of NO transfer between GSNO and Cysβ93 of oxyHb; metHb is not detected in oxyHb/GSNO incubates containing close to the physiological concentration (5 mM) of Hb and CuZnSOD when the Cysβ93/GSNO molar ratio is 0.5 to 1.0, but metHb is detected when the total Hb concentration is low micromolar. These results suggest that erythrocyte CuZnSOD may play a critical role in preserving the biological activity of NO by targeting it from GSNO to Cysβ93 of oxyHb, rather than to its oxyheme.

4.2 Introduction

The interaction between nitric oxide (NO) and the conserved Cysβ93 of hemoglobin (Hb) in red blood cells (RBCs) has been of intense interest recently (60,66,135,136). The allosteric transition of Hb reportedly controls the affinity of Cysβ93 for NO, providing a mechanism for NO capture and delivery that is sensitive to the partial pressure of oxygen. Such a mechanism would allow matching of blood flow and tissue oxygenation. GSNO, the S-nitroso form of the dominant low-molecular weight thiol in RBCs (120), as well as CysSNO, are possible NO donors to Cysβ93 of oxyhemoglobin (oxyHb; $HbFe^{II}O_2$) which has higher affinity for NO than its deoxy form (deoxyHb; $HbFe^{II}$) (56).

A direct *trans*-S-nitrosation reaction (i.e., NO^+ transfer) has been proposed (58). However, unlike direct *trans*-S-nitrosation that is reportedly not metal-catalyzed (7), we have shown that S-nitrosation of oxyHb at Cysβ93 requires the presence of copper (134) as was also reported for Cys34 of bovine serum albumin (BSA) (137). Furthermore, we

have demonstrated (134,138) that neocuproine, a Cu^{I}-specific chelator [$E°(Cu^{II/I})$ = 0.58 V) (139), inhibits NO release from GSNO in solutions of oxyHb or deoxyHb. These observations are consistent with the extensive literature revealing that trace Cu^{I} serves as a highly efficient catalyst of RSNO breakdown (7).

CuZnSOD, a homodimer containing one Cu and one Zn atom per monomer, is the major source of copper in RBCs. Present at a concentration of ~20 μM monomer (140), the assumed function of erythrocyte CuZnSOD is to eliminate O_2^- released from oxyHb (141). The catalytic cycle of CuZnSOD involves redox turnover of copper (142):

$$O_2^- + Cu^{II}ZnSOD \rightleftharpoons O_2 + Cu^{I}ZnSOD \quad (4.1)$$

$$O_2^- + Cu^{I}ZnSOD + 2H^+ \rightleftharpoons H_2O_2 + Cu^{II}ZnSOD \quad (4.2)$$

We demonstrate here that redox turnover of erythrocyte CuZnSOD also allows it to function *in vitro* as an NO S-transferase, catalyzing NO transfer from GSNO to Cysβ93 of oxyHb:

$$GSNO + Cu^{I}ZnSOD + H^+ \rightleftharpoons GSH + NO + Cu^{II}ZnSOD \quad (4.3)$$

$$NO + oxyHb\text{-}SH + Cu^{II}ZnSOD \rightleftharpoons oxyHb\text{-}SNO + Cu^{I}ZnSOD + H^+ \quad (4.4)$$

Results are presented that may support a role for CuZnSOD in catalyzing the reductive cleavage of GSNO (or other RSNOs in the RBC), and in targeting the NO released to Cysβ93 of oxyHb. Our experiments were carried out using GSNO concentrations $>10^6$-fold higher than those expected *in vivo*, which gives rise to stable S-nitrosated Hb (Hb-

SNO) in contrast to the instability of Hb-SNO when overproduced in RBCs (16,66,143). Nonetheless, CuZnSOD-catalyzed S-nitrosation, observed at *physiological* concentrations of oxyHb, may explain in part why RBCs do not convert all the endogenous NO produced in the vascular system to NO_3^- as anticipated from the efficiency of NO trapping experiments (Reaction 4.5) carried out using non-physiological (micromolar) concentrations of oxyHb (16,66,143):

$$\text{oxyHb} + \text{NO} \rightleftharpoons \text{metHb} + NO_3^- \qquad (4.5)$$

Formation of NO_3^- would result in loss of NO bioactivity and as shown here, CuZnSOD may play a critical role in preventing this. Significantly, copper added as $CuSO_4$ does not exhibit the same NO-targeting ability as CuZnSOD.

The reported absence of arterial-venous gradients of Hb-SNO in humans (55) and their presence in rats (12,58) provides contradictory evidence that delivery of O_2 and NO to tissues are allosterically coupled events. However, such gradients are questionable given the widely varying reports of Hb-SNO levels (<20 nM to 5 μM) in arterial and venous blood (51,55,58,62,144). Furthermore, although kinetic and thermodynamic arguments have been made to support the O_2-linked, allosterically mediated release of NO from Hb-SNO (12,58,64) the physiological relevance of such linkage has been challenged on the basis of the very high O_2 affinity of Hb-SNO, which could potentially limit its role in the control of NO delivery (57,65,66,136,145). A detailed understanding of the mechanism of Hb S-nitrosation and denitrosation in RBCs is clearly critical in delineating the role of Hb in NO transport. The present study is an important first step in

this direction since evidence is provided for a possible mechanism involving CuZnSOD-catalyzed S-nitrosation of Cysβ93 of oxyHb.

4.3 Experimental Procedures

4.3.1 Materials

Human hemoglobin A (Sigma) and bovine erythrocyte CuZnSOD (Roche Molecular Biochemicals) were used without further purification except where indicated. A rabbit polyclonal antibody developed against human CuZnSOD (0.85 mg/mL SOD-100) and a goat anti-rabbit HRP-conjugated antibody (SAB-301) were purchased from Stressgen Biotechnologies. All reagents were of the highest quality available and were obtained from the following suppliers: GSNO [glycine, N-(N-L-γ-glutamyl-S-nitroso-L-cysteinyl)] and DEA/NO [diethylammonium (Z)-1-(N,Ndiethylamino) diazen-1-ium-1,2-diolate], Caymen; Na_2EDTA (ethylenediamine-N,N,N',N'-tetraacetic acid, disodium salt), neocuproine (2,9-dimethyl-1,10-phenanthroline), GSH, GSSG, and DEAE-Sephacel anion exchanger, Sigma; trace-metal grade HCl, pyrogallol (1,2,3-trihydroxybenzene), sodium dithionite and sodium phosphate salts, Fisher; DTPA (diethylenetriamine-N,N,N',N",N"-pentaacetic acid) and Tris *Ultra Pure*, ICN; cacodylic acid (dimethylarsenic acid), Aldrich; CuCl and $CuSO_4 \cdot 5H_2O$, Anachemia; isoamyl alcohol, Baker; Omni*Trace* Ultra High Purity concentrated HNO_3, EM Science; 30% H_2O_2, 1000 ppm Cu, Fe, Mn and Zn standard solutions, ACP Chemicals Inc., Montreal; NAP-5 (0.9 x 2.8 cm) and HiTrap 5-mL (1.6 x 2.5 cm) Sephadex G-25 columns, Amersham Pharmacia Biotech. Nanopure water (specific resistance 18 MΩ-cm), obtained from a

Millipore Simplicity water purification system and treated with Chelex-100 (Sigma) to remove trace metal ions, was used to prepare all buffers and H_2O solutions.

4.3.2 Methods

Stock solutions of 250 mM GSNO in 200 mM sodium phosphate buffer, pH 7.2 (NaPi) were prepared <2 min before use in a glove box (MBraun, Model MB-OX-SE1). The final pH was adjusted to pH 7.2 and the GSNO concentration determined spectrophotometrically ($\varepsilon_{333.5}$ = 774 M^{-1} cm^{-1}) (146). Stock DEA/NO was prepared in 0.01 M NaOH at 0°C and added to NaPi in the glove box immediately before use. The DEA/NO concentration was determined using $\varepsilon_{250\ nm}$ = 6,500 $M^{-1}cm^{-1}$. Stock solutions of DTPA (15 mM) and neocuproine (650 μM) were also prepared in NaPi.

4.3.3 Preparation and UV-Vis analysis of the Hb incubates

The Hb samples were prepared as described previously (138). Briefly, lyophilized metHb from the bottle was dissolved in NaPi, centrifuged at 12,000 rpm for 2 min, and the supernatant stored at 4°C prior to use. The metHb ($HbFe^{III}$) concentration was determined spectrophotometrically ($\varepsilon_{500\ nm}$ = 10 and $\varepsilon_{630\ nm}$ = 4.4 mM^{-1} cm^{-1} per heme) (147,148) in an FTIR-type cell with a 6-μm Teflon spacer (Harrick) using a custom-made bracket in a Beckman DU 650 UV-Vis spectrophotometer. Samples of oxyHb were prepared in the glove box by treating metHb with a slight excess of sodium dithionite, desalting on the HiTrap column, and introducing a small volume of air into the sample by syringe (48). The deoxyHb concentrations were determined using $\varepsilon_{555\ nm}$ = 12.5 $mM^{-1}cm^{-1}$ per heme, and oxyHb concentrations using $\varepsilon_{541\ nm}$ = 13.5 and $\varepsilon_{576\ nm}$ = 14.6 $mM^{-1}cm^{-1}$

per heme (48). Use of the FTIR-type cell with a 6-μm pathlength to record the optical spectra of the products formed in the Hb/GSNO incubates allowed measurements to be made close to the physiological concentration of Hb (~5 mM) (45).

Optical spectra were recorded using a scan time of 1200 nm/min and analyzed (138) using multicomponent-analysis software (Beckman, PN 517031) for the DU 600 spectrophotometer. The software uses Full Spectrum Quantitation (FSQ) to calculate the concentration of each component in a mixture by performing a Fourier transform on the scan data. Each point in the calculated absorbance transform contains information from all of the data points in the absorbance scan. The absorbance transform follows Beer's law.

4.3.4 FTIR spectra of the Hb incubates

To record the Fourier transform infrared (FTIR) spectra in the SH stretching ν(SH) region (~2500 cm^{-1}), 20 μL of 7 mM Hb (28 mM heme) in NaPi was added by syringe onto a 13-mm CaF_2 window and the FTIR cell was immediately assembled with a 250-μm Teflon spacer (Harrick). Spectra were recorded at 25°C on a Nicolet Magna-IR 550 spectrometer with a MCT detector cooled to 77 K and purged with dry air from a Whatman FTIR Purge (Model 75-52). All reported spectra are an average of 500 scans recorded in 5.5 min at a resolution of 2 cm^{-1} using a Happ-Genzel apodization with a velocity and aperture of 4.4303 cm/s and 2, respectively. Omnic (Nicolet) software was used for spectral analysis as previously reported (138).

4.3.5 ESI-MS analysis

Hb solutions (7.0 mM) in NaPi were diluted 10^3-fold with H_2O to give ~0.5 μg/μL protein. Aliquots were infused into the ESI source of the mass spectrometer (ThermoFinnigan SSQ7000) by flow injection from the HPLC (Agilent 1090) using a 100 μL loop (but no column) at 50 μL/min with 75% CH_3CN/0.05% TFA as a mobile phase. The 250-mM GSH, GSNO and GSSG stocks in NaPi were diluted 500-fold with H_2O and then 10-fold to 50 μM with 75% CH_3CN/0.05% TFA and their mass spectra obtained as for the Hb solutions.

4.3.6 ICP-MS analysis

A PE Sciex Elan 6000 inductively coupled plasma mass spectrometer (ICP-MS) with cross-flow nebulizer and Scott-type spray chamber was used to determine the amount of Cu, Zn and Fe in the samples and buffers as described previously (138). Stock Hb solutions in NaPi were added to 50 μL of 30% H_2O_2 and 500 μL of ultra high purity concentrated HNO_3 to give a final heme iron concentration of ~5 mM, and the samples ashed using a Bunsen burner. The residue was dissolved in 10 mL of 5% (v/v) HNO_3, and ICP-MS analyses for Cu, Fe and Zn were performed. An internal standard of 9 nM (0.500 ppb) Mn prepared from a 1000 ppm Mn standard solution was added to all samples. Standard analyte curves were prepared by diluting 1000 ppm Cu, Zn and Fe standards in 5% (v/v) HNO_3 and nanopure water to give 0-8 μM (0-0.500 ppm) Cu and Zn, and 0-9 μM (0-0.500 ppm) Fe. The reported Cu and Zn concentrations are normalized to 20 mM Fe (5.0 mM Hb), and all values are the results of at least triplicate experiments with standard deviations of <5%.

4.3.7 Dialysis and DEAE-purification of Hb samples

A solution of metHb from the bottle was extensively dialyzed at 4°C *vs* Na_2EDTA (pH 7.0) followed by H_2O, lyophilized and dissolved in NaPi to a concentration of 30 mM heme as described previously (138). For anion-exchange purification, metHb from the bottle was dissolved in 0.5 mL of NaPi to a concentration of 32 mM heme, and added to a 0.9x2.8-cm DEAE-Sephacel anion-exchange column equilibrated with NaPi. The eluent was 100 mM NaCl in the same buffer, and the Hb that eluted between 1-2 mL was twice reapplied to the column to remove all CuZnSOD. The third DEAE eluate (~3 mL) was desalted on the HiTrap column to give the CuZnSOD-free sample referred to here as 3xDEAE-Hb.

4.3.8 SOD-activity assay

Lyophilized bovine CuZnSOD (10 mg) from the bottle was dissolved in 1 mL of NaPi to give a ~300 μM stock solution ($\varepsilon_{258\ nm}$ = 10.3 mM^{-1} cm^{-1}) (149). Pyrogallol stock (40 mM) in 10 mM HCl (trace-metal grade), and 50 mM Tris (ultra pure) adjusted to pH 8.2 with 0.5 M cacodylic acid were freshly prepared (150). Samples of 0.373 μM metHb in Tris cacodylate buffer (pH 8.2) were added to a 1-cm quartz cuvette at 25°C, followed by 200 μM pyrogallol, and the absorbance at 320 nm read every 15 s over 5 min to monitor rates of pyrogallol oxidation. At the wavelength chosen, the spectra of oxidized pyrogallol and metHb exhibit a maximum and minimum, respectively. Assuming 0% SOD activity in the blank [0.375 μM 3xDEAE-metHb] and 100% in the standard [0.375 μM 3xDEAE-metHb + 1.5 nM CuZnSOD monomer], the relative SOD activities (and

CuZnSOD concentrations) in the unknowns (X) were determined from the initial slopes of the plots of 320-nm absorbance *vs* time:

$$\% \text{ relative SOD activity} = \left(\frac{\text{3xDEAE-metHb slope} - \text{X slope}}{\text{3xDEAE-metHb slope} - \text{standard slope}} \right) \text{x } 100 \qquad (4.6)$$

4.3.9 Western blotting

Western blotting was performed on a 5 mM Hb sample using the polyclonal antibody diluted 1/500 (151). The blot was probed with the goat anti-rabbit-HRP secondary antibody, and the presence of CuZnSOD was detected by chemiluminescence following 1-s X-ray exposure.

4.3.10 Spectrophotometric titration of CuZnSOD with neocuproine

Solutions containing purified CuZnSOD were titrated with neocuproine to establish the time course of removal of active-site Cu^{I} from the protein (152). GSH was added to the CuZnSOD solutions ~30 s before neocuproine to convert Cu^{II} to Cu^{I}, and formation of the $[Cu^{I}(\text{neocuproine})_2]^{+}$ complex was monitored spectrophotometrically (ε_{454} = 7950 M^{-1} cm^{-1}) following extraction with an equal volume of isoamyl alcohol (153).

4.4 Results

4.4.1 ICP-MS analysis

The results summarized in Table 4.1 reveal that ~20 μM Cu and 20 μM Zn are present in 5 mM solutions of commercial human Hb. These concentrations are close to

those found in RBCs, which contain ~5 mM Hb (45) and ~20 μM CuZnSOD monomer (140). Following dialysis or 3xDEAE-purification, the Cu and Zn levels decreased to those (~1 μM) found in the buffer (Table 4.1). The metal ions were removed from CuZnSOD by EDTA chelation during dialysis (149) whereas CuZnSOD (pI = 8.88) (154) was separated from Hb (pI = 7.15) (48) during anion-exchange chromatography because of their different affinities for the DEAE column. A CuZnSOD monomer concentration of ~15 μM per 5 mM Hb was determined by Western blotting from band intensities (data not shown) in good agreement with the ICP-MS data (Table 4.1).

4.4.2 SOD activity assay

The spectra of oxidized pyrogallol and metHb exhibit a maximum and minimum, respectively, at 320 nm (Figure 4.1a). Relative rates of pyrogallol oxidation (Table 4.2) were determined from the initial linear portion of the plots of ΔA_{320} *vs* time (Figure 4.1b). Clearly, 3xDEAE-metHb catalyzes pyrogallol oxidation (Figure 4.1b and Table 4.2) so the blank contained pyrogallol plus 3xDEAE-metHb. In solutions containing both pyrogallol and CuZnSOD, there is competition for the O_2^- produced (150):

$$O_2^- \begin{cases} \xrightarrow{\text{Pyr}} \text{Pyr}^{\bullet+} \\ \xrightarrow{\text{SOD}} H_2O_2 + O_2 \end{cases}$$

$Pyr^{\bullet+}$ is the pyrogallol radical that dimerizes to form the colored product monitored at 320 nm (150), and rates of pyrogallol oxidation decrease in metHb samples when CuZnSOD is present (Figure 4.1b). The standard containing 0.375 μM 3xDEAE-

Table 4.1. Determination of Cu and Zn in stock solutions by ICP-MS

Sample[a]	Cu (μM)	Cu (ppm)	Zn (μM)	Zn (ppm)
5 mM Hb[b]	19 ± 3	1.207 ± 0.190	20 ± 2	1.307 ± 0.130
5 mM G-25-Hb[c]	13 ± 2	0.826 ± 0.127	15 ± 3	0.980 ± 0.196
5 mM 3xDEAE-Hb[d]	0.76 ± 0.1	0.048 ± 0.006	0.15 ± 0.1	0.01 ± 0.006
3xDEAE runoff[e]	17.2 ± 2.7	1.093 ± 0.172	18.3 ± 2.1	1.196 ± 0.137
5 mM dial-Hb[f]	1.7 ± 0.2	0.108 ± 0.01	1 ± 0.4	0.065 ± 0.026
250 mM GSNO	1.2 ± 0.8	0.076 ± 0.05	0.3 ± 0.1	0.019 ± 0.006
300 μM CuZnSOD	612 ± 17	38.890 ± 1.080	578 ± 22	37.79 ± 1.438
15 mM DTPA	0.7 ± 0.3	0.044 ± 0.019	0.5 ± 0.2	0.032 ± 0.013
650 μM neocuproine	1.6 ± 0.5	0.101 ± 0.031	0.9 ± 0.2	0.058 ± 0.013
200 mM NaPi buffer	0.9 ± 0.7	0.057 ± 0.044	1.1 ± 0.4	0.072 ± 0.026

[a] All stock solutions were prepared in 200 mM sodium phosphate buffer (pH 7.2)

[b] Human Hb (Sigma) from the bottle; 5 mM Hb contains 20 mM heme

[c] Hb passed through a 1.6 x 2.5-cm G-25 column

[d] Hb passed 3 times through a 0.9 x 2.8-cm DEAE column

[e] Combined DEAE runoffs collected after each passage of Hb through the DEAE column. Metal ion concentrations were corrected for dilution; 0.50 mL of Hb solution was loaded on the column and a total of 3.0 mL of runoff collected

[f] Hb following dialysis *vs* EDTA

Table 4.2. Relative SOD activities and CuZnSOD concentrations of the metHb samples

Sample[a]	ΔA_{320}/min[b]	% relative activity[c]	CuZnSOD/5 mM Hb (μM) [d]
3xDEAE-Hb[e]	0.702	0	0
3xDEAE-Hb + 1.5 nM SOD	0.381	100 ± 2.0	20 ± 0.4
Dial-Hb[e]	0.656	14 ± 3.0	3 ± 0.6
G-25-Hb[e]	0.463	74 ± 5.0	15 ± 1.0
Hb[e]	0.358	107 ± 3.5	21 ± 0.7
buffer	0.324[f]	—	—

[a] Samples contained 0.375 μM human metHb, and 1.5 nM bovine CuZnSOD monomer where indicated, in Tris cacodylate buffer (pH 8.2) at 25°C. The assay was initiated by adding 200 μM pyrogallol

[b] Initial change in absorbance at 320 nm *vs* time due to pyrogallol oxidation

[c] Defined by equation 6 in the text

[d] Concentrations of active CuZnSOD monomer in the metHb solutions. Values are normalized to 5 mM Hb

[e] See footnotes b, c, d and f, Table 4.1

[f] Rate of 200 μM pyrogallol autoxidation in the Tris cacodylate assay buffer (pH 8.2) at 25°C

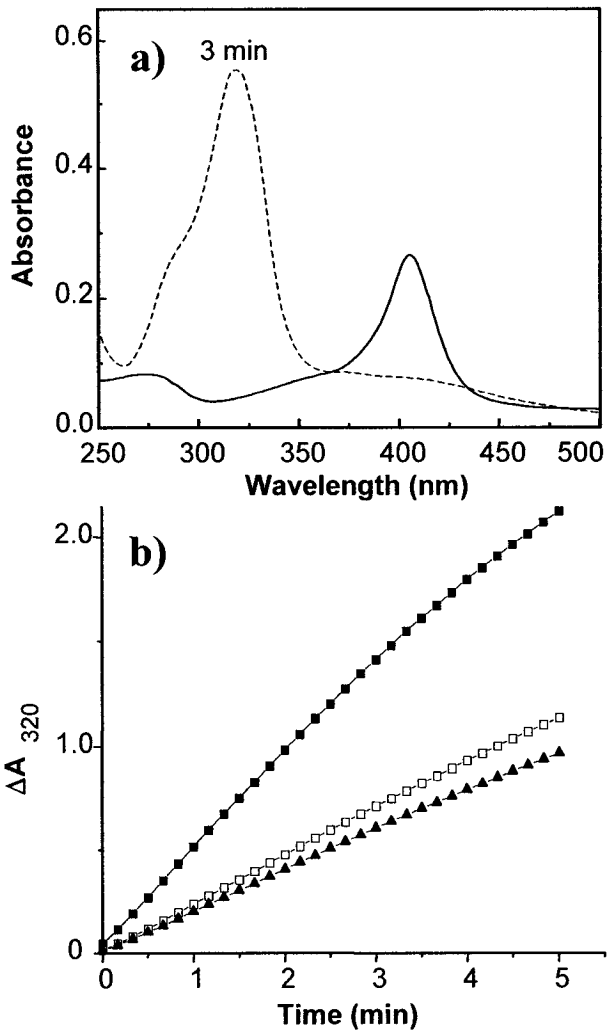

Figure 4.1. SOD-activity assay based on competition between CuZnSOD and pyrogallol for O_2^- in solutions containing metHb. (**a**) Spectrum of 0.375 μM metHb (—) and of 200 μM pyrogallol following autoxidation for 3 min (- - -). Spectra were recorded in a 1-cm quartz cuvette at 25°C with a scan time of 1200 nm/min. (**b**) Time course of absorbance change at 320 nm following addition of 200 μL pyrogallol to (■) 0.375 μM 3xDEAE-metHb; (□) 0.375 μM 3xDEAE-metHb + 1.5 nM CuZnSOD monomer; (▲) buffer only. Assays were carried out in 50 mM Tris cacodylate buffer (pH 8.2) at 25°C in a 3-mL quartz cuvette with a 1-cm path length.

metHb + 1.5 nM CuZnSOD monomer, which coincidently exhibits the same initial rate of pyrogallol oxidation as the buffer alone (Figure 4.1b), is arbitrarily assigned 100% CuZnSOD activity (Table 4.2), and the relative activities of the metHb samples are listed in Table 4.2. The ~107% relative activity in 0.357 μM untreated metHb corresponds to 1.5 nM CuZnSOD monomer, or 20 μM CuZnSOD monomer per 5 mM Hb, in excellent agreement with the ICP-MS data (Table 4.1). Dialysis *vs* EDTA is less effective than 3xDEAE-purification in removing CuZnSOD activity since the Dial-Hb sample exhibits 14% relative SOD activity (Table 4.2). Re-uptake of trace copper and zinc by the apoSOD remaining after dialysis would give rise to the observed SOD activity. G-25-purified metHb (G-25-Hb) retains 74% of its SOD activity, which is not surprising given the fractionation range for globular proteins (1000-5000 Da) of this molecular-exclusion gel (155).

Figure 4.2 shows that neocuproine reacts promptly with $CuSO_4$ but not CuZnSOD in the presence of GSH to form $[Cu^{I}(neocuproine)_2]^{+}$, which absorbs strongly at 454 nm (Figure 4.2, inset). Thus, Cu^{I} removal from CuZnSOD and chelation do not explain the loss of NO-transferase activity (Reactions 4.3 and 4.4) in samples containing neocuproine. Addition of both neocuproine and DTPA do not increase the yield of $[Cu^{I}(neocuproine)_2]^{+}$ formation (Figure 4.2) suggesting that the combination of DTPA and neocuproine does not promote prompt copper removal from the enzyme. We have evidence that DTPA binds to CuZnSOD (156), which could also explain why DTPA inhibits the NO-transferase but not the SOD activity (Reactions 4.1 and 4.2) of CuZnSOD (data not shown). DTPA-binding likely alters interaction of larger molecules

such as GSNO or Hb with CuZnSOD but allows the small O_2^- substrate to access the active site. Further studies on chelator binding to CuZnSOD are underway.

4.4.3 Visible absorption spectra of the Hb incubates

No reaction occurred at the heme during 5-min incubation of 3.75 mM oxyHb (15 mM heme) with 7.5 mM GSNO (Cysβ93/GSNO =1) or 3.75 mM GSNO (Cysβ93/GSNO = 2) (Figure 4.3). This indicates that all NO released from GSNO was directed to Cysβ93, which was confirmed by FTIR (Figure 4.6a) and ESI-MS (Figure 4.7b). The effect of CuZnSOD removal on the visible absorption spectra of 3.75 mM Hb (15 mM heme) incubates was next examined. In a 5-min 3xDEAE-deoxyHb/GSNO incubate (Cysβ93/GSNO = 1) no significant spectral changes were detected while ~100% nitrosylHb ($HbFe^{II}NO$) was formed in the same incubate when bovine CuZnSOD was added (Figure 4.4a). However, when DTPA and neocuproine were also present, CuZnSOD addition had little effect on the spectrum of 3xDEAE-deoxyHb (data not shown), indicating that CuZnSOD-catalyzed GSNO breakdown is inhibited by the copper chelators. Interestingly, only 50% nitrosylHb was formed in the 5-min incubate when copper was added as $CuSO_4$ (Figure 4.4a) although yields at longer times were not determined. Also, nitrosylHb formation was observed in the 5-min 3xDEAE-deoxyHb/DEA/NO incubate (Figure 4.4b), confirming that NO release from DEA/NO is not Cu-catalyzed (10,44). The half-life of DEA/NO is ~8 min at 22°C in 100 mM phosphate (pH 7.4) and it dissociates to give the free amine and 2 NO molecules following first-order kinetics (44).

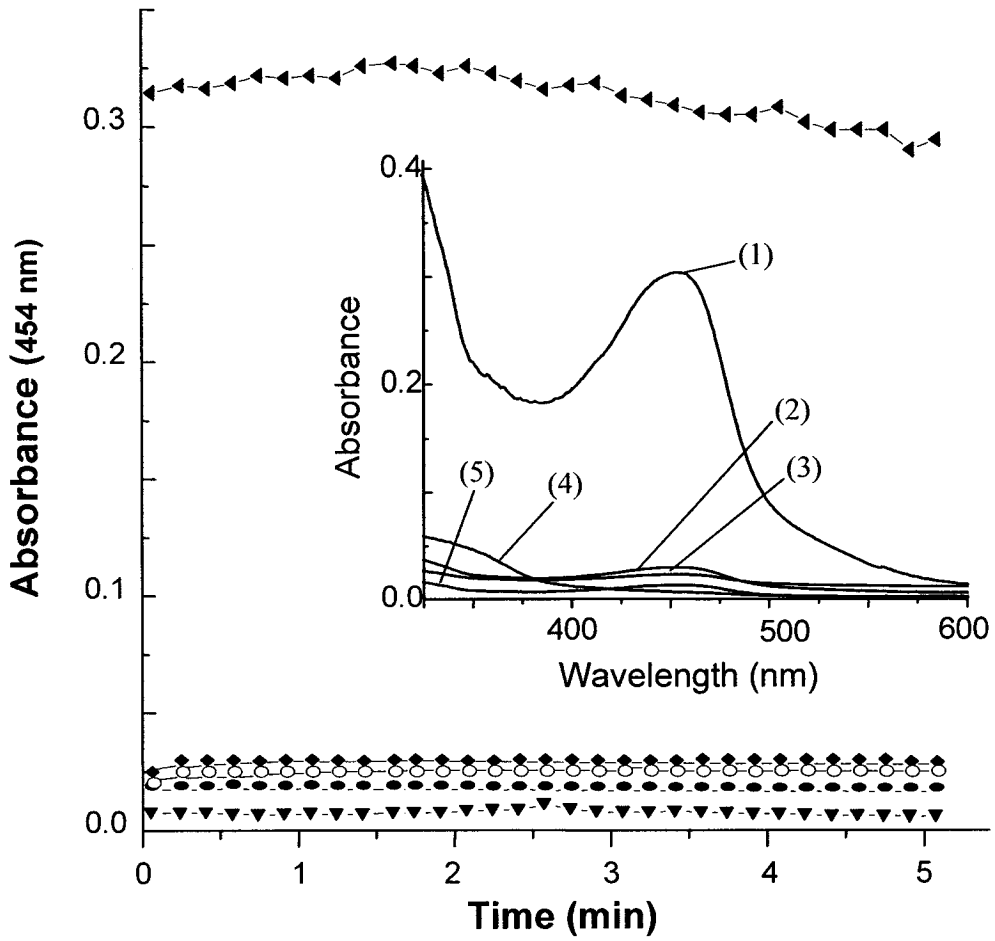

Figure 4.2. Formation of $[Cu(neocuproine)_2]^+$ in copper solutions. 40 μM CuZnSOD monomer or 40 μM $CuSO_4$ was added to 200 μM GSH + 80 μM neocuproine in 200 mM sodium phosphate buffer (pH 7.2), and following isoamyl alcohol extraction the absorbance at 454 nm due to $[Cu(neocuproine)_2]^+$ was monitored *vs* time. The spectra after 5 min are shown in the insert. Sideway triangles (◄) and spectrum 1, neocuproine + $CuSO_4$ + GSH. Diamonds (♦) and spectrum 2, CuZnSOD + neocuproine + GSH. Open circles (o) and spectrum 3, CuZnSOD + neocuproine + 20 μM DTPA + GSH. Solid circles (•) and spectrum 4, neocuproine + GSH. Inverted triangles (▼) and spectrum 5, CuZnSOD + GSH.

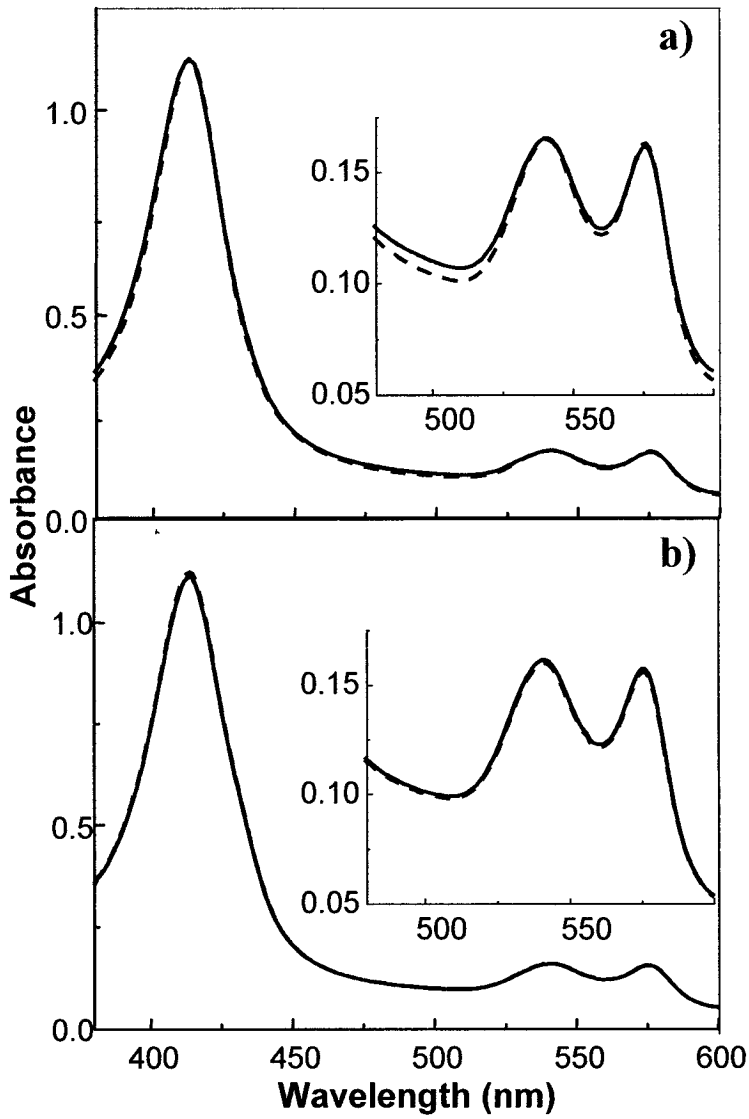

Figure 4.3. Effect of GSNO on the visible absorption spectrum of 3.75 mM oxyHb (15 mM heme). (**a**) oxyHb (---); oxyHb + 7.5 mM GSNO (—). (**b**) oxyHb (---); oxyHb + 3.75 mM GSNO (—). Spectra were recorded 5 min after mixing the reagents in 200 mM sodium phosphate buffer (pH 7.2) at 25°C in an FTIR-type cell with a 6-μm Teflon spacer using a scan time of 1200nm/min. This preparation of Hb was found to contain 20 μM CuZnSOD monomer.

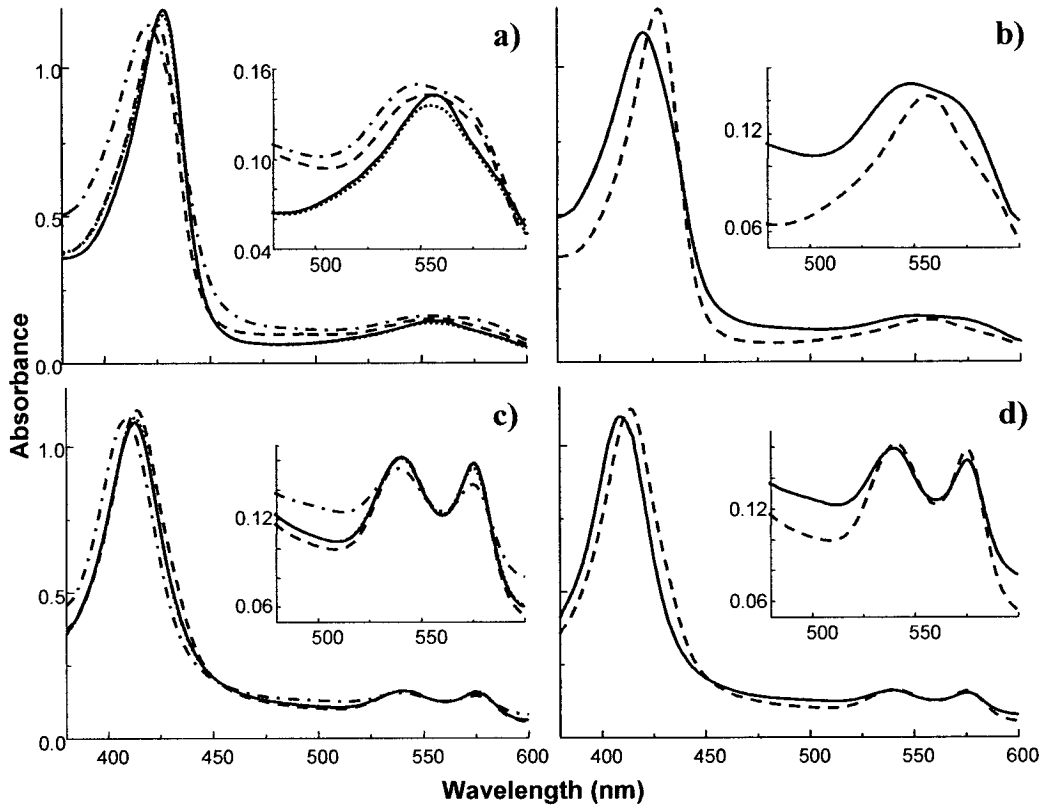

Figure 4.4. Effect of GSNO and 10 μM CuZnSOD monomer or 10 μM $CuSO_4$ on the visible absorption spectrum of 3.75 mM 3xDEAE-Hb (15 mM heme). (**a**) deoxyHb (—); deoxyHb + 7.5 mM GSNO (· · ·); deoxyHb + 7.5 mM GSNO + CuZnSOD (- · -); deoxyHb + 7.5 mM GSNO + $CuSO_4$ (- - -). (**b**) deoxyHb (- - -); deoxyHb + 3.75 mM DEA/NO (—). (**c**) oxyHb (- - -); oxyHb + 7.5 mM GSNO + CuZnSOD + 200 μM DTPA + 200 μM neocuproine (· · ·); oxyHb + 7.5 mM GSNO + $CuSO_4$ (- · -); oxyHb + 7.5 mM GSNO + CuZnSOD (—). (**d**) oxyHb (- - -); oxyHb + 3.75 mM DEA/NO (—). Spectra were recorded 5 min after mixing the reagents in 200 mM sodium phosphate buffer (pH 7.2) at 25°C in a FTIR-type cell with a 6-μm Teflon spacer using a scan time of 1200nm/min. 3xDEAE-Hb contains no SOD activity.

As expected, no reaction at the heme (Figure 4.4c) or Cysβ93 (Figures 4.6b and 7a) was detected in 3xDEAE-oxyHb/GSNO incubates since GSNO breakdown, as monitored by nitrosylHb formation (Figure 4.4a), is prevented by CuZnSOD removal. Also, negligible spectral changes were observed in the 5-min 3xDEAE-oxyHb/GSNO incubate (Cysβ93/GSNO = 1) in the presence of bovine CuZnSOD (Figure 4.4c), indicating that added bovine CuZnSOD, like human CuZnSOD (Figure 4.3), directs NO from GSNO to Cysβ93 of oxyHb. Importantly, copper added as a Cu^{II} salt does not direct all NO to Cysβ93, since formation of metHb was detected in the 3xDEAE-oxyHb/GSNO/$CuSO_4$ incubate (Cysβ93/GSNO = 1; Figure 4.4c). Formation of metHb (via Reaction 4.5) in the 5-min incubate of 3xDEAE-oxyHb/DEA/NO (Figure 4.4d) confirms that CuZnSOD is required to target *all* NO to Cysβ93 of oxyHb.

From Figure 4.5, it can be deduced that NO targeting by CuZnSOD is insignificant in solutions containing 0.5 μM Hb (2 μM heme) and 1 μM GSNO (Cysβ93/GSNO = 1). NitrosylHb and metHb formation can be clearly detected in the 5-min incubates of deoxyHb/GSNO (Figure 4.5a) and oxyHb/GSNO (Figure 4.5b), respectively, with and without chelators. This reveals that CuZnSOD does not target NO to Cysβ93 at protein concentrations much lower than their physiological values. Also, the 100-fold lower concentration of chelators used in the experiments in Figure 4.5 *vs* Figure 4.4 does not inhibit redox turnover of CuZnSOD.

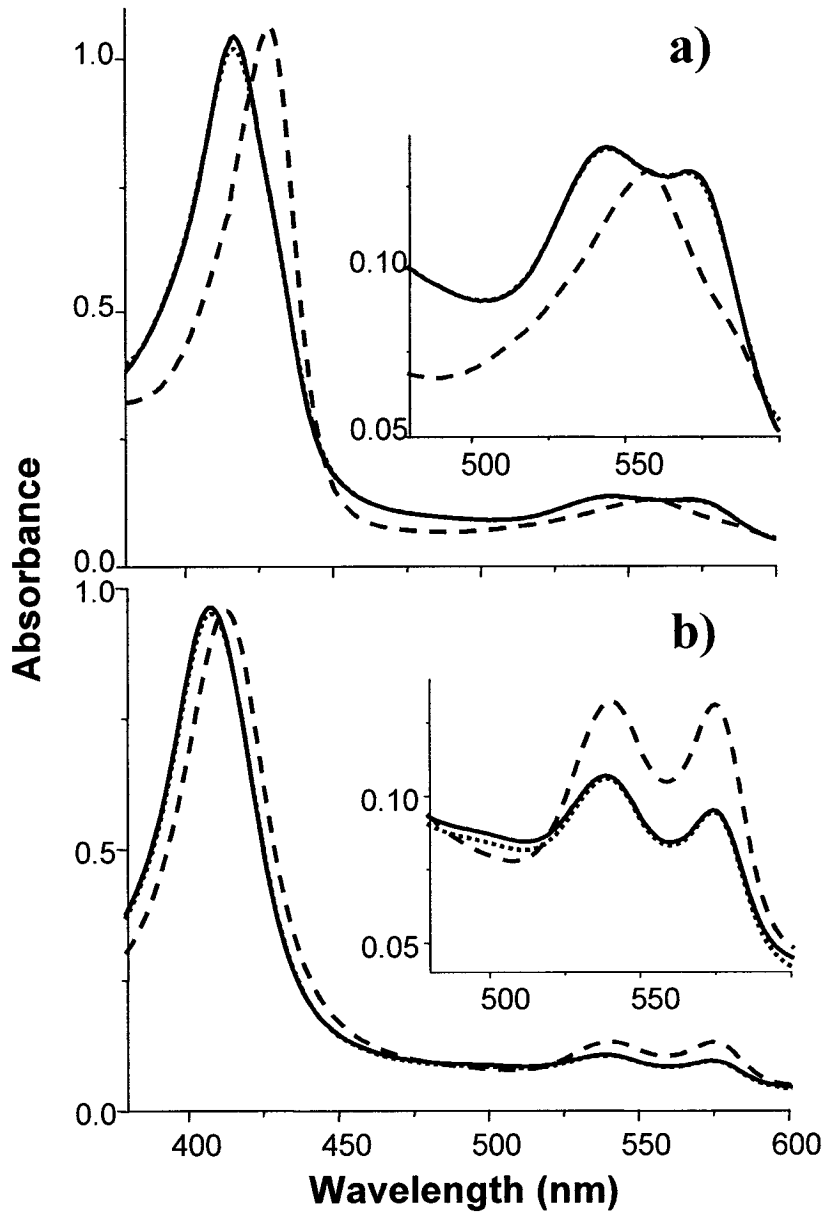

Figure 4.5. Effect of 1 μM GSNO on the visible absorption spectrum of 0.5 μM Hb (2 μM heme). (**a**) deoxyHb (- - -); deoxyHb + GSNO (——); deoxyHb + GSNO + 2 μM DTPA + 2 μM neocuproine (· · ·). (**b**) oxyHb (- - -); oxyHb + GSNO (——); oxyHb GSNO + 2 μM DTPA + 2 μM neocuproine (· · ·). Spectra were recorded 5 min after mixing the reagents in 200 mM sodium phosphate buffer (pH 7.2) at 25°C in a 1-cm quartz cuvette using a scan time of 1200nm/min.

4.4.4 FTIR spectra of the Hb incubates

FTIR spectroscopy is a valuable probe of protein thiols since ν(SH) falls in a spectral window (~2500 cm^{-1}) with minimum H_2O and protein absorption (122,123). Although >1 mM Hb is necessary to observe the weak IR ν(SH) absorption (122,123), the concentrations used are comparable to those found in RBCs (~5 mM Hb) (45). The FTIR spectrum of 7 mM oxyHb recorded in the absence of GSNO (Figure 4.6) clearly exhibits the three ν(SH) peaks at 2586, 2566, and 2553 cm^{-1} assigned previously to Cysβ93, Cysβ112 and Cysα104, respectively (123).

A 5-min incubation of oxyHb with GSNO results in total loss of the Cysβ93 ν(SH) band when Cysβ93/GSNO = 1 while 50% intensity remains in incubates with Cysβ93/GSNO = 2 (Figure 4.6a). A 3xDEAE-oxyHb/GSNO incubate (Cysβ93/GSNO = 1) did not show any loss of Cysβ93 ν(SH) intensity but the band disappeared when 20 μM monomer bovine CuZnSOD was added (Figure 4.6b). In contrast, < 50% loss of Cysβ93 absorbance was observed on addition of 20 μM $CuSO_4$ (Figure 4.6b), confirming the partial oxyheme scavenging of NO released in the presence of free copper (Figure 4.4c). Addition of DTPA and neocuproine inhibited the NO-transferase activity of CuZnSOD (Figure 4.6b) consistent with the inhibition of CuZnSOD-catalyzed GSNO breakdown seen in Figure 4.4a.

4.4.5 ESI-MS results

The deconvolved mass spectrum of Hb from the 5-min incubate of 7 mM 3xDEAE-oxyHb (28 mM heme) and 14 mM GSNO showed no evidence of β-subunit

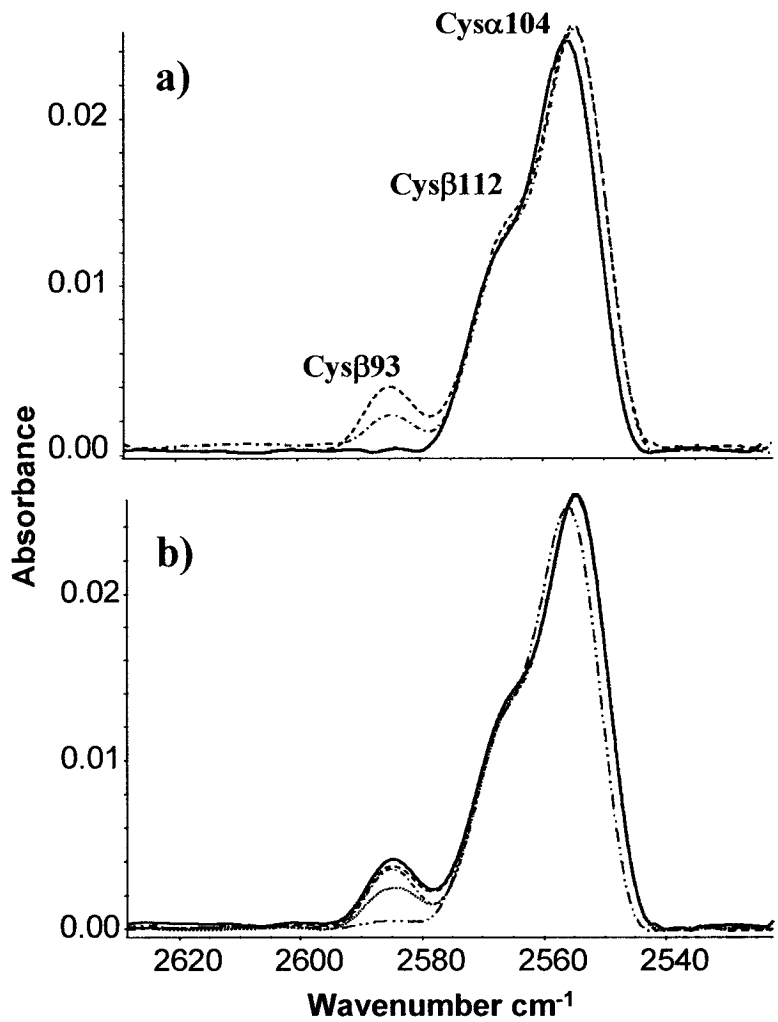

Figure 4.6. Effect of GSNO on the FTIR spectrum in the ν(SH) region of 7.0 mM oxyHb (28 mM heme). (**a**) oxyHb (– – –); oxyHb + 7 mM GSNO (– · –); oxyHb + 14 mM GSNO (——). (**b**) 3xDEAE-oxyHb (——); 3xDEAE-oxyHb + 14 mM GSNO (– – –); 3xDEAE-oxyHb + 14 mM GSNO + 20 μM CuZnSOD monomer + 500 μM DTPA + 200 μM neocuproine (– · –); 3xDEAE-oxyHb + 14 mM GSNO + 20 μM $CuSO_4$ (– – –); 3xDEAE-oxyHb + 14 mM GSNO + 20 μM CuZnSOD monomer (– · · –). Spectra were recorded in a 250-μm pathlength FTIR cell 5 min after mixing the reagents in 200 mM sodium phosphate buffer (pH 7.2) at 25°C, and are the average of 500 scans at 2-cm^{-1} resolution. Background subtraction, baseline correction, smoothing and Fourier transform self-deconvolution were performed on the displayed spectra (Section 4.4.4).

S-nitrosation (Figure 4.7a), while a peak with an increased mass of 29 Da is observed when bovine CuZnSOD was added to the incubate (Figure 4.7b). Interestingly, no Hb nitrosation is detected in the 5-min incubate of 0.5 μM oxyHb (2 μM heme) with 1 μM GSNO (Figure 4.7c).

An intense peak due to $GSSGH^+$ (m/z 613.5) is observed in the ESI mass spectrum of a 5-min GSH/GSNO/CuZnSOD incubate (Figure 4.8a, insert). Presumably, GSSG is formed in the CuZnSOD-catalyzed reductive cleavage of GSNO:

$$GSH + Cu^{II}ZnSOD \rightleftharpoons \tfrac{1}{2}GSSG + Cu^{I}ZnSOD + H^+ \qquad (4.7)$$

$$GSNO + Cu^{I}ZnSOD + H^+ \rightleftharpoons GSH + NO + Cu^{II}ZnSOD \qquad (4.3)$$

In contrast, no $GSSGH^+$ peak appears in the spectrum of the 5-min 3xDEAE-oxyHb/GSNO/CuZnSOD incubate (Figure 4.8b, insert) indicating that the GSH formed *in situ* (eqn 4.3) does not supply electrons for GSNO reductive cleavage in this incubate. GSSG formation in the 3xDEAE-oxyHb/GSNO/$CuSO_4$ (data not shown) and deoxyHb/GSNO incubates (138), and in all incubates containing 0.5 μM Hb (data not shown) signals that GSH is oxidized. Combined, these results reveal that GSH acts an electron donor in all the Hb/GSNO incubates examined except in those containing oxyHb(mM)/GSNO/CuZnSOD where *all* of the released NO is directed to Cysβ93.

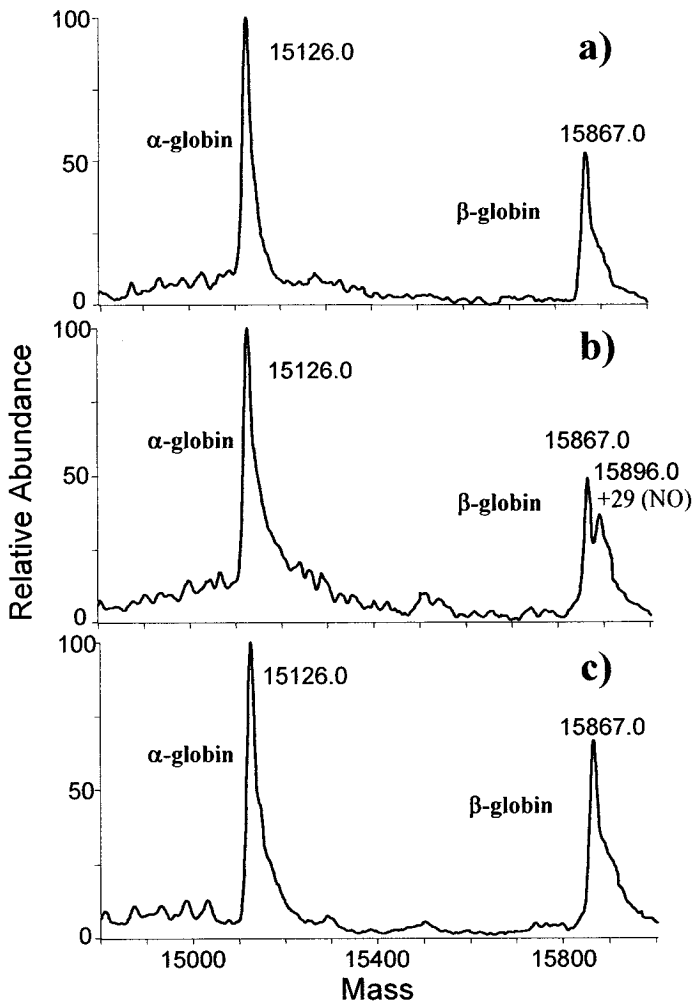

Figure 4.7. Effect of GSNO on the deconvolved electrospray mass spectra of the heme-free Hb subunits. (**a**) Hb from 7.0 mM 3xDEAE-oxyHb + 14 mM GSNO incubate; (**b**) Hb from 7.0 mM 3xDEAE-oxyHb + 14 mM GSNO + 20 μM CuZnSOD monomer incubate; (**c**) Hb from 0.5 μM Hb + 1 μM GSNO incubate. Experimental conditions: following incubation of the reactants in 200 mM sodium phosphate buffer (pH 7.2) for 5 min at 25°C, the Hb concentration in (**a**) and (**b**) was adjusted to 7 μM (~0.45 μg/μL) by dilution in H_2O. Aliquots (100 μL) were infused into the ESI source of the mass spectrometer by flow injection at 50 μL/min with 75% CH_3CN/0.05% TFA as a mobile phase. The capillary temperature was 180°C and the spray voltage 4.0 kV. Hb dissociated into free heme and α- and β-subunits under the MS conditions. The unresolved shoulders on the subunit peaks at high mass are due to sodium adducts.

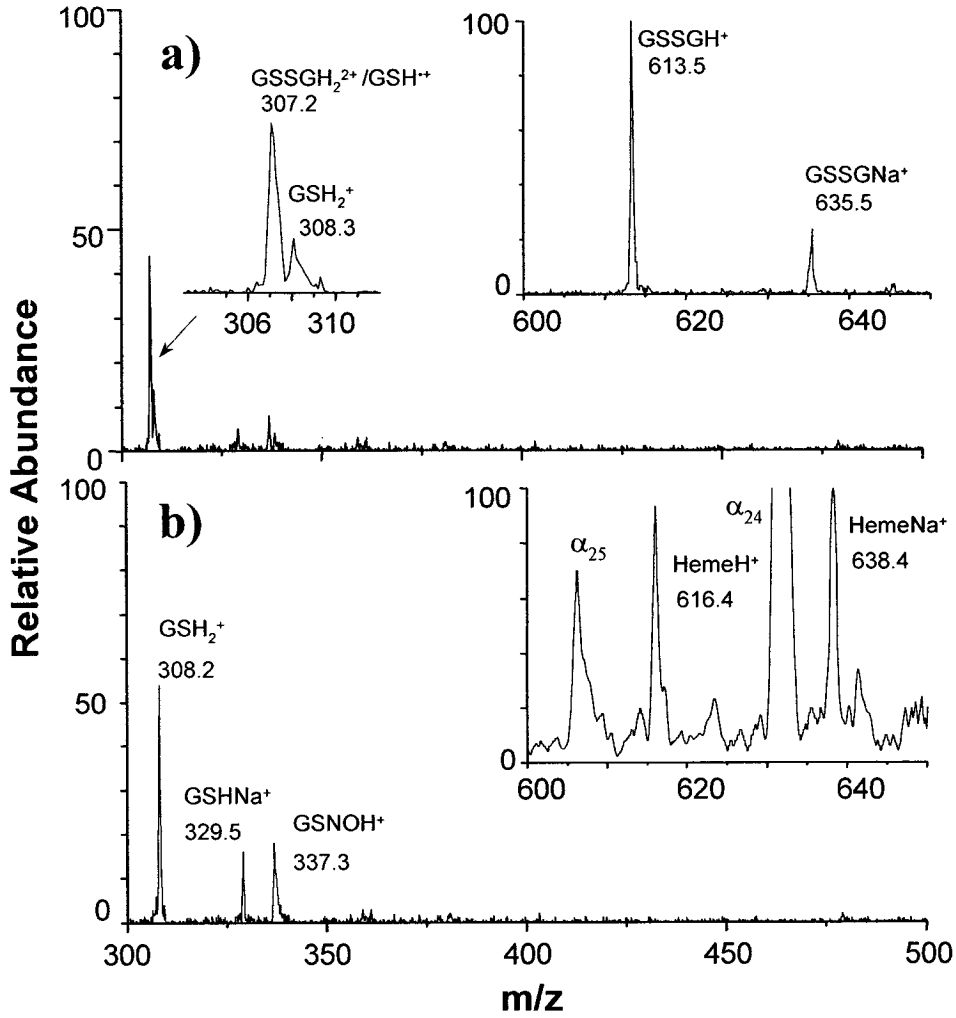

Figure 4.8. Electrospray mass spectral analysis of the glutathione-derived products. (**a**) 14 mM GSNO + 14 mM GSH + 20 μM CuZnSOD monomer; (**b**) 7.0 mM 3xDEAE-oxyHb + 14 mM GSNO + 20 μM CuZnSOD monomer. Experimental conditions: following incubation of the reactants in 200 mM sodium phosphate buffer (pH 7.2) for 5 min at 25°C, the samples were diluted 10^3-fold and the mass spectra recorded as outlined in Figure 4.7. Peaks labeled α_{24} and α_{25} are due to α-globinH_{24}^{24+} and α-globinH_{25}^{25+}, respectively. Peak intensities in spectrum (a) are relative to the $GSSGH^+$ peak at m/z 613.5 (100%) and, in spectrum (b), to the $hemeNa^+$ peak at m/z 638 (100%). $GSH^{\bullet+}$ formed on the homolysis and protonation in the ESI source of residual GSNO could also contribute to the intensity of the peak at m/z 307 in spectrum (a).

4.5 Discussion

We have previously shown that copper redox turnover is required for oxyHb S-nitrosation by GSNO (134). In the present work, we demonstrate that commercial human Hb contains ~20 μM CuZnSOD monomer, and that the latter is a highly efficient catalyst of NO transfer from millimolar GSNO to Cysβ93 of oxyHb at the concentrations of Hb (~5 mM) (45) and CuZnSOD (20 μM monomer) (140) found in RBCs. The well-documented (16,40) reaction of NO with oxyHb (equation 4.5) dominates at micromolar Hb (Figure 4.5), but not at physiological concentrations of oxyHb and CuZnSOD, where all the NO released is directed to Cysβ93 (Figures 4.3 and 4.6). The following mechanism for CuZnSOD-catalyzed NO transfer from GSNO to Cysβ93 is proposed:

$$\text{oxyHb-SH} + \text{Cu}^{\text{II}}\text{ZnSOD} \rightleftharpoons \text{oxyHb-S}^{\bullet} + \text{Cu}^{\text{I}}\text{ZnSOD} + \text{H}^{+} \qquad (4.8)$$

$$\text{GSNO} + \text{Cu}^{\text{I}}\text{ZnSOD} + \text{H}^{+} \rightleftharpoons \text{GSH} + \text{NO} + \text{Cu}^{\text{II}}\text{ZnSOD} \qquad (4.3)$$

$$\text{NO} + \text{oxyHb-S}^{\bullet} \rightleftharpoons \text{oxyHb-SNO} \qquad (4.9)$$

Formation of a thiyl radical on Cysβ93 should produce an efficient scavenger of the NO released on reductive cleavage of GSNO. Since glutathiolation of Cysβ93 (Hb-SSG formation) (157) was not detected by mass spectrometry, the putative thiyl radical would have to be more reactive with NO than with the GSH generated in Reaction 4.3.

It is further proposed that at ~5 mM oxyHb, Reactions 4.8, 4.3 and 4.9 all occur within an oxyHb-CuZnSOD encounter complex. The proteins are presumably oriented with respect to each other within this complex to target or channel the nascent NO to the thiyl radical on Cysβ93 and thereby prevent its scavenging by the $Fe^{II}O_2$ heme (Reaction

4.5). Our key finding is that *all* the NO released from GSNO is targeted to Cysβ93 at physiological concentrations of oxyHb and CuZnSOD (Figures 4.3 and 4.6). When CuZnSOD is removed, and GSNO breakdown is catalyzed by added $CuSO_4$, the released NO is scavenged by both Cysβ93 (Figure 4.6b) and the $Fe^{II}O_2$ heme (Figure 4.4c). Thus, in the presence of CuZnSOD, the transient oxyHb-$S^{\bullet}$ would have to be formed close to the site of NO generation to prevent scavenging by the $Fe^{II}O_2$ heme. Such efficient channeling of NO would require the formation of an oriented encounter complex between oxyHb and CuZnSOD. Furthermore, since product analysis revealed that no GSSG was formed in the 3xDEAE-oxyHb/GSNO/CuZnSOD incubate (Figure 4.8b), the GSH generated *in situ* (Reaction 4.3) is not kinetically competitive with Cysβ93 as an electron donor to Cu^{II}ZnSOD. The dominance of Reaction 4.8 over Reaction 4.7 provides additional evidence for the formation of an encounter complex between the proteins, since positioning Cysβ93 close to the active site of CuZnSOD in an oxyHb-CuZnSOD complex would ensure that the protein-bound thiol acts as an electron donor to the Cu^{II}. Complex formation could also allow Cysβ93 (~10 mM) (45) to compete with GSH (~5 mM) (158) as an electron donor to Cu^{II}ZnSOD under physiological conditions although the kinetics are yet to be determined. On dilution of the reagents, most of the NO released from GSNO is scavenged by the $Fe^{II}O_2$ heme (Figure 4.5b), no Cysβ93 S-nitrosation is detected (Figure 4.7c), and GSSG is formed (data not shown) revealing that GSH is an electron donor. These observations suggest the absence of an oxyHb/CuZnSOD encounter complex at low Hb concentrations, and the loss of NO channeling to Cysβ93.

The levels of GSNO used here are up to 10^6-fold higher than those expected *in vivo*, which are generally reported to be in the nanomolar range (51,55,58,62,144). The mechanism of NO transfer from nanomolar GSNO to millimolar Hb cannot be probed *directly* using visible and infrared absorption measurements as done here. However, if 20 μM CuZnSOD monomer catalyzes the channeling of *all* NO from 3.25 or 7.5 mM GSNO to 7.5 mM Cysβ93 of oxyHb (Figures 4.3 and 4.6), we assume that it catalyzes the channeling of *all* NO from nanomolar GSNO to 10 mM Cysβ93 in RBCs. The critical factor for NO channeling suggested by the results reported here is the presence of oxyHb-CuZnSOD encounter complexes, which are expected to be present in similar concentrations in RBCs and in cell-free solutions containing 5 mM Hb and 20 μM CuZnSOD monomer.

Control of NO capture at Cysβ93 by the allosteric transition of Hb can also be rationalized based on Reaction 4.8. In T-state Hb, which occurs on release of O_2, Cysβ93 must be a poor electron donor to $Cu^{II}ZnSOD$ since high concentrations of GSSG were detected in the ESI mass spectrum of deoxyHb/GSNO incubates (138). This reveals that GSH formed *in situ* is the electron donor to $Cu^{II}ZnSOD$, and in the absence of thiyl radical formation on Cysβ93, the NO released (Reaction 4.3) is captured by the deoxyheme (Figure 4.4a) consistent with reports that Cysβ93 of deoxyHb is not S-nitrosated (124,138). In summary, the proposed reactions occurring in deoxyHb/GSNO incubates are the following:

$$GSH + Cu^{II}ZnSOD \rightleftharpoons \tfrac{1}{2}GSSG + Cu^{I}ZnSOD + H^{+} \qquad (4.7)$$

$$GSNO + Cu^{I}ZnSOD + H^{+} \rightleftharpoons GSH + NO + Cu^{II}ZnSOD \qquad (4.3)$$

$$NO + deoxyHb \rightleftharpoons nitrosylHb \qquad (4.10)$$

Since Cu^{II}-catalyzed RSNO formation is not kinetically competitive with disulfide formation for low-molecular-weight thiols (128,134), the $GS^{\bullet}$ radicals, formed as intermediates in Reaction 4.7, dimerize faster than they react with NO. This permits the nascent NO to be scavenged by the deoxyheme (Reaction 4.10) in deoxyHb/GSNO incubates as seen in Figure 4.4a.

Copper added as $CuSO_4$ is less efficient than CuZnSOD in catalyzing reductive cleavage of GSNO, giving rise to only ~50% yield of nitrosylHb within 5 min (Figure 4.4a). This could be explained by the binding of free Cu^{II} to Hb, which possesses two well-characterized copper binding sites (114), and/or complexation of Cu^{II} by GSSG (128). However, $CuSO_4$ is not only a less efficient catalyst of GSNO reductive cleavage, it also does not target *all* the NO released from GSNO to Cysβ93 in oxyHb incubates (Figures 4.4b and 4.6b). As mentioned previously, this observation supports channeling of NO from GSNO to Cysβ93 within an oxyHb-CuZnSOD encounter complex. Also, the NO spontaneously released from DEA/NO (44) is directed to the $Fe^{II}O_2$ heme (Figure 4.4d), presumably because no protein thiyl radicals are formed in oxyHb incubates with DEA/NO to scavenge the NO (Reaction 4.9).

To fully assess on a chemical basis the highly controversial hypothesis that Hb delivers NO to tissues in a pO_2-dependent manner (135), elucidation of the conditions that promote NO release from Cysβ93, as well as from nitrosylHb, is necessary. Hb denitrosation could conceivably also involve redox turnover of CuZnSOD. Using electrons donated from GSH (Reaction 4.7), Cu^{I}ZnSOD could catalyze Cysβ93-SNO

breakdown to give the free thiol and NO. This would be reversible for oxyHb, which undergoes Reactions 4.8 and 4.9, but not for deoxyHb, consistent with the proposal that O_2 release from Hb promotes NO release from Cysβ93 (56). We are currently investigating the stability of *preformed* Hb-SNO in the presence of CuZnSOD and different concentrations of GSH. Given the complexity of these reactions, to understand the possible mechanisms of Hb-SNO formation and breakdown *in vivo* it is necessary to separate the S-nitrosation and denitrosation steps.

4.6 Conclusions

Erythrocyte CuZnSOD may play a role in vasorelaxation by targeting NO to Cysβ93 of oxyHb and thereby preventing NO scavenging by the $Fe^{II}O_2$ heme at physiological concentrations of the proteins. The allosteric transition of Hb controls the products formed in CuZnSOD-catalyzed NO transfer from GSNO to Hb since NO is channeled to Cysβ93 in oxyHb incubates but scavenged by the heme in deoxyHb incubates. Although millimolar GSNO was used to *directly* probe the products formed, the results may also be relevant at physiological (nanomolar) GSNO concentrations since a critical factor appears to be the formation of an oxyHb-CuZnSOD encounter complex to ensure NO channeling. Conversion of NO to NO_3^-, which is non vasoactive, occurs in the absence of CuZnSOD or at oxyHb concentrations ~10^3-fold below physiological values, conditions that may eliminate or disrupt oxyHb-CuZnSOD complexation.

The results presented here may also hold far-reaching implications in cell signaling. Like protein phosphorylation, protein S-nitrosation may represent a fundamental mechanism for the reversible post-translational control of protein activity

and cellular function (159). The reaction scheme defined by eqns 4.8, 4.3 and 4.9 suggests a general mechanism for selectively in protein S-nitrosation. Only proteins with cysteine residues that can act as donors to an NO-transferase such as CuZnSOD will be S-nitrosated. Co-localization of the donor and transferase, as occurs in RBCs for oxyHb and CuZnSOD, will promote S-nitrosation of the target, which in the present *in vitro* study serves to prevent the conversion of NO to NO_3^-.

4.7 Acknowledgements

This research was supported by grants from CIHR, NSERC (Canada), FQRNT (Quebec) to A. M. E. and J. A. C., and by a Graduate Fellowship (Concordia University) to A. A. R. We would like to thank Professor Eric Salin and Margaret Antler from the Department of Chemistry, McGill University, for helping us with the ICP-MS measurements and for the use of their ICP-MS instrumentation. Drs Jeff Agar and Heather Durham from the Montreal Neurological Institute are thanked for their help in the Western blotting experiments.

5.0 Heme Nitrosylation of Deoxyhemoglobin by S-Nitrosoglutathione Requires Copper

5.1 Abstract

NO reactions with hemoglobin (Hb) likely play a role in blood pressure regulation. For example, NO exchange between Hb and S-nitrosoglutathione (GSNO) has been reported *in vitro*. Here we examine the reaction between GSNO and deoxyHb ($HbFe^{II}$) in the presence of both Cu^{I} (neocuproine) and Cu^{II} (DTPA) chelators, and using a Cu-depleted Hb solution. Spectroscopic analysis of deoxyHb/GSNO incubates show prompt formation (<5 min) of ~100% heme-nitrosylated Hb ($HbFe^{II}NO$) in the absence of chelators, 46% in the presence of DTPA and 25% in the presence of neocuproine. Negligible (<2%) nitrosylHb ($HbFe^{II}NO$) was detected when neocuproine was added to Cu-depleted deoxyHb/GSNO incubates. Thus, nitrosylHb formation *via* a mechanism involving *free* NO generated by Cu^{I}-catalysis of GSNO breakdown is proposed. GSH is a source of reducing equivalents since extensive GSSG was detected in deoxyHb/GSNO incubates in the absence of metal chelators. No S-nitrosation of deoxyHb was detected under any conditions. In contrast, the NO released from GSNO is directed to Cysβ93 of oxyHb in the absence of chelators but only metHb formation is observed in the presence of chelators. Our findings reveal that the reactions of GSNO and Hb are controlled by copper, and that metal chelators do not fully inhibit NO release from GSNO in Hb-containing solutions.

5.2 Introduction

Possible exchange of NO between thiols and hemoglobin (Hb) in red blood cells (RBCs) has been the focus of intense interest recently (60,66). It has been suggested that GSNO or CysSNO could act as an NO^+ donor to Cysβ93 of oxyHb ($HbFe^{II}O_2$) in a *trans*-S-nitrosation reaction (58). However, we have shown that free NO must first be released from GSNO (134), the S-nitroso form of the dominant thiol in the RBC(120), or CysSNO (unpublished work) in a Cu^I-catalyzed reaction. S-nitrosation of Cysβ93 then occurs in a Cu^{II}-catalyzed reaction (134) as reported also for Cys34 of bovine serum albumin (BSA) (137). For Hb to function as a blood-pressure regulator in an O_2-sensitive manner, release of NO from Cysβ93 of deoxyHb is necessary (160). One possibility is that NO is delivered to tissues *via* S-nitrosation from Cysβ93 to GSH or another thiol (161) that promotes NO transport across the RBC:

$$\text{Hb-SNO} + \text{RSH} \rightleftharpoons \text{Hb-SH} + \text{RSNO} \qquad (5.1)$$

Recently it has been suggested that delivery to tissues of all the NO bound to Cysβ93 of Hb would result in extensive vasodilation which would be fatal (63). Hence, it was proposed that most of the NO released from Cysβ93 is actually captured by deoxyHb. Capture of NO released from GSNO is also possible and would compete with the exit of NO from the RBC. In fact, Spencer and coworkers reported direct reductive cleavage of GSNO by deoxyHb and capture of the released NO by another Fe^{II} center ($Hb'Fe^{II}$) (124):

$$HbFe^{II} + \text{GSNO} + H^+ \rightleftharpoons HbFe^{III} + \text{GSH} + \text{NO} \qquad (5.2)$$

$$Hb'Fe^{II} + NO \rightleftharpoons Hb'Fe^{II}NO \qquad (5.3)$$

A trace amount of Cu^{I} serves as a highly efficient catalyst of RSNO breakdown (7). We have suggested that neocuproine, a Cu^{I}-specific chelator, inhibits NO release from GSNO in solutions of oxyHb (134). Therefore, we considered it likely that neocuproine would also inhibit NO release from GSNO in solutions containing deoxyHb. To distinguish between direct reductive cleavage of GSNO by deoxyHb (Reaction 5.2) and Cu^{I}-catalyzed release (Reaction 5.4), it is necessary to remove all trace Cu or prevent its turnover *via* redox cycling using GSH (Reaction 5.5) or another donor in the Hb-containing solutions.

$$Cu^{I} + GSNO + H^{+} \rightleftharpoons Cu^{II} + GSH + NO \qquad (5.4)$$

$$Cu^{II} + GSH \rightleftharpoons Cu^{I} + \tfrac{1}{2}\,GSSG + H^{+} \qquad (5.5)$$

Here we report the results of a detailed examination of deoxyHb/GSNO incubates after 5 min in the presence of preferential chelators of Cu^{I} (neocuproine) and Cu^{II} (DTPA). Solutions of deoxyHb that were not dialyzed and solutions that underwent exhaustive dialysis *vs* EDTA were used. Our direct spectroscopic and ESI-mass spectrometric analyses reveal that NO release from GSNO is <2% in the presence of neocuproine in deoxyHb/GSNO solutions containing dialyzed Hb. NitrosylHb formation, and hence GSNO breakdown, is ~100% within 5 min in the absence of chelators. NitrosylHb formation is decreased by ~50 to 75% in the presence of DTPA and neocuproine, and in solutions containing dialyzed Hb without neocuproine. Since trace

copper was found in all reagents by ICP-MS, these observations are consistent with Cu^{I}-catalyzed release of NO (Reaction 5.4).

The source of the reducing equivalents for the prompt Cu^{I}-catalyzed reductive cleavage of GSNO is also of interest. Extensive GSSG was formed in deoxyHb/GSNO incubates in the absence of metal chelators indicating that GSH is the main source of reducing equivalents under these conditions (Reaction 5.5). Less than expected GSSG was detected by ESI-MS in deoxyHb/GSNO incubates containing DTPA although ~50% GSNO breakdown was observed. This suggested deoxyHb as a possible additional source of reducing equivalents to $[Cu^{II}(DTPA)]^{2-}$ since related EDTA complexes were shown to be redox-active with Hb (162). Careful examination of the absorption (optical and FTIR) spectra revealed the presence of metHb. Thus, our results indicate that the direct reduction of GSNO by deoxyHb is unlikely to play a role in NO transport in RBCs. Nonetheless, deoxyHb may indirectly provide a source of electrons for the reductive cleavage of GSNO or other RSNOs *in vivo*.

The realization that commonly used Cu^{I} (neocuproine) and Cu^{II} chelators (EDTA, DTPA) may not always prevent Cu turnover is an important consideration in deciphering mechanisms of S-nitrosothiol signaling and NO biochemistry in general. Although neocuproine, a tight-binding Cu^{I} chelator (K_d = 1.2 x 10^{-19} M^2) (139,163), is a better inhibitor than DTPA of GSNO breakdown (Reaction 5.4) in Hb-containing solutions, dialysis of the Hb samples as well as neocuproine addition, was necessary to obtain negligible GSNO breakdown.

Finally, the prompt changes in oxyHb on incubation with GSNO are compared to those observed for the deoxyHb incubates. The key results of this comparison are that in

the absence of chelators, S-nitrosation of Cysβ93 of the oxy protein is extensive, and this competes with NO capture by the $Fe^{II}O_2$ heme to form metHb and NO_3^-. In contrast, no S-nitrosation of the deoxy protein is detected suggesting that *all* NO released from GSNO is captured by the Fe^{II} heme.

5.3 Experimental Procedures

5.3.1 Materials

Human hemoglobin A was obtained from Sigma and used without further purification. Nanopure water (specific resistance 18 MΩ-cm), obtained from a Millipore Simplicity water purification system and treated with Chelex-100 (Sigma) to remove trace metal ions, was used to prepare all H_2O solutions. Reactions were carried out in 200 mM sodium phosphate buffer, pH 7.2 (NaPi) prepared from sodium phosphate salts (Fisher) in nanopure H_2O. Stock solutions of 15 mM diethylenetriamine-N,N,N',N",N"-pentaacetic acid (DTPA, ICN) and 650 μM 2,9-dimethyl-1,10-phenanthroline (neocuproine, Sigma) were prepared in NaPi. Stock solutions of 250 mM GSNO [glycine, N-(N-L-γ-glutamyl-S-nitroso-L-cysteinyl), Cayman] in NaPi were prepared just before use in a glove bag (Aldrich) under nitrogen, and the GSNO concentrations determined spectrophotometrically ($\varepsilon_{333.5}$ = 774 M^{-1} cm^{-1}) (146). GSH and GSSG were obtained from Sigma, and N_2 and NO gases from Praxair. NO was purged into a 10% KOH water solution before use (164).

5.3.2 Methods

5.3.2.1 Preparation and Optical Spectroscopy of Hb Samples

Typically 1 g of lyophilized metHb ($HbFe^{III}$) from the bottle was dissolved in 2 mL of NaPi. After 2 min centrifugation at 12,000 rpm the precipitate was discarded and the dark-red solution of metHb stored at 4°C prior to use. An aliquot (10 μL) of the Hb solution was pipetted onto a 13-mm CaF_2 window of a dismountable FTIR-type cell (Harrick). The cell was immediately assembled using a 6-μm Teflon spacer (Harrick) and placed in a custom-made bracket in a Beckman DU 650 UV-Vis spectrophotometer. metHb concentrations were found to be 32 mM in heme assuming $\varepsilon_{500\ nm} = 10$ and $\varepsilon_{630\ nm} = 4.4\ mM^{-1}\ cm^{-1}$ per heme (147,148). This was confirmed by diluting the samples 10^3-fold, adding potassium ferricyanide and excess KCN (BDH) and reading the absorbance of the CN^- adduct at 540 nm ($\varepsilon_{540} = 11.0\ mM^{-1}\ cm^{-1}$ per heme) in a 1-cm cuvette on the Beckman instrument.

DeoxyHb was prepared in the glove bag under N_2 by treating metHb with equimolar sodium dithionite (Fisher) (125) followed by desalting on a 1.6 x 2.5-cm HiTrap Sephadex G-25 column (Amersham Pharmacia), and the deoxyHb concentration was calculated using $\varepsilon_{555\ nm} = 12.5\ mM^{-1}cm^{-1}$ per heme (48). OxyHb was prepared from deoxyHb by introducing a small volume of air into the sample using a syringe; for example, 720 μL of air was added to 200 μL of a 32-mM heme sample. A single addition of O_2 in slight excess (8.5 μmol of O_2 per 8 μmol of heme) yielded fully oxygenated Hb as indicated by the Soret spectrum recorded following a 5-min equilibration. NitrosylHb and nitrosylmetHb were prepared from deoxyHb and metHb on exposure to NO gas. Optical spectra were recorded using a scan time of 1200 nm/min. Use of the FTIR-type cell to record the optical spectra of the products formed in the deoxyHb/GSNO incubates

allowed measurements to be made at close to physiological concentrations of Hb (2-4 mM) (165).

5.3.2.2 Preparation of Dialyzed Hb samples

Approximately 500 mg of metHb was dissolved in 5 mL of 100 mM Na_2EDTA (Sigma), pH 7.0, and allowed to stand for 30 min. This solution was dialyzed at 4°C *vs* 500 mL of 10 mM Na_2EDTA, pH 7.0, which was replaced with fresh solution 6 times in 24 h. The dialysis was continued *vs* EDTA-free H_2O, which was replaced with fresh solution 12 times in 48 h. After dialysis, metHb was lyophilized and dissolved in NaPi to a concentration of 30 mM heme.

5.3.2.3 ICP-MS Analysis

A PE Sciex Elan 6000 inductively coupled plasma mass spectrometer (ICP-MS) with cross-flow nebulizer and Scott-type spray chamber was used to determine the amount of Cu in the Hb and GSNO samples and in the buffers (Table 5.1). The RF power was 1000 W and the argon flow 0.85 L/min, which gave the best sensitivity as determined by the recommended optimization procedure. The optimum lens voltage was determined by maximizing rhodium sensitivity, and data were acquired in the pulse-count mode (166). Stock Hb solutions in NaPi were added to 50 µL of 30% H_2O_2 (ACP) and 500 µL of concentrated HNO_3 (Omni*Trace* Ultra high purity, EM Science) to give a final heme (Fe) concentration of 4.3 mM, and the samples were ashed using a Bunsen burner. The residue was dissolved in 10 mL of 5% (v/v) HNO_3, and ICP-MS analyses for Cu and Fe were performed. An internal standard of 9 nM (0.500 ppb) Mn prepared from a 1000

ppm Mn standard solution (ACP) was added to all solutions. Standard curves were prepared by diluting 1000 ppm Cu and Fe standard solutions (ACP) in 5% (v/v) HNO_3 and nanopure water to give 0-8 μM (0-0.500 ppm) Cu and 0-9 μM (0-0.500 ppm) Fe. All reported ICP-MS data are the result of at least triplicate experiments, and in all cases the standard deviations were <5%.

5.3.2.4 FTIR Analysis

Approximately 20 μL Hb (28 mM heme) in NaPi was added by syringe onto a 13-mm CaF_2 window in the glove bag under N_2 where necessary. The FTIR cell was immediately assembled with a 250-μm Teflon spacer (Harrick), and the spectra were recorded at 25°C on a Nicolet Magna-IR 550 spectrometer with a MCT detector cooled to 77 K and purged with dry air from a Whatman FTIR Purge (Model 75-52). All reported spectra are an average of 500 scans recorded in 5.52 min at a resolution of 2 cm^{-1} using a Happ-Genzel apodization with a velocity and aperture of 4.4303 cm/s and 2, respectively. Omnic (Nicolet) software was used for subtraction, baseline correction, smoothing, and Fourier transform self-deconvolution employing a half-width-at-half-height of 0.6 cm^{-1} and an enhancement (K factor) of 1. Subtraction of water-vapor absorption from the spectra was performed by the method of Dong *et al.* (91,167).

5.3.2.5 ESI-MS Analysis

Stock Hb solutions (28 mM heme) in NaPi were diluted 10^{-3}-fold with H_2O to give ~0.5 μg/μL protein. Aliquots were infused into the ESI source of the mass

Table 5.1. ICP-MS analysis of Cu in stock solutions

Sample[a]	Cu (μM)	Cu (ppm)
5 mM Hb[b]	19 ± 3	1.207 ± 0.191
5 mM dialyzed Hb[c]	2.0 ± 0.7	0.127 ± 0.045
250 mM GSNO	1.2 ± 0.8	0.076 ± 0.050
250 mM GSH	1.0 ± 0.6	0.063 ± 0.038
250 mM GSSG	1.1 ± 0.7	0.070 ± 0.044
15 mM DTPA	0.7 ± 0.3	0.044 ± 0.019
650 μM neocuproine	1.6 ± 0.5	0.102 ± 0.032
200 mM NaPi buffer	0.9 ± 0.7	0.057 ± 0.044

[a] All stock solutions were prepared in 200 mM sodium phosphate buffer (pH 7.2)

[b] Human Hb (Sigma) from the bottle; 5 mM Hb contains 20 mM heme

[c] Human Hb following dialysis *vs* EDTA (see Section 5.3.2.2)

spectrometer (ThermoFinnigan SSQ7000) by flow injection from the HPLC (Agilent 1090) using a 100 μL loop (but no column) at 50 μL/min with 75% CH_3CN (0.05% TFA) as a mobile phase. Stock (250 mM) GSH, GSNO and GSSG solutions in 200 mM NaPi (pH 7.2) were diluted 500-fold with H_2O and 10-fold to 50 μM with 75% CH_3CN (0.05% TFA) and their mass spectra obtained as for the Hb solutions.

5.3.2.6 Multi-Component Analysis of the Optical Spectra of Incubates

The absorbance at a given wavelength is the sum of the absorbances (A) of all species at that wavelength: $A = A_x + A_y + A_z + \quad = \varepsilon_x b [X] + \varepsilon_y b [Y] + \varepsilon_z b [Z] + \quad$, where ε_x is the molar extinction of X at the selected wavelength, b the pathlength (6 μm) and [X] the molar concentration of X. Assuming a limited number of oxidation and coordination states for Fe of Hb, the spectra recorded for the incubates were mathematically disassembled into those of their components. Absorbances at the Soret maxima of the Hb species were used to generate n Beer's law expressions from which the concentrations ([X], [Y], [Z],) of the n species present in the incubates were obtained. Solutions to the *n* equations with *n* unknowns were obtained using a program at http://www.1728.com/indexalg.htm. For the deoxyHb/GSNO incubates, absorbances were recorded at the Soret maxima of the expected heme species metHb, nitrosylmetHb, nitrosylHb and deoxyHb. The millimolar extinction coefficients (ε, mM^{-1} cm^{-1}) and wavelengths (nm; in parentheses) used are the following: 169 (405), 110 (416), 97 (418), 50 (430) for metHb; 95.5 (405), 129 (416), 130 (418), 95 (430) for nitrosylHb; 113 (405), 137 (416), 136 (418), 64 (430) for nitrosylmetHb; and 62 (405), 92 (416), 99 (418), 133 (430) for deoxyHb. The corresponding values for the expected Fe states in the were

recorded at the Soret maxima of the expected heme species metHb, nitrosylmetHb, nitrosylHb and deoxyHb. The millimolar extinction coefficients (ε, mM^{-1} cm^{-1}) and wavelengths (nm; in parentheses) used are the following: 169 (405), 110 (416), 97 (418), 50 (430) for metHb; 95.5 (405), 129 (416), 130 (418), 95 (430) for nitrosylHb; 113 (405), 137 (416), 136 (418), 64 (430) for nitrosylmetHb; and 62 (405), 92 (416), 99 (418), 133 (430) for deoxyHb. The corresponding values for the expected Fe states in the oxyHb/GSNO incubates are: 169 (405), 116 (415) for metHb; and 102 (405), 125 (415) for oxyHb. The spectra of the components and mixtures were graphed using Origin 6.0 software (Microcal).

5.4 Results

5.4.1 ICP-MS Analysis

Since the stability of S-nitrosothiols is highly dependent on the Cu content, all solutions were examined by ICP-MS for trace Cu. The results are summarized in Table 5.1, which reveal that 19 μM Cu was found in 5 mM Hb (20 mM heme) solutions. This decreased to 2 μM Cu following dialysis *vs* EDTA. NaPi buffer (200 mM) and the 250 mM stock solutions of GSH and its derivatives were found to contain ~1 μM Cu (Table 5.1). These values differ from those reported previously using atomic absorption spectroscopy, where ~50 μM Cu was found in solutions containing 5 mM Hb, but <1 μM Cu in 5 mM dialyzed Hb as well as in NaPi (134). Since ICP-MS is more sensitive, more accurate and did not show matrix effects (as verified using a Mn internal standard) compared to atomic absorption spectroscopy (168), the present Cu analyses are considered more reliable.

5.4.2 Optical Absorption Spectra

Figure 5.1a compares the spectra of deoxyHb and metHb and their NO adducts in the Soret and visible regions. As expected, high-spin Fe^{II} and Fe^{III} hemes exhibit Soret maxima at 430 and 405 nm, respectively, and visible bands at 556 (Fe^{II}) and 500, 540 and 580 nm (Fe^{III}). Soret maxima are observed at 418 nm (ε = 130 mM^{-1} cm^{-1}; $Fe^{II}NO$) and 416 nm (ε = 137 mM^{-1} cm^{-1}; $Fe^{III}NO$) for the heme-NO adducts of Hb. The corresponding visible bands are at 545 and 575 nm ($Fe^{II}NO$), and 540 and 565 nm ($Fe^{III}NO$). These values agree with those reported previously (125,169). The products formed on mixing deoxyHb and GSNO under anaerobic conditions were directly probed by comparing their spectra with those in Figure 5.1a. Evidence for heme-iron nitrosylation is clearly seen in the Soret and visible bands of the deoxyHb/GSNO incubates without chelators (Figure 5.1b). The Soret maximum blue-shifted from 430 to ~418 nm within 5 min of mixing deoxyHb and GSNO and the visible region resembles that of nitrosylHb in Figure 5.1a. Multi-component analysis of the 5-min spectrum reveals almost complete conversion of deoxyHb to nitrosylHb (Table 5.2). Thus, rapid release of NO from GSNO occurred in the deoxyHb/GSNO sample.

Heme nitrosylation is also evident 5 min after mixing deoxyHb and GSNO in the presence of 200 μM DTPA (Figure 5.1c). The extent of nitrosylation is less since the blue-shifting of the Soret maximum is less and the visible maximum of deoxyHb at 556 nm is still evident, indicating that DTPA decreases the amount of NO released from GSNO. Multi-component analysis of the spectrum of the 5-min deoxyHb/GSNO/DTPA incubate reveals the presence of 46% nitrosylHb, 44% deoxyHb, 8.5% metHb and 1%

Figure 5.1. Effect of 15 mM GSNO and metal chelators on the visible absorption spectra of 15 mM (heme) deoxyHb. (**a**) metHb (—), nitrosylmetHb (. . .), nitrosylHb (- . -) and deoxyHb (- - -). (**b**) deoxyHb (- - -), deoxyHb + GSNO after 5 min (—). (**c**) deoxyHb (- - -), and deoxyHb + GSNO + 200 μM DTPA after 5 min (- - -). (**d**) deoxyHb (- - -), and deoxyHb + GSNO + 150 μM neocuproine after 5 min (- - -). (**e**) dialyzed deoxyHb (- - -), and dialyzed deoxyHb + GSNO after 5 min (—). (**f**) dialyzed deoxyHb (- - -), and dialyzed deoxyHb + GSNO + 150 μM neocuproine after 5 min (—). All spectra were recorded in 200 mM sodium phosphate buffer (pH 7.2) at 25°C in a FTIR cell with a 6-μm Teflon spacer using a scan time of 1200 nm/min.

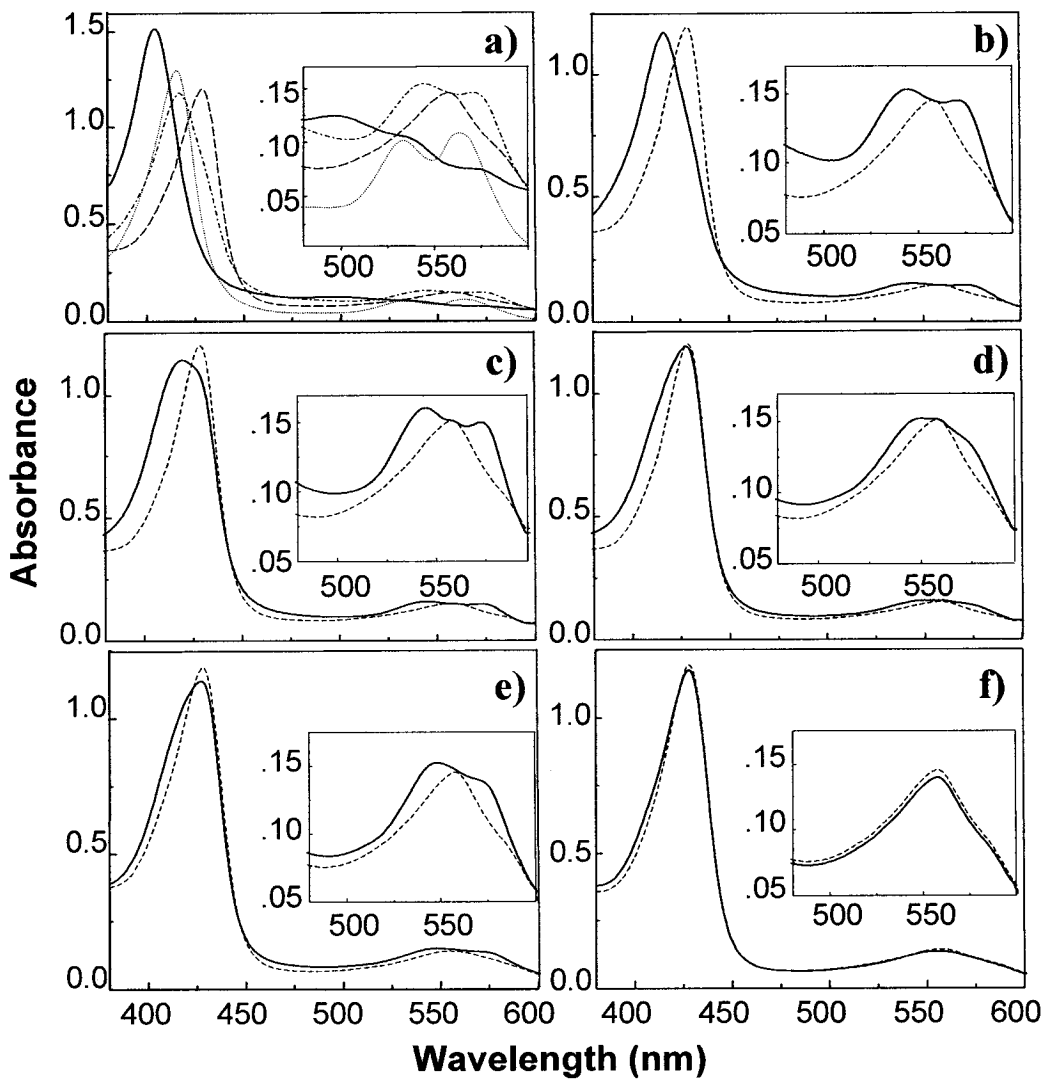
a)
b)
c)
d)
e)
f)
Absorbance
Wavelength (nm)
0.0
0.5
1.0
1.5
.05
.10
.15
400
450
500
550
600

nitrosylmetHb (Figure 5.2a and Table 5.2). When deoxyHb and GSNO were mixed in the presence of neocuproine, the spectral changes revealed that significantly less heme nitrosylation occurred (Figure 5.1d) than in the presence of DTPA, which was confirmed by multi-component analysis (Table 5.2). Approximately 33% heme nitrosylation was found in the incubate of dialyzed deoxyHb in the absence of chelators (Figure 5.1e and Table 5.2), but addition of 150 μM neocuproine essentially shut down NO release from GSNO (Figure 5.1f) since 98% deoxyHb was found in the 5-min incubate of dialyzed-deoxyHb/GSNO/neocuproine (Table 5.2). To compare the heme species formed in deoxyHb/GSNO incubates with those formed in oxyHb/GSNO incubates, the spectra of the latter were recorded. The Soret spectra of oxyHb/GSNO (Figure 5.3a and c) reveal that metHb is formed within 5 min, and multi-components analysis uncovered the presence of ~46% metHb and ~54% oxyHb (Table 5.2). Significantly less metHb formation is detected following mixing of oxyHb with GSNO in the presence of DTPA (Figure 5.3b). This is confirmed by multi-component analysis of the 5-min spectrum, which reveals only 23% and 12% metHb formation in oxyHb/GSNO incubates containing DTPA and neocuproine, respectively. The formation of metHb likely occurs from the well characterized reaction of free NO and oxyHb (16,40):

$$\text{oxyHb} + \text{NO} \rightleftharpoons \text{metHb} + \text{NO}_3^- \qquad (5.6)$$

5.4.3 **FTIR Spectra**

Table 5.2. Hb species present in Hb/GSNO incubates[a] based on analysis of their visible spectra[b]

Incubate	DeoxyHb mM	MetHb mM	NitrosylHb mM	NitrosylmetHb mM	oxyHb mM
DeoxyHb/GSNO	0.15		14.85		
DeoxyHb/GSNO/DTPA	6.59	1.28	6.97	0.16	
DeoxyHb/GSNO/neo	11.2		3.8		
DeoxyHb(dial)/GSNO[c]	10.05		4.95		
DeoxyHb(dial)/GSNO/neo	14.72		0.28		
OxyHb/GSNO		6.85			8.15
OxyHb/GSNO/DTPA		3.5			11.5
OxyHb/GSNO/neo		1.8			13.2

[a] 15 mM (heme) Hb plus 15 mM GSNO were incubated at room temperature in 200 mM NaPi buffer (pH 7.2).with 200 μM DTPA and 150 μM neocuproine where indicated. Spectra were recorded 5 min after the start of the incubation

[b] The wavelengths used in the multi-component analysis were the Soret maxima of the expected components and the extinction coefficients are given in Section 5.3.2.6

[c] DeoxyHb(dial) was dialyzed *vs* EDTA (see Section 5.3.2.2)

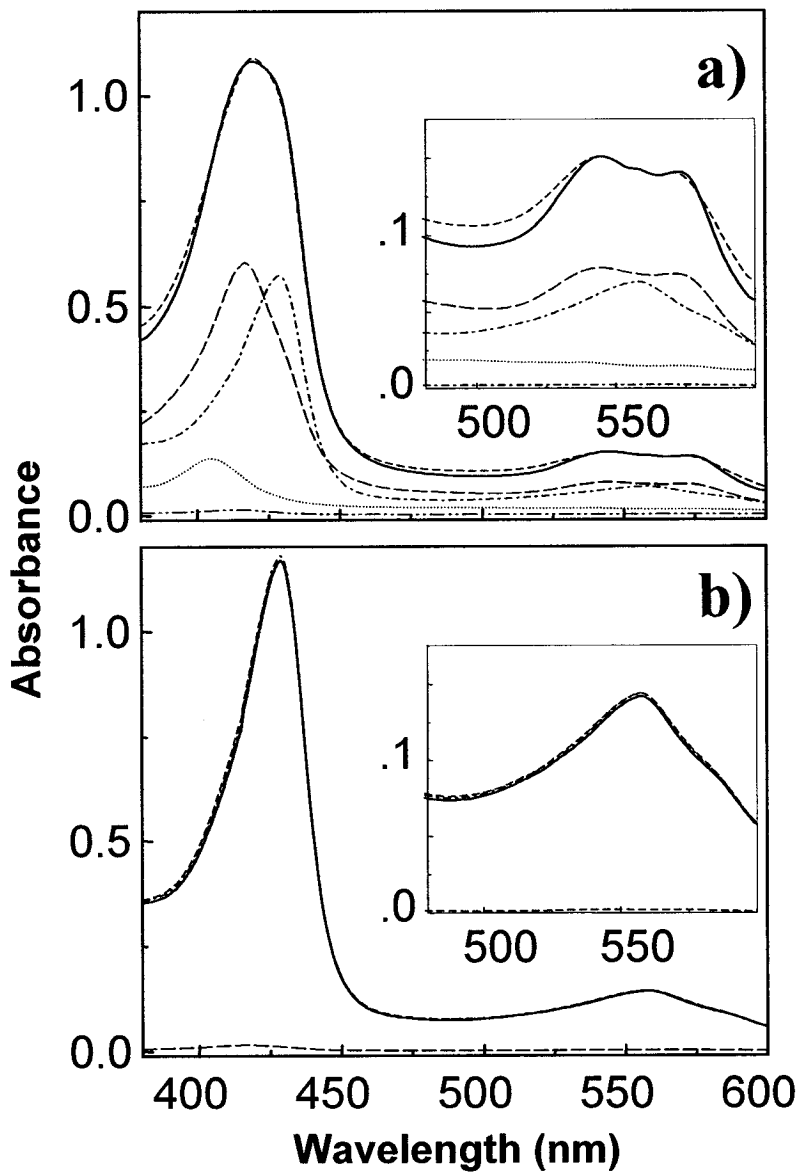

Figure 5.2. Multi-component analysis of mixtures of the visible absorption spectra obtained 5 min after mixing 15 mM (heme) deoxyHb and 15 mM GSNO. (a) Observed spectrum from Figure 5.1c for deoxyHb + GSNO + DTPA (—); sum (- - -) of the spectra of 1.28 mM metHb (. . .), 0.16 mM nitrosylmetHb (- . . -), 6.97 mM nitrosylHb (— — —) and 6.59 mM deoxyHb (- . -). **(b)** Observed spectrum from Figure 5.1f for dialyzed deoxyHb + GSNO + 150 μM neocuproine (—); sum (- - -) of the spectra of 0.28 mM nitrosylHb (— — —) and 14.72 mM deoxyHb (- . -).

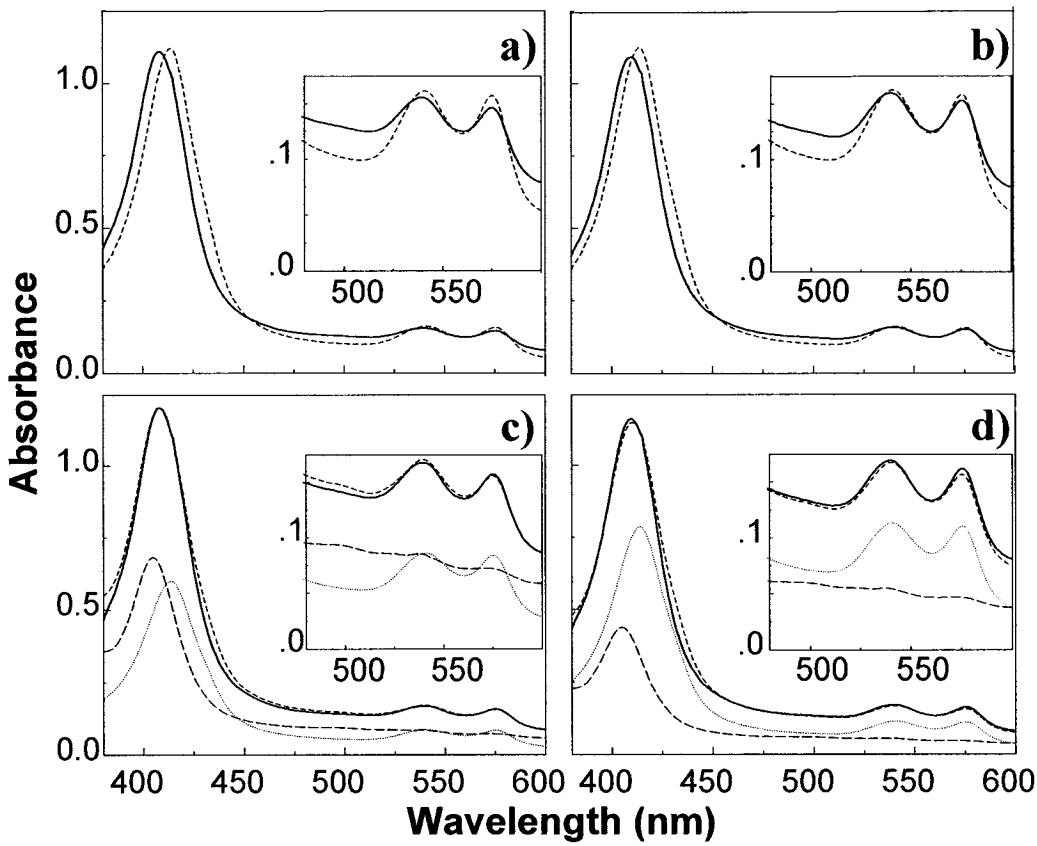

Figure 5.3. Effect of 15 mM GSNO and DTPA on the visible absorption spectra of 15 mM (heme) oxyHb. (a) oxyHb (- - -), and oxyHb + GSNO after 5 min (—). **(b)** oxyHb (- - -) and oxyHb + GSNO + 200 μM DTPA after 5 min (—). **(c)** Observed spectrum from 5.3a for oxyHb + GSNO after 5 min (—); sum (- - -) of the spectra of 6.85 mM metHb (— — —) and 8.15 mM deoxyHb (. . .). **(d)** Observed spectrum from 5.3b for oxyHb + GSNO + 200 μM DTPA after 5 min (—); sum (- - -) of the spectra of 3.1 mM metHb (- - -) and 11.9 mM deoxyHb (. . .). See Figure 5.1 for experimental details.

Fourier transform infrared (FTIR) spectroscopy is a valuable probe of protein thiols since the SH stretching vibration ν(SH) falls in a spectral window (~2500 cm^{-1}) with minimum H_2O and protein absorption (90,122,123). Although ~5 mM Hb is necessary to observe the weak IR ν(SH) absorption (90,122,123), comparable Hb concentrations are found in RBCs (~3 mM) (165). The FTIR spectrum of deoxyHb in the ν(SH) region recorded in the absence and presence of GSNO and metal chelators (Figure 5.4a, spectrum 1) exhibits the three ν(SH) peaks at 2576, 2563, and 2558 cm^{-1} assigned previously to Cysβ93, Cysβ112 and Cysα104, respectively (90,123).

The spectrum of deoxyHb plus GSNO (Figure 5.4a, spectrum 4) exhibits a peak for Cysβ93 ν(SH) at 2584 cm^{-1}, which is close to that of nitrosylHb (2585 cm^{-1}). The ν(SH) band for Cysβ93 is also at 2584 cm^{-1} in the deoxyHb/GSNO/DTPA spectrum (Figure 5.4a, spectrum 5), but in the presence of *both* DTPA and neocuproine (Figure 5.4a, spectrum 2) Cysβ93 possesses the same ν(SH) (2576 cm^{-1}) as deoxyHb alone (Figure 5.4a, spectrum 1). These results corroborate those from the analysis of the visible spectra, which revealed that the major Hb species are nitrosylHb and deoxyHb in the 5-min deoxyHb /GSNO incubates in the presence of DTPA and neocuproine, respectively. Furthermore, no evidence for Hb-SNO formation is seen in Figure 5.4a, since the ν(SH) absorption of Cysβ93 does not appear to lose intensity on exposure to GSNO (Figure 5.4a, spectrum 1 *vs* 2, 3 and spectrum 6 *vs* 4, 5).

Loss of Cysβ93 ν(SH) absorption is clearly evident in Figure 5.4b, spectrum 1. Thus, Hb-SNO formation does occur in the oxyHb/GSNO incubates in the absence of metal chelators as we reported previously (134). Addition of DTPA prevents loss of Cysβ93 ν(SH) intensity but the spectrum is not identical to that of oxyHb alone (Figure

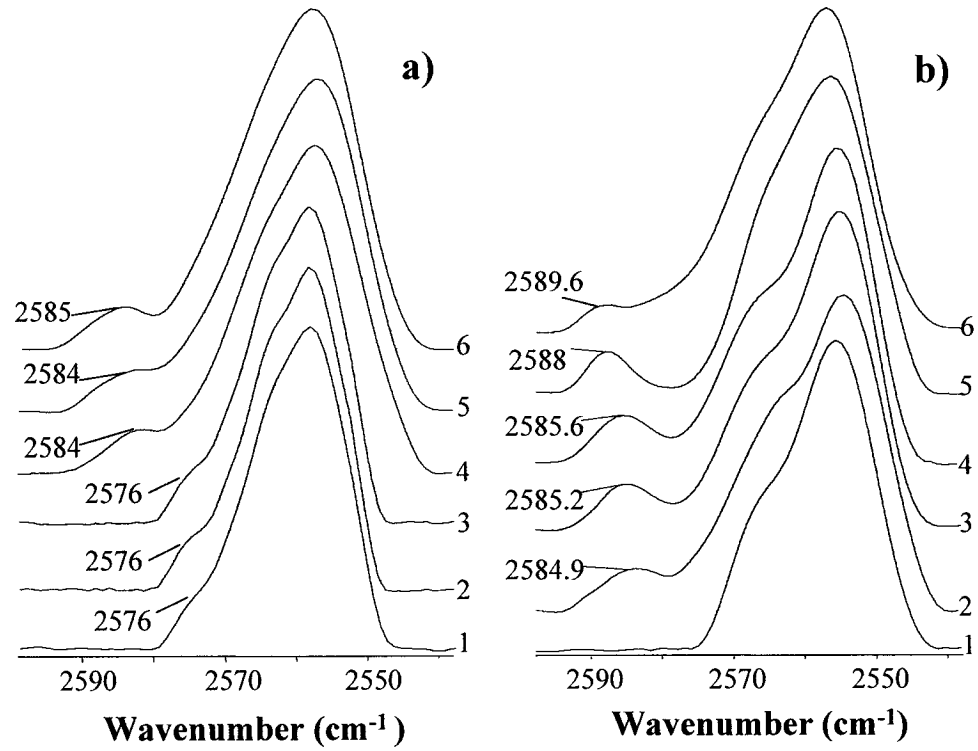

Figure 5.4. Effect of 28 mM GSNO and metal chelators on the FTIR spectra in the ν(SH) region of 28 mM (heme) Hb. (a) Spectrum 1, deoxyHb; spectrum 2, deoxyHb + GSNO + 200 μM DTPA + 150 μM neocuproine; spectrum 3, deoxyHb + GSNO + 150 μM neocuproine; spectrum 4, deoxyHb + GSNO; spectrum 5, deoxyHb + GSNO + 200 μM DTPA; spectrum 6, nitrosylHb. **(b)** Spectrum 1, oxyHb + GSNO; spectrum 2, oxyHb + GSNO + 200 μM DTPA; spectrum 3, oxyHb + GSNO + 150 μM neocuproine; spectrum 4, oxyHb; spectrum 5, nitrosylmetHb; spectrum 6, metHb. All spectra were recorded in a 250-μm pathlength FTIR cell 5 min after mixing Hb and GSNO in 200 mM sodium phosphate buffer (pH 7.2) at 25°C, and are the average of 500 scans at 2-cm^{-1} resolution. Background subtraction, baseline correction, smoothing and Fourier transform self-deconvolution were performed on the displayed spectra (see Section 5.3.2.4).

5.4b, spectrum 2 *vs* 4). Direct monitoring of the heme shows 23% conversion of oxyHb to metHb within 5 min in the oxyHb/GSNO/DTPA incubate (Figure 5.3, and Table 5.2). Thus, the FTIR data confirm that DTPA does not prevent release of NO from GSNO (Reaction 5.4), but it does inhibit S-nitrosation of Cysβ93 (Figure 5.4b, spectrum 2 *vs* 1). The FTIR spectrum of the oxyHb/GSNO/neocuproine incubate is essentially identical to that of oxyHb alone (Figure 5.4b, spectrum 3 *vs* 4), which is consistent with the optical results where 88% oxyHb was found in the neocuproine incubate (Table 5.2).

5.4.4 Mass Spectral Analysis

ESI-MS was used to probe Hb-SNO formation in the deoxyHb/GSNO incubates (134). No peak corresponding to S-nitrosation of the β-subunit of deoxyHb was observed under any conditions with or without metal chelators (Figure 5.5a), or in the dialyzed deoxyHb samples. On the other hand, S-nitrosation of the β-subunit was detected following incubation of oxyHb with GSNO in the absence of metal chelators (Figure 5.5b), but not in their presence (data not shown). These MS results support those from FTIR spectroscopy in that Hb-SNO is formed only in the oxyHb/GSNO incubates in the absence of metal chelators (Figure 5.4b, spectrum 1).

In the low-m/z region of the ESI mass spectra, the low-molecular-weight products formed in the deoxyHb/GSNO incubates can be monitored. In the absence of metal chelators, a weak GSNO (m/z 337) and an intense GSSG peak (m/z 613) are observed (Figure 5.6b), which are not present in the spectrum of Hb alone (Figure 5.6a). In mass spectrum of the deoxyHb/GSNO/neocuproine incubate (Figure 5.6d), GSNO is the

Figure 5.5. Deconvolved electrospray mass spectra of the heme-free Hb subunits following incubation with GSNO. (a) deoxyHb + GSNO; **(b)** oxyHb + GSNO. Experimental conditions: Hb and GSNO were incubated in 200 mM NaPi buffer (pH 7.2) for 5 min at 25°C and diluted 10^{-3}-fold with H_2O to give 28 μM heme (~0.5 μg/μL Hb) and 28 μM GSNO. Aliquots (100 μL) were infused into the electrospray source of the mass spectrometer by flow injection at 50 μL/min with 75% CH_3CN (0.05% TFA) as a mobile phase. The capillary temperature was 180°C and the spray voltage 4.0 kV. Under the MS conditions, Hb dissociated into free heme and α- and β-subunits. The unresolved shoulders on the subunit peaks at high mass are due to sodium adducts.

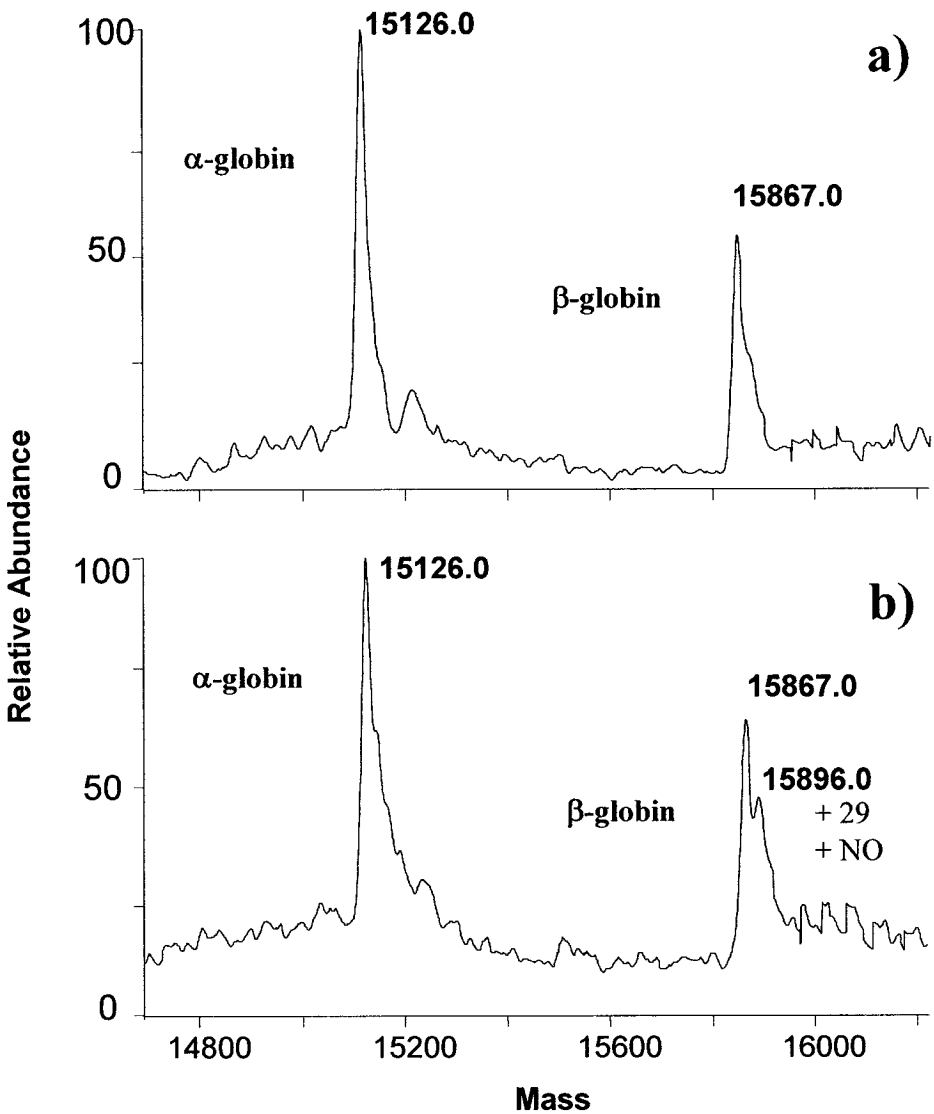
a)
15126.0
α-globin
15867.0
β-globin
100
50
0
b)
15126.0
α-globin
15867.0
15896.0
+ 29
+ NO
β-globin
100
50
0
Relative Abundance
14800
15200
15600
16000
Mass

dominant glutathione species and little GSH is present, consistent with decreased GSNO breakdown in the presence of the Cu^{I}-specific chelator. In Figure 5.6c, the GSNO intensity is ~50% of that in the presence of neocuproine indicating that DTPA is less effective in inhibiting the release of NO from GSNO in Hb solutions. However, a well-defined GSSG peak (m/z 613) is not observed in Figure 5.6c as expected if GSH were the major source of electrons for the reductive cleavage of GSNO (Reactions 5.4 and 5.5). A relatively intense GSH peak persists in Figure 5.6c and also the optical spectra reveal that metHb is formed in the deoxyHb/GSNO/DTPA incubate (Table 5.2). Since metHb is not observed in the deoxyHb incubates in the absence of DTPA, $[Cu^{II}(DTPA)]^{2-}$ was added to a solution of deoxyHb to determine if this complexed form of copper could oxidize the heme. Multi-component analysis of the absorption spectrum of 4 μM deoxyHb and 16 μM $[Cu^{II}(DTPA)]^{2-}$ after 5 min incubation revealed the presence of 21% metHb (Figure 5.7). This can be compared to 19% metHb formation in the deoxyHb/GSNO/DTPA incubates (Table 5.2).

* **Note added to the thesis:** The ESI mass spectrum of GSNO has been reexaminated using a high-resolution (10000 FWHM) mass spectrometer with accurate mass capability (5 ppm) (QTOF2, Waters Micromass). The base peak was found to be the MH^+ ion of GSNO, $GSNOH^+$ at m/z 337. Additional peaks were observed at m/z 307 and 306. These are assigned to $GSH^{\bullet+}$ and GS^+ ions, respectively, which arise from homolytic cleavage of GSNO (GSNO $\rightarrow$ $GS^{\bullet}$ + $NO^{\bullet}$) in the ESI source. The abundance of the $GSH^{\bullet+}$ and GS^+ ions are expected to be greater in the SSQ7000 due to homolysis of GSNO in the heated capillary present in the ESI source of this instrument but not in the

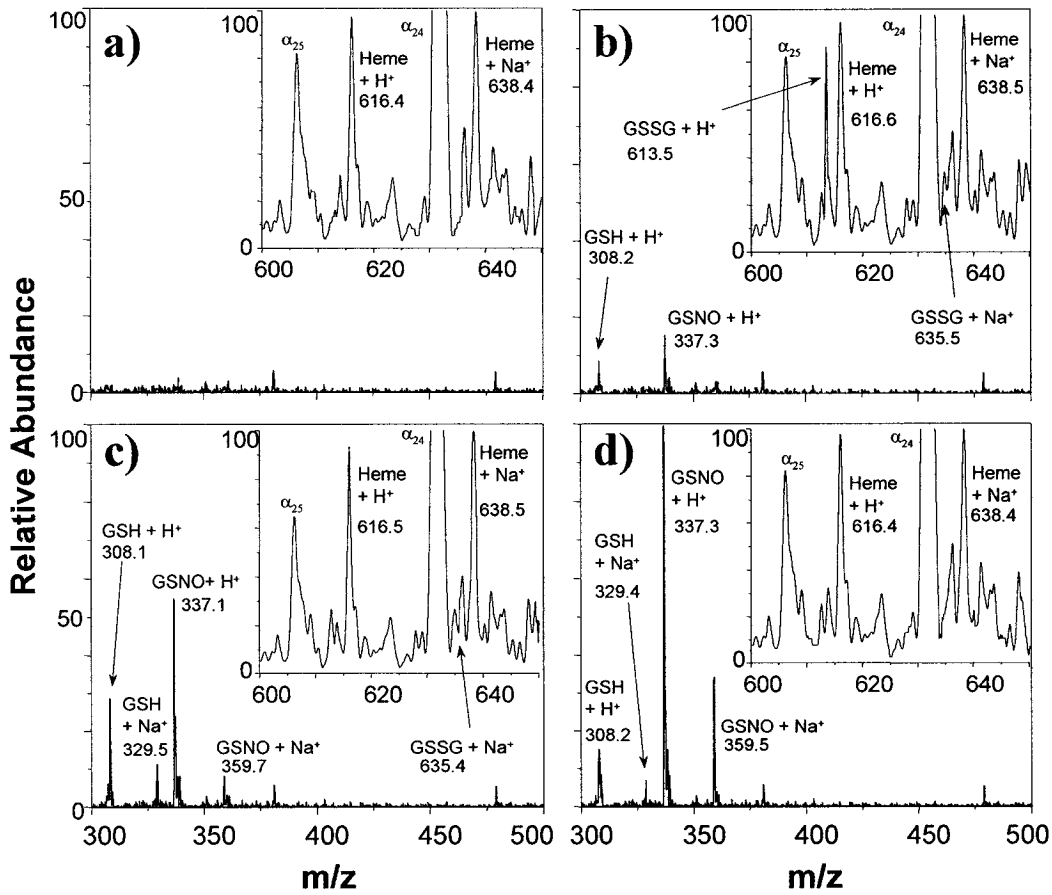

Figure 5.6. Electrospray mass spectra of glutathione products following incubation with deoxyHb. **(a)** deoxyHb; **(b)** deoxyHb + GSNO; **(c)** deoxyHb + GSNO + 200 μM DTPA. **(d)** EDTA-dialyzed deoxyHb + GSNO + 150 μM neocuproine. The experimental conditions are given in Figure 5.5. Peaks labeled α_{24} and α_{25} are due to α-globin + 24 H^+ and α-globin + 25 H^+, respectively. All peak intensities are relative to the (heme + Na)$^+$ peak at m/z 638 (100%).

QTOF2. Hence, the peaks observed at m/z 308 in Figures 5.6b-d most likely arise from mainly $GSH^{\bullet+}$ ions. Given the unit-mass resolution (2000 FWHM) and mass accuracy (100 ppm) of the SSQ7000, ions at m/z 307 and 308 are not always resolved. Since the GSH_2^+ peak in Figures 5.6b-d was incorrectly assumed to be derived from GSNO cleavage in the ESI source, the product analysis remains the same.

5.4 Discussion

Spencer and coworkers have reported that deoxyHb can directly reduce GSNO and that the released NO is captured by additional Fe^{II} heme (124). Since the release of NO from GSNO is known to be Cu^I-catalyzed (128), we monitored deoxyHb/GSNO incubates by optical and FTIR spectroscopies to probe changes occurring at the heme and Cysβ93 centers, respectively. In addition, the incubates were analyzed by ESI-MS to examine changes in the mass of the protein and to determine the low-molecular-weight species produced.

The optical spectra shown in Figure 5.1 clearly reveal that trace Cu^I is required for the release of NO from GSNO (Reaction 5.4). Essentially no nitrosylHb is formed in the deoxyHb/GSNO incubate containing *both* Cu-depleted Hb (i.e., dialyzed Hb in Table 5.1) and neocuproine. The combined data in Tables 5.1 and 5.2 indicate that total inhibition of Cu^I-catalysis of GSNO breakdown requires removal of most of the Cu as well as neocuproine addition to Hb-containing solutions. Thus, the results summarized in Table 5.2 are *not* consistent with direct reduction of GSNO by deoxyHb (124) (Reaction 5.2) when equimolar heme and GSNO are present. Given the rapid (<5 min) Cu^I-

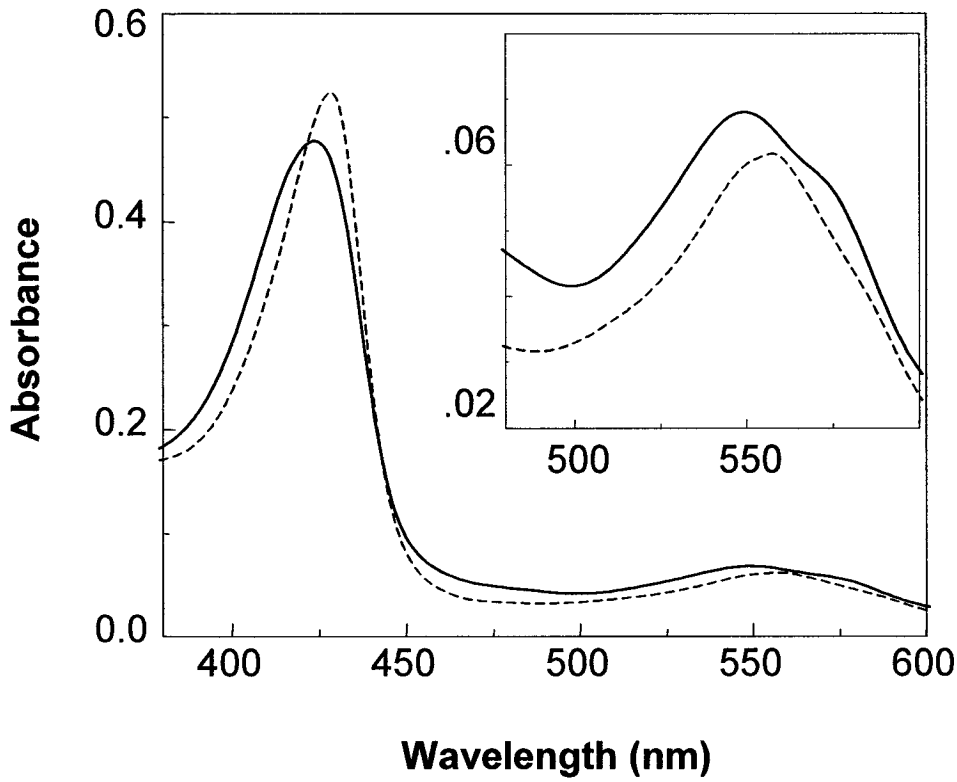

Figure 5.7. Visible absorption spectra of 4 μM (heme) deoxyHb with 16 μM $[Cu^{II}(DTPA)]^{2-}$. **(a)** $HbFe^{II}$ (- - -). **(b)** $HbFe^{II}$ + $[Cu^{II}(DTPA)]^{2-}$ after 5 min (—). $[Cu^{II}(DTPA)]^{2-}$ was prepared by mixing equimolar solutions of $CuSO_4$ and DTPA. Experimental details are given in Figure 5.1 except that a 1-cm quartz cuvette was used.

catalyzed release of NO from GSNO (Figure 5.1b), it is likely that Cu-catalyzed reductive cleavage of GSNO also occurs in *vivo*.

The next question that arises is, of course, what is the source of reducing equivalents to regenerate Cu^{I} following electron transfer to GSNO to release NO (Reaction 5.4)? Possible electron donors to Cu^{II} are GSH (Reaction 5.5) and deoxyHb. With GSH as a donor, 2 molecules of NO would be released or 2 heme $Fe^{II}NO$ adducts formed per molecule of GSSG produced. The mass spectrum reveals extensive formation of GSSG in the deoxyHb/GSNO incubates in the absence of chelators (Figure 5.6b). Although a peak corresponding to its Na^{+} adduct occurs at m/z 635, the expected GSSG peak at m/z 613 is not clearly evident in deoxyHb/GSNO incubates containing DTPA. Nonetheless, GSNO does release NO as evidenced by the loss of GSNO peak intensity relative to the base peak at m/z 638 (Figure 5.6c *vs* 5.6d) and the formation of nitrosylHb (Figure 5.1c, Table 5.2). Thus, reduction of $[Cu^{II}(DTPA)]^{2-}$ by deoxyHb was considered, which would account for the metHb absorbance seen in Figure 5.2a. From Table 5.2, 7.13 mM NO is released (6.97 mM nitrosylHb + 0.16 mM nitrosylmetHb) from the 15 mM GSNO present in the deoxyHb/GSNO/DTPA incubate. If all the reducing equivalents were to come from GSH oxidation (Reaction 5.5), then 3.56 mM GSSG should be produced. However, deoxyHb oxidation provides 1.44 milliequivalents of reductant (1.28 mM metHb + 0.16 mM nitrosylmetHb), which would decrease the concentration of GSSG produced to 2.84 mM. This is ~1/3 of the GSSG produced in deoxyHb/GSNO incubates where a strong GSSG peak is observed at m/z 613. The lower than expected intensity of the GSSG (m/z 613) peak in Figure 5.6c is attributed to ion suppression. The production of metHb in the deoxyHb incubates in the presence but *not* the absence of

DTPA (Table 5.2) suggested that $[Cu^{II}(DTPA)]^{2-}$ may accept an electron from deoxyHb, which was confirmed. Addition of authentic $[Cu^{II}(DTPA)]^{2-}$ to deoxyHb led to oxidation of 21% of the heme (Figure 5.7). Electron transfer between $[Fe^{II}(EDTA)]^{2-}$ and metHb has been reported previously (162).

No loss of ν(SH) intensity was detected by FTIR when deoxyHb was treated with GSNO with or without metal chelators (Figure 5.4a). This is consistent with the proposal that Hb's allosteric transition controls Cysβ93 S-nitrosation (56). The FTIR results also show that Cu^{I} is required for nitrosylHb formation since neocuproine inhibited blue-shifting of the Cysβ93 ν(SH) peak (Figure 5.4a, spectra 2 and 3) that accompanies heme nitrosylation (123). Scheme 5.1 summarizes the reactions in the deoxyHb/GSNO incubates reported here:

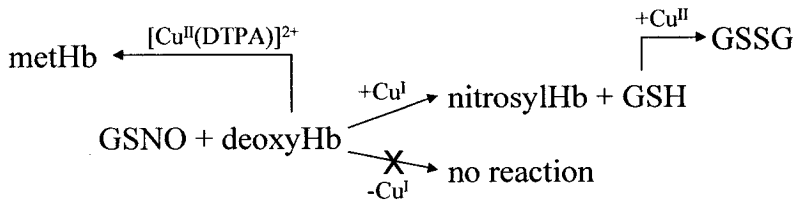

(5.1)

Clearly the oxidation of deoxyHb by $[Cu^{II}(DTPA)]^{2+}$is unlikely to be of importance *in vivo*, but the requirement of Cu for NO release from GSNO shown in Scheme 5.1 could well have physiological relevance.

The key result that Cu is also required for S-nitrosation of Cysβ93 of oxyHb (134) can be deduced from Figures 5.4b and 5.5b. S-nitrosation of Cysβ93 is observed only in the absence of metal chelators (Figure 5.4b, spectrum 1 and Figure 5.5b). Thus, we propose Scheme 5.2 for the reactions of NO with oxyHb:

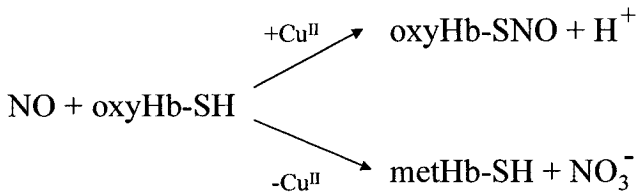

(5.2)

NO is targeted to Cysβ93 in the absence of chelators, but in the presence of DTPA, all the NO released from GSNO is targeted to the $Fe^{II}O_2$ heme (Figures 5.3 and 5.4b) and converted to NO_3^- (Reaction 5.6). Scheme 5.2 predicts that efficient Cu^{II}–catalyzed S-nitrosation of Cysβ93 will preserve the biological activity of NO by preventing its conversion to nonvasoactive NO_3^-. The capture of NO by deoxyHb (Scheme 5.1) should not lead to loss of its vasoactive power as long as Fe^{II}-NO adduct formation is reversible on a physiologically relevant time scale. It has been proposed that the Fe^{II} heme centers of partially oxygenated Hb, as found in the RBC (60), have a much lower affinity for NO than fully deoxygenated deoxyHb (63). Thus, Cu-control of NO reactivity with Hb, plus weaker binding of NO to deoxyHb *in vivo* than *in vitro*, could explain why RBC Hb does not act a sink for most of the NO produced in the vascular system. A possible Cu-catalyst *in vivo* is Cu,Zn superoxide dismutase which is abundant in the RBC (140).

It is of interest to compare the extent of the prompt changes in deoxyHb and oxyHb on incubation with GSNO. When 15 mM GSNO is incubated with 15 mM (heme) deoxyHb in the absence of metal chelators 99% is converted to nitrosylHb within 5 min whereas only 46% of oxyHb is converted to metHb under the same conditions. This is easy to understand when we consider that ~7.5 mM NO released from GSNO was targeted to Cysβ93 in oxyHb but not in deoxyHb (Figure 5.4 and 5.5). In the DTPA

incubates, 44% deoxyHb *vs* 77% oxyHb remain, and in neocuproine incubates 75% deoxyHb *vs* 88% oxyHb remain after the same 5-min period. Clearly, the increased stability of the Hb reactants in the presence of metal chelators is due to inhibition of GSNO breakdown, but the lower consumption of oxyHb relative to deoxyHb cannot be attributed to NO trapping by Cysβ93 in the former since this does not occur in the presence of chelators (Figure 5.4b). More efficient NO trapping by deoxyHb (127) than by oxyHb ($k = 3\text{-}5 \times 10^7\ M^{-1}\ s^{-1}$ for Reaction 5.6) (170) would give rise to the higher deoxyHb consumption in the incubates. Also, the reaction of NO with any free O_2 in the oxyHb incubate would decrease the amount of oxyHb consumed.

In this work we also examined the spectra of the deoxyHb/GSNO incubates after 1 h. The results obtained indicate that the prompt products undergo further reaction over longer times. For example, the Soret maximum after 1 h of deoxyHb/GSNO incubate still shows a maximum at 418 nm but with decreased intensity (data not shown). Since the spectrum of authentic nitrosylHb in the absence of any glutathione-derived species is stable for >1 h, the nitrosylHb initially formed must react with some reagent in the incubate (work in preparation). The Soret maximum of the deoxyHb/GSNO/DTPA incubate after 1 h (data not shown) is blue-shifted (409 nm) from that at 5 min (411 nm) (Figure 5.1c). We initially attributed this blue-shift to increased nitrosylHb formation due to NO-driven reduction of metHb using reducing equivalents from GSH. However, addition of GSH to authentic nitrosylmetHb also gave rise to a Soret maximum at 411 nm and not the expected nitrosylHb peak at 418 nm. The biological relevance of these slow reactions is questionable since, for example, any metHb formed in the RBC would be rapidly converted to deoxyHb by methemoglobin reductase (171).

5.5 Conclusions

The results reported here provide insight into the mechanism of heme nitrosylation following mixing of deoxyHb with GSNO. The data presented are *inconsistent* with direct reduction of GSNO by deoxyHb, but are consistent with catalysis of GSNO breakdown by trace Cu and *free* NO generation in the reactions. Since deoxyHb is stable in the presence of GSNO when free Cu is rigorously excluded from the system, direct reduction of GSNO by deoxyHb is unlikely to be of biological significance. Trace Cu also controls targeting of NO released from GSNO to the Cysβ93 and $Fe^{II}O_2$ centers of oxyHb. Thus, we conclude that Cu-catalysis of S-nitrosation and S-denitrosation plays a key role in preserving the vasoactivity of NO in the RBC.

5.6 Acknowledgements

This research was supported by the Natural Sciences and Engineering Research Council of Canada (NSERC), the Canadian Institutes for Health Research (CIHR), the Fonds pour la Formation des Chercheurs et L'Aide à la Recherche (FCAR) to A. M. E. and J. A. C., and by a Graduate Fellowship (Concordia University) to A. A. R.

We would like to thank Professor Eric Salin and Dr. John Tromp from the Department of Chemistry, McGill University, for helping us with the ICP-MS measurements and for the use of their ICP-MS instrumentation.

6.0 Spin Scavenging of a Thiyl Radical on Cysβ93 in Human Hemoglobin as Detected by ESI-MS

6.1 Abstract

Cu^{II} acceleration of CO/H_2O-driven reduction of methemoglobin (metHb) has been proposed to involve electron transfer from Cysβ93 to the β-heme, thereby forming a thiyl radical and reducing Fe^{III} to Fe^{II}. MetHb was incubated with CO at high (millimolar) Hb concentration. The formation of carbonylHb ($HbFe^{II}CO$) was confirmed by monitoring the Soret and visible absorption during the copper-enhanced CO/H_2O-driven reaction. In addition, formation of a peak at 1951 cm^{-1} corresponding to ν(CO) was observed by FTIR. To confirm thiyl radical formation, spin scavenging using 4-hydroxy-2,2,6,6-tetramethylpiperidine 1-oxyl (TEMPOL$^{\bullet}$), followed by peptide mass mapping of Hb was attempted. Since copper aids in the formation of carbonylHb, the spin scavenging experiments were performed in the presence of copper ions added as $CuSO_4$, and also in the presence of the metal chelator DTPA. The mass spectrometry results provide evidence of thiyl radical scavenging on Cysβ93 in metHb incubates during copper-enhanced CO/H_2O-driven heme reduction since signals corresponding to TEMPOL-labeled peptides 83-95 were observed in the peptide mass map of the tryptic digest of β-globin. The results are interpreted in light of the mechanism of Hb S-nitrosation *in vivo*.

6.2 Introduction

It has been proposed that the interaction of nitric oxide (NO) with hemoglobin (Hb) plays a role in blood-pressure regulation. Oxygenation of the heme-iron promotes

the binding of NO to Cysβ93 of Hb to form S-nitroso-Hb (Hb-SNO) and deoxygenation promotes release of NO from Hb-SNO (63). A facile mechanism of Hb S-nitrosation would be to generate a thiyl radical on Cysβ93, which should react rapidly with NO, itself a radical species. It has been proposed that NO transfer from a low-molecular-weight S-nitrosothiol (RSNO), such as CysSNO or GSNO, to Cysβ93 of Hb could occur *via* a *trans*-S-nitrosation mechanism (Reaction 1.20), involving direct NO^+ transfer between the thiols. However, data presented in Chapters 3, 4 and 5 of this thesis show that NO transfer from GSNO and CysSNO to Hb is a copper-catalyzed process. Both free copper and the copper present in Cu,Zn-superoxide dismutase (CuZnSOD) catalyze the reductive elimination of NO from GSNO (Reaction 4.3), but only in the presence of CuZnSOD is all of the released NO directed to Cysβ93 at physiological concentrations of Hb. The proposed mechanism of NO targeting to Cysβ93 involves thiyl radical fomation on this residue (Reactions 4.11 and 4.12).

It has been reported that addition of copper ions accelerates metHb reduction by CO/H_2O (172). This copper-induced rate enhancement was inhibited by blocking Cysβ93 with *N*-ethylmaleimide (172) suggesting a mechanism whereby electron transfer occurs via an internal pathway coupling CO/H_2O oxidation to Fe^{III} and Cu^{II} reduction (172,173). Electron donation from Cysβ93 *via* the peptide backbone to the heme-iron in β-globin is suspected. The sulfur atom can lose its proton becoming S^-, which then becomes a thiyl radical by transferring one electron to the β–Fe^{III}. The published work can be summarized by two important findings: (i) binding of Cu^{II} to Hb at the high affinity site involving Hisβ2 and N-terminal amino group is ineffective in promoting electron exchange

between Cu^{II} and the β-heme Fe^{III}, (ii) effective electron transfer between Cu^{II} and the β-heme is not governed by the R ⇌ T conformational equilibrium of Hb.

The goal of the present work is to investigate the formation of a thiyl radical on Cysβ93 of Hb and the role of added copper ions in this process. Hence, the CO/H_2O-driven reduction of metHb was re-examined here at a copper/heme ratio of 1:2 and at micromolar and millimolar metHb. Given that 5 mM Hb is present in RBCs (165), bimolecular reactions between Hb molecules are likely to be highly favourable. We show in the present work that copper-enhanced CO/H_2O driven metHb reduction is much faster at high *vs* low Hb concentrations. These results are inconsistent with the presence of an *efficient* electron-transfer pathway between Cysβ93 and the heme.

6.3 Experimental Procedures

6.3.1 Materials

Human hemoglobin A (Hb) was obtained from Sigma and used without further purification. Nanopure water (specific resistance 18 MΩ-cm), obtained from a Millipore Simplicity water purification system and treated with Chelex-100 (Sigma) to remove trace metal ions, was used to prepare all H_2O solutions. Reactions were carried out in 200 mM sodium phosphate buffer, pH 7.2 (NaPi) prepared from sodium phosphate salts (Fisher) in nanopure H_2O. Stock solutions of 15 mM diethylenetriamine-N,N,N',N",N"-pentaacetic acid (DTPA, ICN) were prepared in NaPi. L-ascorbic acid sodium salt, $CuSO_4$, the spin traps 3,5-dibromo-4-nitrosobenzenesulfonic acid sodium salt (DBNBS), and 5,5-dimethyl-1-pyrroline N-oxide (DMPO), and the spin label 4-hydroxy-2,2,6,6-

tetramethylpiperidine 1-oxyl (TEMPOL•) were purchased from Sigma. Trypsin, modified, sequencing grade (from bovine pancreas) was obtained from Roche.

6.3.2 Methods

6.3.2.1 Preparation and Optical Spectroscopy of Hb Samples

MetHb (32 mM) was prepared as described in Chapter 5. An aliquot (10 μL) of the Hb solution was pipetted onto a 13-mm CaF_2 window of a dismountable FTIR-type cell (Harrick). The cell was immediately assembled using a 6-μm Teflon spacer (Harrick) and placed in a custom-made bracket in a Beckman DU 650 UV-Vis spectrophotometer. deoxyHb was also prepared as described in Chapter 5. Authentic carbonylHb ($HbFe^{II}CO$) exhibits two characteristic peaks at 540 and 569 nm (ε_{540} = 13.4 and ε_{569} = 13.4 $mM^{-1}cm^{-1}$), while metHb absorbs at 500 and 540 nm (ε_{500} = 10.0 and ε_{540} = 11.0 $mM^{-1}cm^{-1}$). Use of the FTIR-type cell to record the optical spectra of Hb incubates allowed measurements to be made at close to physiological concentrations of Hb (~5 mM) (165). Authentic carbonylHb was prepared from deoxyHb by introducing pure CO (at 1 atmosphere pressure) from a CO tank (Praxair) into the sample using a needle. All samples were deaerated by purging with nitrogen to ensure that no oxygen was present in the samples before CO incubation. Fully carbonylated Hb was obtained as indicated by the Soret and visible spectra recorded following a 5-min equilibration (Figures 6.4 and 6.5). Soret absorption differentiates between metHb and carbonylHb since the maxima are 405 (ε_{405} = 169 $mM^{-1}cm^{-1}$) and 419 (ε_{419} = 191 $mM^{-1}cm^{-1}$), respectively (125). Optical spectra were recorded using a scan time of 1200 nm/min.

6.3.2.2 FTIR Analysis of Hb Samples

For analysis of the ν(SH) vibration in the region of 2400-2600 cm^{-1}, Hb (20 μL, 28 mM heme) in NaPi was added by syringe onto a 13-mm CaF_2 window. The FTIR cell was immediately assembled with a 250-μm Teflon spacer (Harrick). For ν(CO) analysis of the heme-bound CO (1900-2000 cm^{-1}), Hb (10 μL, 14 mM heme) in NaPi was added by syringe onto the window and the FTIR cell was immediately assembled with a 6-μm Teflon spacer. Spectra were recorded at 25°C on a Nicolet Magna-IR 550 spectrometer with a MCT detector cooled to 77 K and purged with dry air from a Whatman FTIR Purge (Model 75-52). All reported spectra are an average of 500 scans recorded in 5.52 min at a resolution of 2 cm^{-1} using a Happ-Genzel apodization with a velocity and aperture of 4.4303 cm/s and 2, respectively. Omnic (Nicolet) software was used for subtraction, baseline correction, smoothing, and Fourier transform self-deconvolution employing a half-width-at-half-height of 0.6 cm^{-1} and an enhancement (K factor) of 1. Subtraction of water-vapor absorption from the spectra was performed as in Chapter 5.

6.3.2.3 Analysis of CO/H_2O-Driven Reduction of MetHb and Hb Thiyl Radical Formation

Electron transfer from Cysβ93 to Fe^{III} of metHb under CO has been proposed (172). Therefore, an attempt was made to trap or scavenge the thiyl radical formed on Cysβ93 using the spin traps DBNBS and DMPO (174-177) and the spin scavenger TEMPOL$^{\bullet}$ (178-181) for ESI-MS analysis (39,182). Solutions of 28 mM (heme) metHb under 1 atm CO or N_2 with or without $CuSO_4$ and DTPA were prepared (Table 6.1).

Table 6.1. Samples for ESI/LC/MS analysis of (28 mM heme) metHb/CO incubates

Incubates [a,b]	1 atm CO or N_2	Spin trap/scavenger [c,d]	$CuSO_4$	DTPA	Δm [e]
MetHb	N_2				
MetHb/CO	CO				
MetHb/DBNBS	N_2	30 mM DBNBS			
MetHb/CO/DBNBS	CO	30 mM DBNBS			
MetHb/CO/Cu^{II}/DBNBS	CO	30 mM DBNBS	15 mM		β + 48
MetHb/CO/Cu^{II}/DTPA/DBNBS	CO	30 mM DBNBS	15 mM	30 mM	
MetHb/TEMPOL$^{\cdot}$	N_2	50 mM TEMPOL$^{\cdot}$			
MetHb/CO/TEMPOL$^{\cdot}$	CO	50 mM TEMPOL$^{\cdot}$			
MetHb/Cu^{II}/TEMPOL$^{\cdot}$	N_2	50 mM TEMPOL$^{\cdot}$			
MetHb/CO/Cu^{II}/TEMPOL$^{\cdot}$	CO	50 mM TEMPOL$^{\cdot}$	15 mM		β + 171
MetHb/CO/Cu^{II}/DTPA/TEMPOL$^{\cdot}$	CO	50 mM TEMPOL$^{\cdot}$	15 mM	30 mM	β + 48
MetHb/CO/DMPO	CO	30 mM DMPO	15 mM	30 mM	
MetHb/CO/Cu^{II}/DMPO	CO	30 mM DMPO	15 mM	30 mM	β + 113
MetHb/CO/Cu^{II}/DTPA/DMPO	CO	30 mM DMPO	15 mM	30 mM	β + 32

[a] All samples were incubated in 200 mM NaPi (pH 7.2) at 25°C for 30 min in the dark under 1 atm CO or N_2 in a 1-mL sealed vial and constantly spun with a magnetic stirrer

[b] Incubates contained the reagents listed at the concentrations given in the table

[c] After 30 min incubation, DBNBS, DMPO or TEMPOL$^{\cdot}$ was added for 10 min prior LC-MS analysis

[d] After 10 min incubation with DBNBS or DMPO, samples were incubated for a further 5 min with 30 mM sodium ascorbate just prior to LC/MS analysis

[e] Δm is the change in mass observed for β-globin. No mass changes were observed for α-globin (see Section 6.4.3)

After 30 min incubation, excess DBNBS, DMPO or TEMPOL$^{\bullet}$ was added for 10 min prior to LC-MS analysis.

6.3.2.4 ESI-MS Analysis

MetHb incubates in NaPi were diluted 10^3-fold into H_2O to give 0.3 μg protein per μL before injection into the HPLC. LC-MS analysis was performed using an Agilent 1090 Series II HPLC with a diode-array detector (DAD) coupled to a ThermoFinnigan SSQ7000 mass spectrometer with an ESI source. The source voltage and capillary temperature were 3.5 kV and 180°C, respectively, in all experiments. The DAD detector of the HPLC 1090 allowed monitoring of the eluate at 405 for the heme, 241 for TEMPOL$^{\bullet}$ and 210 nm for α- and β-globin and DBNBS.

Thiyl radical formation was probed in the incubates listed in Table 6.1. Samples containing the spin traps DBNBS and DMPO were incubated for 5 min with 30 mM ascorbate to convert any Hb-DBNBS$^{\bullet}$ spin adduct formed to a more stable species by reducing the nitroso radical to the hydroxylamine, R'RN-O$^{\bullet}$ → R'RN-OH. Aliquots (20 μL, ~7 μg of protein) of each sample were loaded onto a Vydac reversed-phase C_{18} column (4.6x250 mm), and the protein was separated from buffer salts and excess reactants with a 20-55% CH_3CN gradient in 0.05% TFA at 1 mL/min over 20 min. Fractions eluted from the HPLC were split and 20% was directly injected into the ESI source. The remainder was collected (~1 mL), lyophilised, dissolved in 100 μL of 50% CH_3OH in 5% CH_3COOH and directly injected into the ESI source using a 100-μL syringe at a flow rate of 5 μL/min. To locate the label, the modified Hb was lyophilized and digested with 1:50 trypsin/protein (w/w) at 40°C for 20 h in 200 mM NaPi buffer.

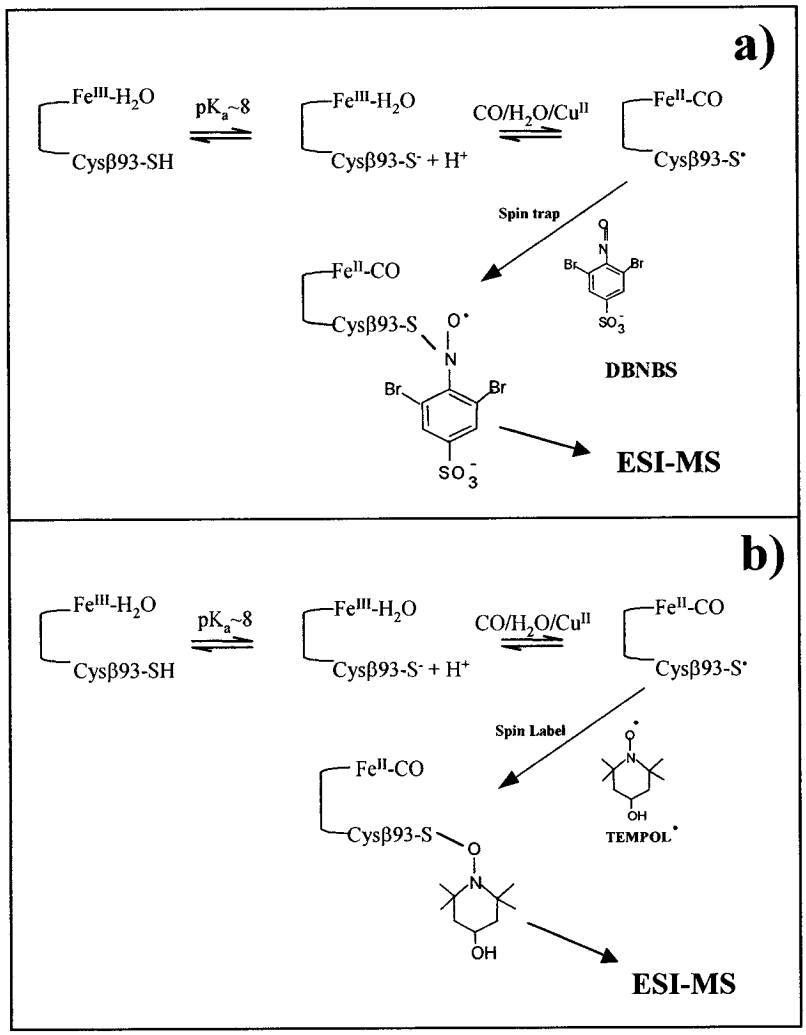

Figure 6.1. Schemes for thiyl radical formation in Hb and its analysis by ESI-MS during copper enhanced CO/H_2O driven metHb reduction. A thiyl radical is formed on Hb Cysβ93 in the metHb/CO/Cu^{II} incubate following intramolecular and/or bimolecular electron transfer to the Fe^{III} heme. The thiyl radical is trapped with (**a**) the spin trap DBNBS or scavenged by (**b**) the stable nitroxide radical TEMPOL$^•$. The resultant mass adducts are characterized by ESI-MS.

The digests were loaded on a Vydac microbore C_{18} column (1x250 mm) and the peptides eluted with a 5-60% CH_3CN gradient in 0.05% TFA at 40 μL/min over 100 min. Figure 6.1 summarizes the scheme for thiyl formation and detection in Hb

6.4 Results

6.4.1 CO/H_2O-Driven Reduction of MetHb as Monitored by Visible and FTIR Absorption

Both DBNBS and TEMPOL$^{\bullet}$ are water soluble and their UV-Vis absorption spectra in NaPi are shown in Figure 6.2. The absorbance of their solutions did not change over 30 min, indicating that they are stable under these conditions.

The UV-Vis spectrum of a 7 μM (heme) metHb/CO incubate in 200 mM NaPi, after 12 h under 1 atm CO (Figure 6.3) shows ~10% decrease in absorbance at 405 nm of metHb (ε_{405} = 169 $mM^{-1}cm^{-1}$). Also, ~10% increase in absorbance at 419 nm, corresponding to carbonylHb (ε_{419} =191 mM^{-1} cm^{-1}) is observed. The percentages were calculated using multicomponent analysis as previously described (Section 5.3.2.6). In a metHb/CO/Cu^{II} incubate, which contained 3.5 μM Cu^{II}, ~100% formation of carbonylHb was observed after 12 h (Figure 6.3). Addition of 7 μM DTPA inhibited carbonylHb formation (Figure 6.3). Since DTPA chelates Cu^{II}, these results indicate the important role of redox-active copper in the CO/H_2O-driven reduction of metHb.

In the spectrum of the 14 mM heme metHb/CO incubate an intensity decrease at 405 nm and increase at 419 nm were observed after only 30 min (Figure 6.4) corresponding to ~40% carbonylHb formation as determined by multicomponent

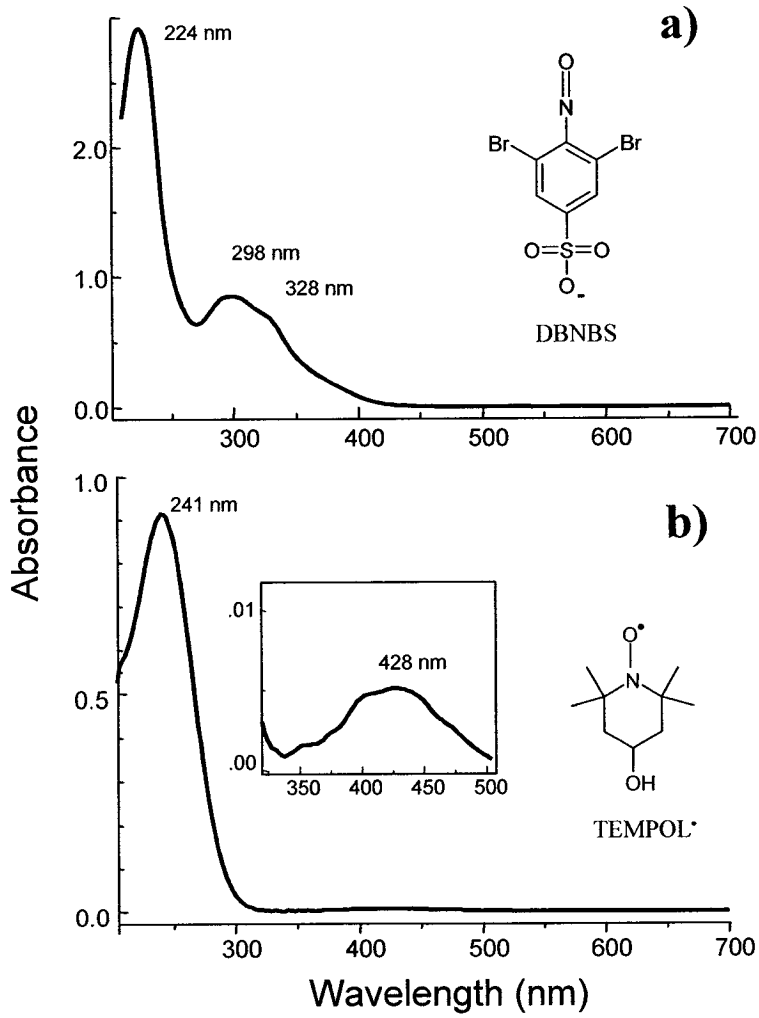

Figure 6.2. Structures and UV-Vis absorption spectra of DBNBS and TEMPOL•. (a) Spectrum of 625 μM DBNBS in 200 mM NaPi (pH 7.2). The maxima are labelled: $\varepsilon_{224\ nm}$ = 4.64, $\varepsilon_{298\ nm}$ = 1.28 and $\varepsilon_{328\ nm}$ = 1.04 $mM^{-1}\ cm^{-1}$. **(b)** Spectrum of 20 μM TEMPOL• in 200 mM NaPi (pH 7.2). The maximum ($\varepsilon_{241\ nm}$ = 46.5 $mM^{-1}\ cm^{-1}$) and a weak band ($\varepsilon_{428\ nm}$ = 0.26 $mM^{-1}\ cm^{-1}$) are labelled. Spectra were collected at 25°C in a 1-cm quartz cuvette using a scan time of 1200/min.

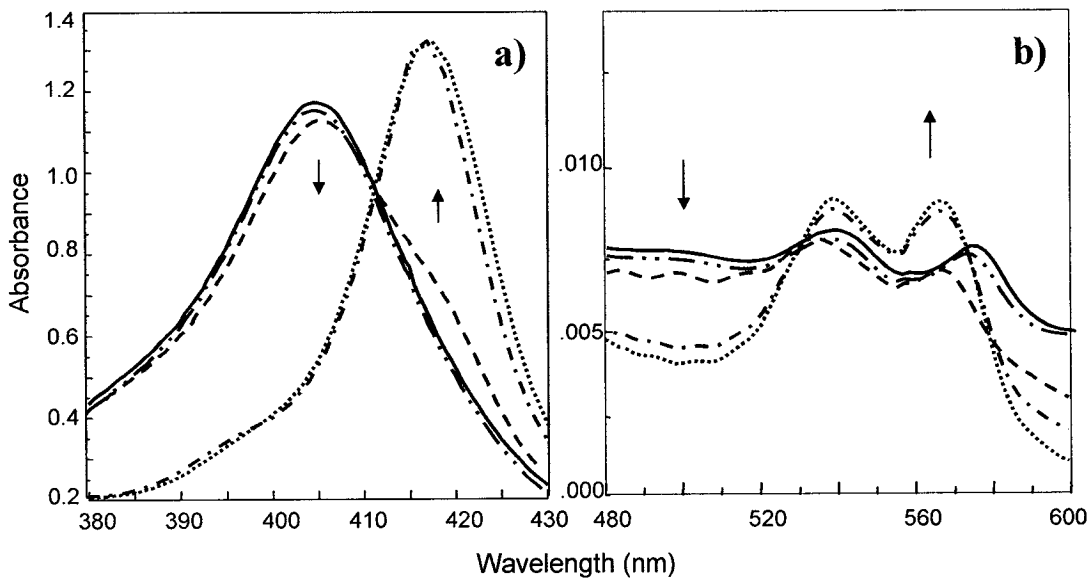

Figure 6.3. Spectral changes during copper-enhanced CO/H_2O driven reduction of 7 μM (heme) metHb. (**a**) Soret absorption of metHb (—); authentic carbonylHb (· · ·); metHb/CO (- - -); metHb/CO/Cu^{II} (- · - · -) and metHb/CO/Cu^{II}/DTPA (- · · - · · -). (**b**) Absorption in the visible region of the samples in (a). The Hb incubates were left standing at 25°C for 12 h under 1 atm CO with 3.5 μM $CuSO_4$ and 7 μM DTPA where indicated. Authentic carbonylHb was prepared by exposing deoxyHb to CO (125). All samples were in 200 mM NaPi (pH 7.2) at 25°C and spectra were recorded in a 1-cm quartz cuvette using a scan time of 1200 nm/min.

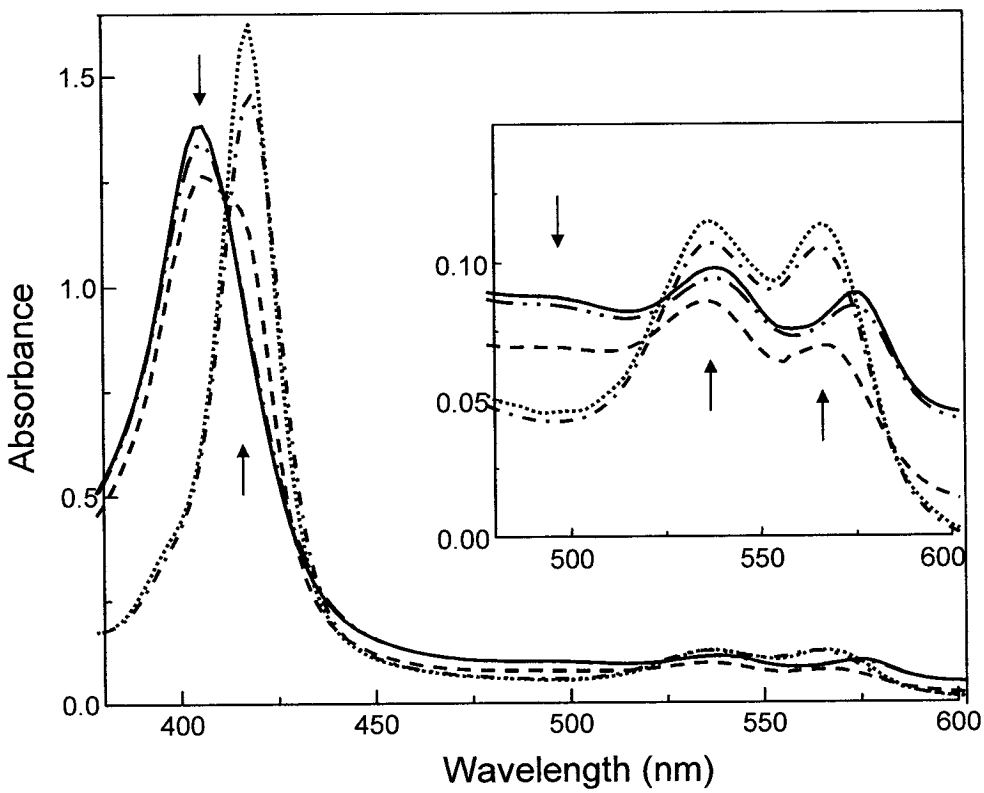

Figure 6.4. Spectral changes during copper-enhanced CO/H_2O driven reduction of 14 mM (heme) metHb. Spectra of metHb (—), authentic carbonylHb (···), metHb/CO (- - -), metHb/CO/Cu^{II} (-·-·-) and metHb/CO/Cu^{II}/DTPA (-···-···-). The Hb incubates were left standing at 25°C for 30 min under 1 atm CO with 7.5 mM $CuSO_4$ and 15 mM DTPA where indicated. Authentic carbonylHb was prepared as in Figure 6.3. Spectra were recorded in 200 mM NaPi (pH 7.2) at 25°C using an FTIR cell with a 6-μm Teflon spacer and a scan time of 1200 nm/min.

analysis. Addition of 15 mM $CuSO_4$ resulted in ~100% carbonylHb formation in 30 min whereas in the metHb/CO/Cu^{II}/DTPA incubate, which contained 30 mM DTPA, only ~5% carbonylHb formation occurred within 30 min (Figure 6.4).

The 30-min FTIR spectra of the 28 mM metHb/CO incubate show decreased Cysβ93 ν(SH) absorption relative to metHb (2589 cm^{-1}) and a peak due to ν(CO) at 1951 cm^{-1} (Figure 6.5). The intensity of the CO band corresponds to ~40% carbonylHb formation when compared to the ν(CO) intensity of the authentic carbonylHb sample. After 30 min, the spectrum of the metHb/CO/Cu^{II} incubate showed no Cysβ93 ν(SH) absorption, indicating possible thiyl radical formation on Cysβ93. The ν(CO) intensity is comparable to that of authentic carbonylHb (Figure 6.5), which reveals that both the α– and β-hemes were converted to $Fe^{II}CO$ forms. In the metHb/CO/Cu^{II}/DTPA incubate no loss of Cysβ93 ν(SH) relative to metHb was observed and <5% carbonylHb was formed after 30 min (Figure 6.5) indicating the key role of Cu^{II} in accelerating CO/H_2O driven heme reduction.

6.4.2 Analysis of Electron-Transfer Pathway Between Cysβ93 and the β-Heme

A computer program, HARLEM (183-185), was used to examine intramolecular electron transfer in Hb. The best pathway between the donor (sulfur atom of Cysβ93) and the acceptor (heme Fe^{III} of β-globin) was found to be Cysβ93-Hisβ92-heme-Fe^{III} (Figure 6.6). This pathway is also the shortest, and it is the same in both deoxyHb and oxyHb. This suggests that intramolecular electron transfer from Cysβ93 to the heme should be equally efficient in R- and T-state Hb corroborating the previous report on Cu^{II}-enhanced

Figure 6.5. Comparison of FTIR spectra change in ν(SH) and ν(CO) regions during copper-enhanced CO/H_2O driven reduction of 28 mM (heme) metHb. (**a**) ν(SH) spectra of metHb (—), authentic carbonylHb (···), metHb/CO (– – –), metHb/CO/Cu^{II} (–·–·–) and metHb/CO/Cu^{II}/DTPA (–···–···–). (**b**) ν(CO) spectra of the samples in (**a**). The Hb incubates were left standing at 25°C for 30 min under 1 atm CO with 15 mM $CuSO_4$ and 30 mM DTPA where indicated. Authentic carbonylHb was prepared as in Figure 6.3. Spectra were recorded in 200 mM NaPi (pH 7.2) at 25°C, and are the average of 500 scans at 2-cm^{-1} resolution. Spectra in ν(SH) and ν(CO) regions were recorded using a 250- and 6-μm Teflon spacers, respectively. Background subtraction, baseline correction, smoothing and Fourier transform self-deconvolution were performed on the displayed spectra as described in Section 5.3.2.4.

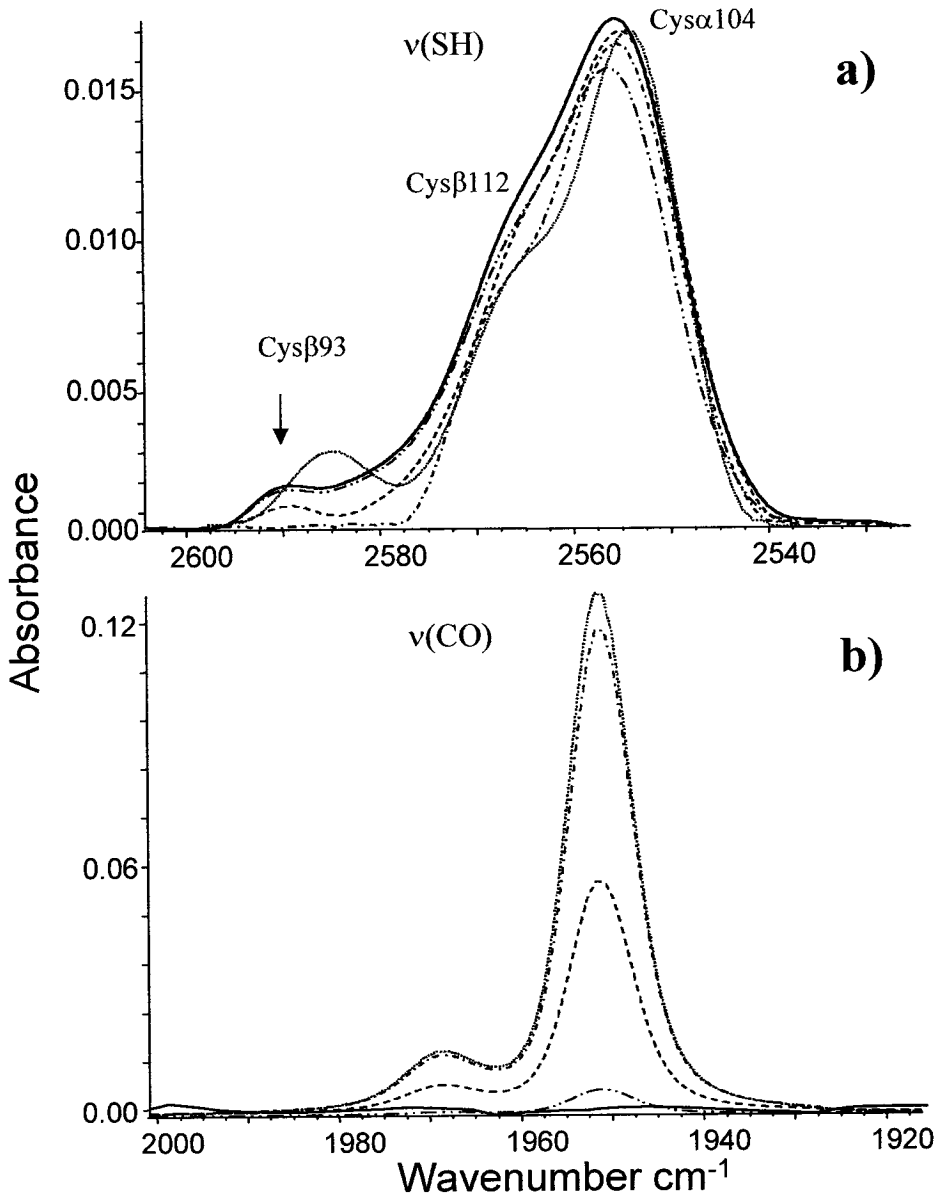
ν(SH)
Cysα104
a)
Cysβ112
Cysβ93
0.015
0.010
0.005
0.000
2600
2580
2560
2540
Absorbance
ν(CO)
b)
0.12
0.06
0.00
2000
1980
1960
1940
1920
Wavenumber cm-1

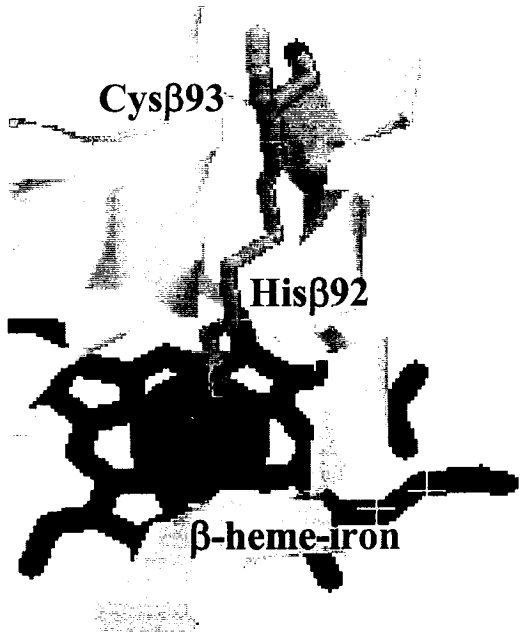

Figure 6.6. Best pathway for intramolecular electron transfer between Cysβ93 and the β-heme Fe^{III} in human metHb. The electron transfer begins at the γ-sulfur of Cysβ93 (yellow), proceeds through the proximal Hisβ92 and ends at the β-heme Fe^{III} (red). The γ-sulfur to Fe^{III} distance is 13 Å. The pathway analysis was carried out using HARLEM (183-185) and the coordinates of metHb from PDB file 1HGB.

heme reduction that effective electron transfer is not governed by the R ⇌ T conformational equilibrium (172).

6.4.3 LC-MS Analysis of the MetHb (28 mM Heme) Incubates

Figure 6.7 shows that the α- and β-subunits of Hb are readily separated from the low-molecular-weight reagents and products by HPLC. The buffer salts were eluted at ~2.7 min, β-globin at 16.5 min, α-globin at 17.5 min and the heme at 19 min (Figure 6.7a). Under the same conditions, DBNBS was eluted at 7.7 min and TEMPOL$^{\bullet}$ at 3.8 min (Figures 6.7a,b). The deconvolved ESI mass spectra of Hb α- and β-globin yielded average masses in agreement with the theoretical ones based on the amino acid sequences shown in Table 1.1 (186): 15,126 Da for α-globin and 15,867 Da for β-gobin (Figures 6.8a,b).

The mass spectrum of β-globin from the metHb/CO/Cu^{II}/TEMPOL$^{\bullet}$ incubate showed a peak corresponding to β-globin + 171 (16,038 Da) (Figure 6.8c), which matches the mass expected for a TEMPOL$^{\bullet}$ (MW 172.1) adduct [β-globin - H + TEMPOL$^{\bullet}$] while the α-globin spectrum showed only a peak corresponding to the unmodified subunit (data not shown). In contrast, the spectrum of the metHb/CO/Cu^{II}/DTPA/TEMPOL$^{\bullet}$ incubate showed no peak corresponding to TEMPOL-labelled β-globin but a peak at β-gobin + 48 (15,915 Da) was observed (Figure 6.8d). This could be due to the binding of three oxygen atoms to the β-subunit in the incubate containing DTPA. No spin adducts were observed in the LC-MS spectra of the DBNBS incubates and controls (Table 6.1). Modified β-globin with an increased mass of +48 Da was detected in the mass spectra of the metHb/CO/Cu^{II}/DBNBS incubate, but again the

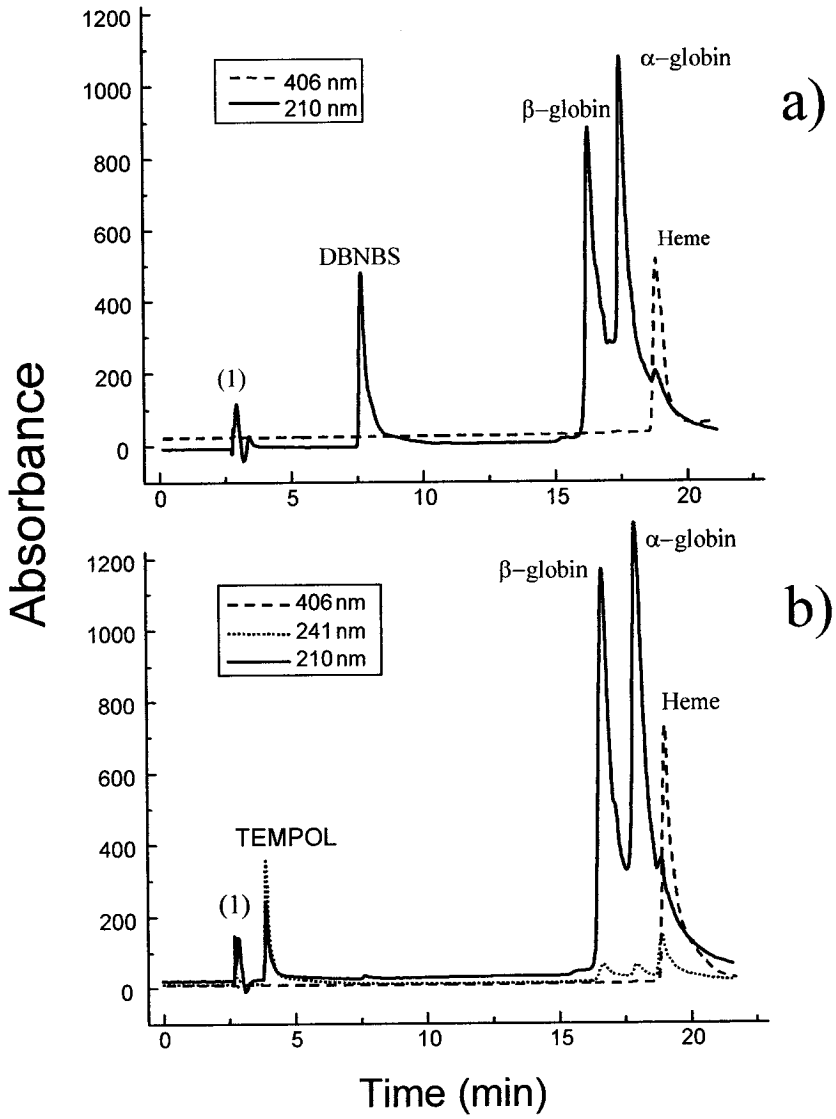

Figure 6.7. HPLC reversed-phase separation of Hb α-globin, β-globin and heme from buffer salts and excess reactants in the 28 mM (heme) metHb/CO incubate. Separation was performed using a C_{18} column (4.6x250 mm), 20-55% CH_3CN gradient and 0.05% TFA, at 1 mL/min over 20 min. (**a**) MetHb/CO/Cu^{II}/DBNBS incubate. (**b**) MetHb/CO/Cu^{II}/TEMPOL$^{\bullet}$ incubate. Peak (1) corresponds to the buffer salts eluted at 2.7 min. The Hb incubates were left standing at 25°C for 30 min in 200 mM NaPi (pH 7.2) with 15 mM $CuSO_4$ and 30 mM DBNBS or 50 mM TEMPOL$^{\bullet}$ where indicated. The chromatogram obtained for the metHb/CO incubate was essentially identical to that in **(a)** except that no DBNBS peak was present.

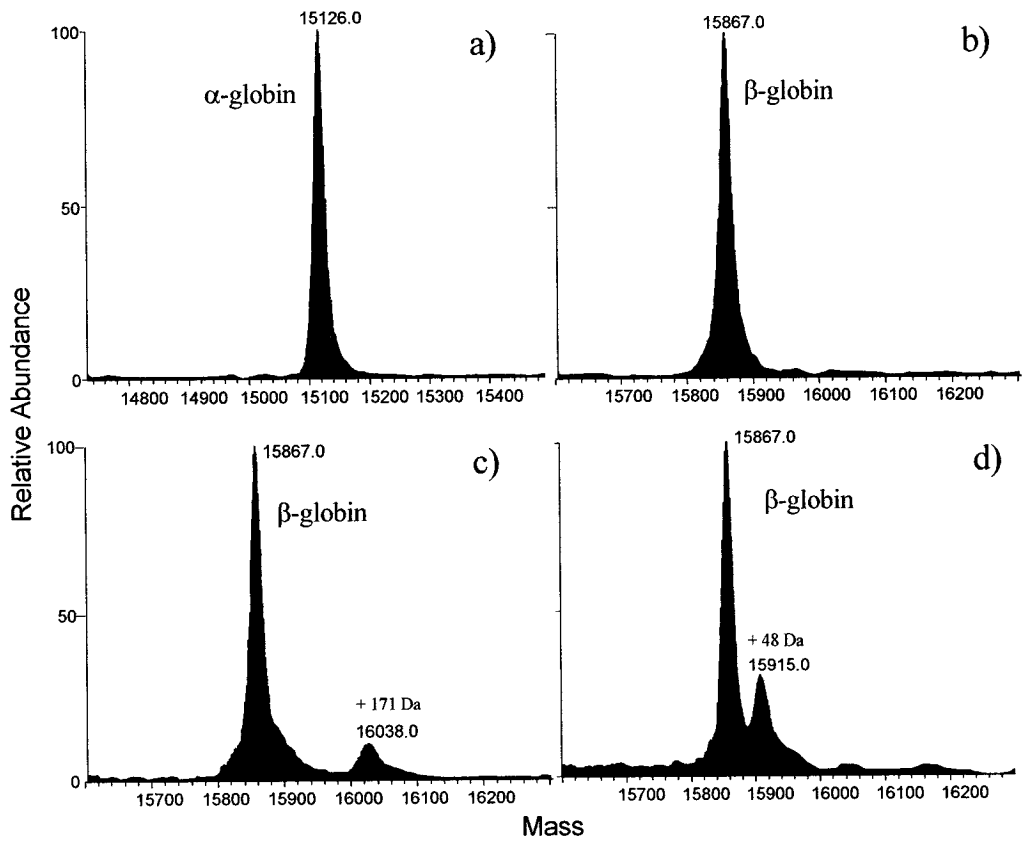

Figure 6.8. ESI mass spectra of the globin subunits from the 28 mM (heme) metHb/CO incubate. Deconvolved mass spectra of: (**a**) α-globin from a metHb/CO incubate; (**b**) β-globin from the metHb/CO/TEMPOL• incubate; (**c**) β-globin from the metHb/CO/Cu^{II}/TEMPOL• incubate, and (**d**) β-globin from metHb/CO/Cu^{II}/DTPA/TEMPOL• incubate. MetHb was incubated under 1 atm CO for 30 min with 15 mM $CuSO_4$, 30 mM DTPA and 50 mM TEMPOL• where indicated. The Hb samples were diluted 10^3-fold in H_2O immediately before injection into the HPLC 1090 for LC-MS analysis. The ESI source voltage and capillary temperature were 3.5 kV and 180°C, respectively, and the on-line flow rate into the source was 5 μL/min.

α-globin was unmodified (data not shown). The mass spectrum of β-globin from the metHb/CO/Cu^{II}/DMPO incubate showed a weak band just above the noise corresponding to β-globin + 113 ±1 (15,979 Da) (data not shown), which matches the mass expected for a DMPO (MW 113.2) spin adduct [β-globin - H + DMPO] or a reduced diamagnetic adduct [β-globin – H + DMPO + H]. Modified β-globin with an increased mass of +32 Da was detected in the mass spectrum of the metHb/CO/Cu^{II}/DTPA/DMPO incubate (data not shown), which could be due to the binding of two oxygen atoms to the β-subunit. No modification of the α-globin was detected in the DMPO incubates.

The DBNBS- and TEMPOL$^{\bullet}$-containing fractions from the HPLC separation (Figure 6.7) were collected (~0.5 mL) and also analysed by ESI-MS. The DBNBS fraction was lyophilised and redissolved in 500 μL of 20 mM CH_3COONH_4 in 80% ACN and its ESI mass spectrum recorded in negative-ion mode. Figure 6.9a shows the $(M + NH_2)^-$ ammoniated ion of DBNBS at m/z 357.6, and peaks at m/z 359.6 and 361.7 are assigned to ions containing one and two ^{81}Br atoms, respectively. The 1:2:1 intensity ratio of the three peaks is as expected for an ion containing two Br atoms (187). The ESI mass spectrum performed in positive-ion mode of TEMPOL$^{\bullet}$ collected from the HPLC, lyophilised and redissolved in 500 μL of 75 % ACN in 0.05 % TFA is shown in Figure 6.9b. The two abundant peaks at m/z 173.2 and 158.1 are assigned to the $MH^{\bullet+}$ and $(MH-{}^{\bullet}CH_3 + H)^+$ ions, respectively, of TEMPOL$^{\bullet}$.

6.4.3 Tryptic Digestion and Peptide Mass Mapping by LC/MS

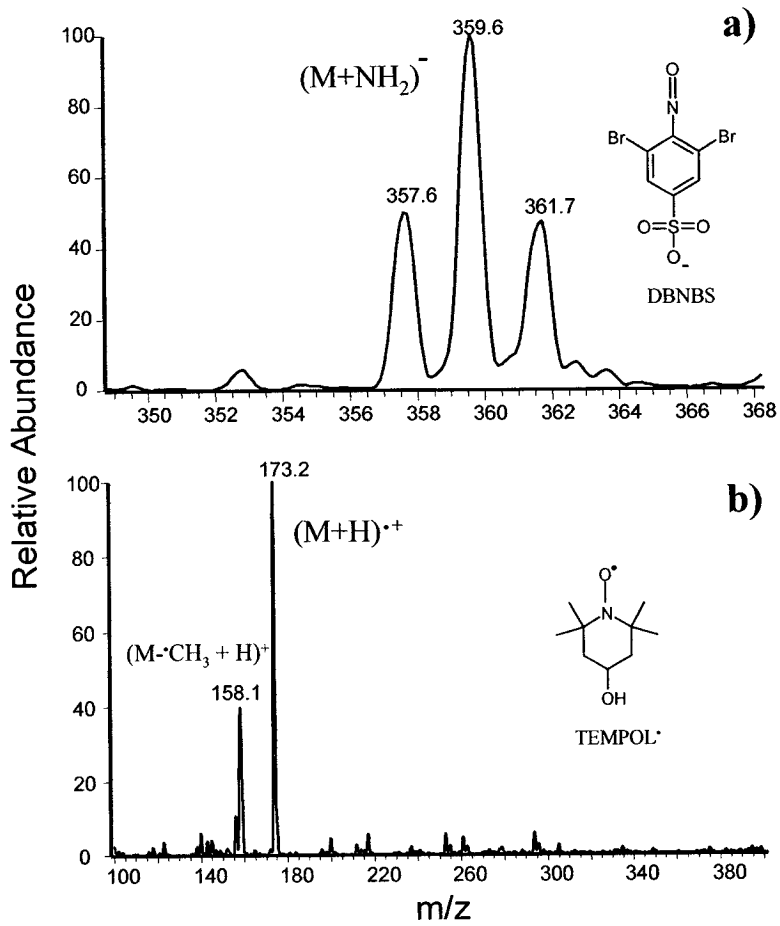

Figure 6.9. ESI mass spectra of DBNBS and TEMPOL·. (**a**) Negative-ion spectrum of DBNBS in 20 mM CH_3COONH_4 in 80 % ACN. (**b**) Positive-ion spectrum of TEMPOL· in 75 % ACN in 0.05 % TFA. The DBNBS and TEMPOL· samples were obtained from the HPLC separation of the metHb/CO incubates (Figure 6.7), lyophilised and redissolved immediately before direct injection at a flow rate of 5 µL/min into the ESI source. The source voltage and capillary temperature were 3.5 kV and 180°C, respectively.

Table 6.2. Theoretical and observed tryptic peptides of human Hb β-globin

Peptide		Mass (Da)[a]	Sequence[b]	Observed Sequence[c]
(1)	1-8	952.1	VHLTPEEK	VHLTPEEK
(2)	9-17	932.1	NAVTTLWGK	NAVTTLWGK
(3)	18-30	1314.4	VNVDEVGGEALGR	VNVDEVGGEALGR
(4)	31-40	1274.5	LLVVYPWTQR	LLVVYPWTQR
(5)	41-59	2059.3	FFESFGDLSSPDAVMGNPK	
(6)	60-61	245.3	VK	VK
(7)	62-65	411.5	AHGK	
(8)	66-66	146.2	K	
(9)	67-82	1669.9	VLGAFSDGLNHLDNLK	
(10)	83-95	1421.6	GTFAQLSELHCDK	GTFAQLSELHCDK
(11)	96-104	1126.2	LHVDPENFK	LHVDPENFK
(12)	105-120	1720.1	LLGNVLVCVLAHHFGK	
(13)	121-132	1378.5	EFTPQVQAAYQK	EFTPQVQAAYQK
(14)	133-144	1149.4	VVAGVANALAHK	
(15)	145-146	318.3	YH	YH

[a] Hb β-globin total mass = 15867.2

[b] *In silico* digestion of Hb with trypsin was carried out using Paws software from ProteoMetrics (http://65.219.84.5/paws.html)

[c] The sequence coverage based on the number of residues in the peptides observed in the mass map was 60%

Online analysis by ESI-MS was performed to detect the TEMPOL-labelled peptides following digestion with trypsin. Peptide mass mapping of the α-globin and β-globin (Table 6.2) yelded ~50% sequence coverage of α- (data not shown) and 60% of β-globin (Table 6.2). More interestingly, the β-globin tryptic peptide 83-95 containing Cysβ93 was detected in all the Hb incubates, and the peptide mass map of β-globin from the 28 mM (heme) metHb/CO/Cu^{II}/TEMPOL$^{\bullet}$ incubate (Figure 6.8c) shows a weak band at 56.9 min that corresponds to peptide 83-95 + TEMPOL$^{\bullet}$ (Figures 6.10a,b). The mass spectrum of the 56.9-min band shows two peaks corresponding to the $(M+H)^{+}$ and $(M+2H)^{2+}$ ions of peptide 83-95 + TEMPOL$^{\bullet}$ at m/z 1593.4 and 798.5, respectively (Figure 6.10c).

6.5 Discussion

Cu^{II} is often present as an impurity in water-buffer components (~μM) and it has been found that Cu^{II} bound to amino acids, peptides, and proteins can oxidize the thiolate anion. Two copper-binding sites (114) have been identified in human Hb (Figure 6.11). A high-affinity Cu^{II}-binding site (K_d ~200 nM) is located at the N-terminus region of each β-globin. The binding appears to involve the amino-terminal nitrogen, as well as the imidazole group of Hisβ2. A low-affinity Cu^{II}-binding (K_d ~2 μM) site is in the proximity of the β-heme and Cysβ93 sulfhydryl group (114,188). A sulfur radical has been detected in oxyHb by EPR at low temperature and this has been assigned to Cysβ93 (189). Electron transfer from Cysβ93 to superoxide formed in the β-heme pocket is assumed to give rise to the observed thiyl radical. Using the spin trap, DMPO, trapping of

Figure 6.10. Peptide mass mapping of β-globin from the 28 mM (heme) metHb/CO/Cu^{II}/TEMPOL$^{\bullet}$ incubate. The β-globin HPLC fraction (Figure 6.7c), was lyophilised and digested with 1:50 trypsin/protein (w/w) at 40°C for 20 h in 200 mM NaPi buffer (pH 7.2). The digest (20 μL) was loaded on a Vydac microbore C_{18} column (1x300 mm) and the peptides eluted with a 5-60% CH_3CN gradient in 0.05% TFA at 40 μL/min over 100 min. (**a**) Absorbance at 210 and 280 nm *vs* time of the HPLC eluate. (**b**) TIC vs time of the HPLC eluate. (**c**) ESI mass spectrum of the 56.9-min band in (**b**). The ESI source voltage and capillary temperature were 3.5 kV and 180°C, respectively.

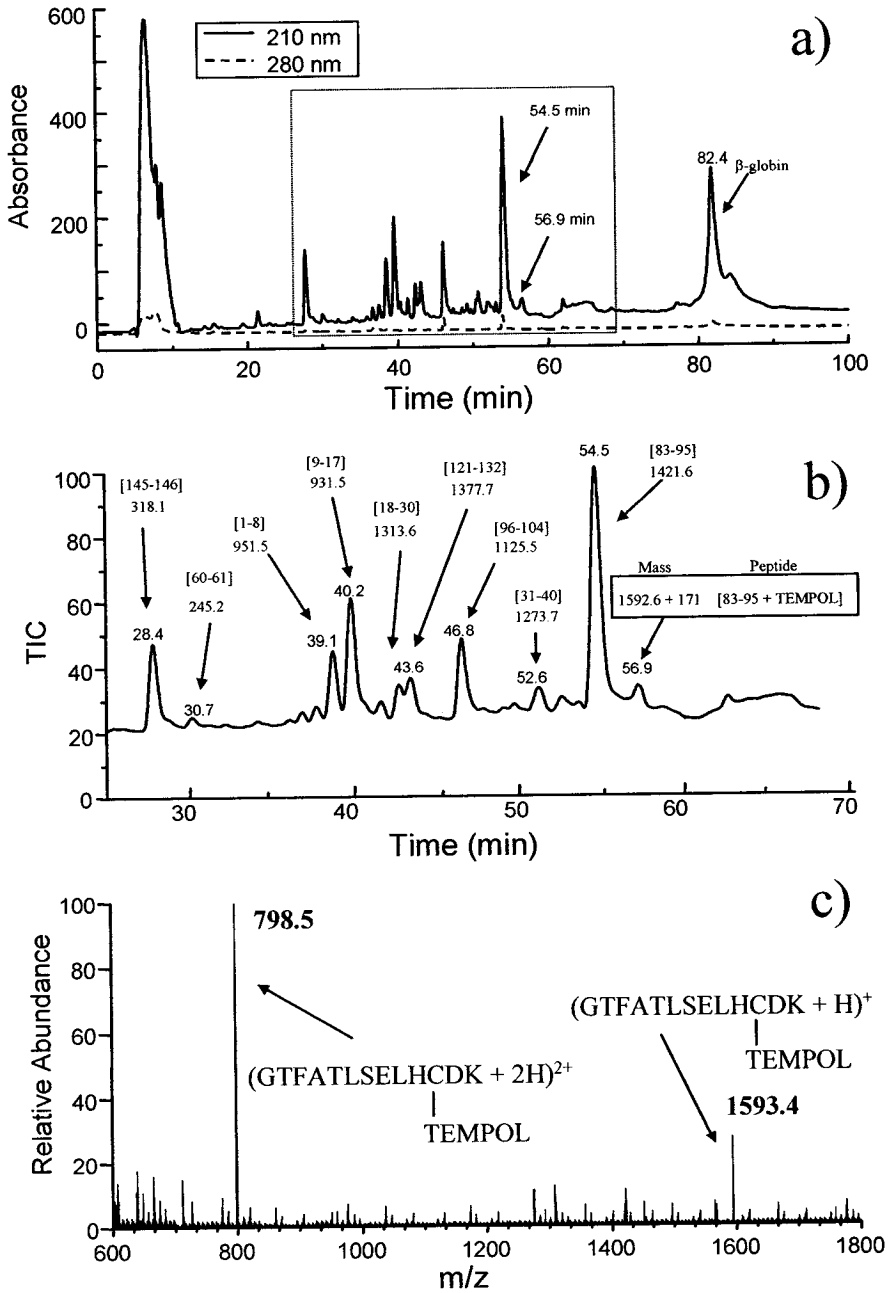
a)
210 nm
280 nm
Absorbance
Time (min)
54.5 min
56.9 min
82.4
β-globin
b)
TIC
Time (min)
[145-146] 318.1
[60-61] 245.2
[1-8] 951.5
[9-17] 931.5
[18-30] 1313.6
[121-132] 1377.7
[96-104] 1125.5
[31-40] 1273.7
[83-95] 1421.6
54.5
Mass
Peptide
1592.6 + 171
[83-95 + TEMPOL]
28.4
30.7
39.1
40.2
43.6
46.8
52.6
56.9
c)
Relative Abundance
m/z
798.5
(GTFATLSELHCDK + 2H)2+
TEMPOL
(GTFATLSELHCDK + H)+
TEMPOL
1593.4

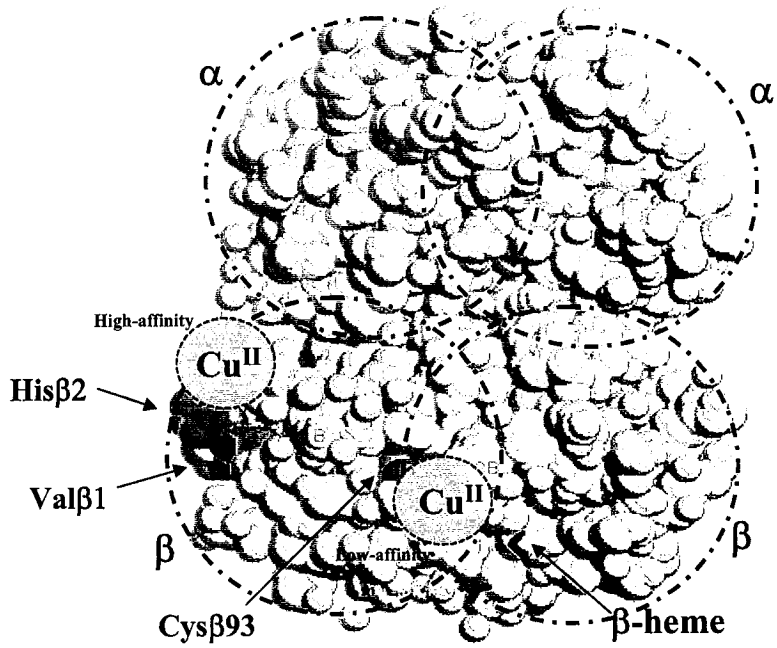

Figure 6.11. Copper-binding sites in human Hb. The high-affinity Cu^{II}-binding site (K_d ~200 nM) is located in the N-terminal region of each β-globin. The binding appears to involve the nitrogen of the amino terminal residue Valβ1 as well as the imidazole side chain of Hisβ2. A low-affinity Cu^{II}-binding site (K_d ~2 μM) is located in the proximity of the β-heme and Cysβ93. This space-filling model was generated using RasWin Molecular Graphics 2.6 and the coordinates of human deoxyHb in PDB file 2HHB.

a thiyl radical on Hb *in vivo* has also been reported following phenylhydrazine administration to rats (190). The DMPO spin adduct was detected by EPR (191) and the mechanism of thiyl radical formation was proposed to involve a ferryl-Hb (Fe^{IV}=O) intermediate that oxidized Cysβ93. (191).

Copper-enhanced CO/H_2O-driven reduction in samples containing 13 μM (heme) metHb has been reported (172). Approximately 100% $Fe^{II}CO$ was formed in 12 h and reportedly this involves electron transfer from Cysβ93 to the β-heme to reduce Fe^{III} to Fe^{II}, which is trapped by CO (172). Although a short (13 Å) intramolecular electron-transfer pathway is shown in Figure 6.6, CO/H_2O-driven reduction of metHb in metHb/CO/Cu^{II} incubates is complete only after ~12 h at 7 μM (heme) Hb (Figure 6.3), while it appears to be complete within 30 min at 14 mM (heme) Hb (Figure 6.4). The dramatic Hb concentration dependence of heme reduction indicates that this is likely a bimolecular process at high protein concentrations:

$$Hb_A\text{-}S^- + Hb_B\text{-}Fe^{III} + CO \rightleftharpoons Hb_A\text{-}S^\bullet + Hb_B\text{-}Fe^{II}CO \qquad (6.4)$$

Furthermore, since copper accelerates Reaction 6.4, another possibility could be oxidation of the Cysβ93 thiolate by Cu^{II} and reduction of metHb by Cu^{I} (Reactions 6.5 and 6.6):

$$Hb_A\text{-}S^- + Cu^{II} \rightleftharpoons Hb_A\text{-}S^\bullet + Cu^{I} \qquad (6.5)$$

$$Hb_B\text{-}Fe^{III} + Cu^{I} + CO \rightleftharpoons Hb_B\text{-}Fe^{II}CO + Cu^{II} \qquad (6.6)$$

The rapid reduction of the Hb heme at millimolar *vs* micromolar Hb concentrations in the presence of copper (Figure 6.4 *vs* 6.3) is consistent with the mechanism defined by Reactions 6.5 and 6.6. The added Cu^{II} ion oxidizes Cysβ93 on Hb_A and the Cu^{I} formed reduces the heme of Hb_B. But what is the fate of Cysβ93 thiyl radical? Loss of the ν(SH) absorption of Cysβ93 is seen in the 28 mM (heme) metHb/CO/Cu^{II} incubate in Figure 6.5a. In this incubate carbonylHb formation is ~100% as evidenced by the intensity of its ν(CO) band (Figure 6.5b). Given that heme/Cysβ93 ratio in Hb is 2:1, reducing equivalents must come from the water-gas shift reaction (eq. 6.7):

$$CO + H_2O \rightleftharpoons CO_2 + 2\,H^+ + 2\,e^- \qquad (6.7)$$

Do electrons supplied by Reaction 6.7 also re-reduce Cysβ93? Loss of the ν(SH) absorption in the 28 mM (heme) metHb/CO/Cu^{II} incubate (Figure 6.5a) suggests that this is not the case, except of course, copper may coordinate to Hb *via* the sulfur atom of Cysβ93 in the lower-affinity copper-binding site of Hb (Figure 6.11). The effects of adding $CuSO_4$ on the ν(SH) of authentic carbonylHb and also of metHb should be examined to establish if the metal coordinates the sulfur atom of Cysβ93.

Evidence of TEMPOL$^{\bullet}$ spin scavenging in the metHb/CO/Cu^{II}/TEMPOL$^{\bullet}$ incubate is obtained from the LC/ESI/MS experiments. The β-globin is singly TEMPOL-labelled in the 28 mM (heme) metHb/CO/Cu^{II}/TEMPOL$^{\bullet}$ incubate (Figure 6.8d) and the peptide mass of this singly labelled β-globin reveals that the label is located on peptide 83-95 containing Cysβ93 (Figure 6.10). In the presence of 2-fold molar excess DTPA to chelate the Cu^{II} there is no evidence of Hb-TEMPOL labelling. The ESI mass spectrum

of the 28 mM (heme) metHb/CO/Cu^{II}/DTPA/TEMPOL$^{\bullet}$ incubate showed a peak at the m/z of β-globin +48 (Figure 6.8d) corresponding to the addition of three atoms of oxygen. This likely is due to sulfoxide ($-SO_3^-$) formation on Cysβ93 and not a TEMPOL-derived adduct (Figure 6.8d). If the side chain of Cysβ93 is partially converted to a sulfoxide then the yield of thiyl radical reduction *via* Reaction 6.7 is clearly not 100%.

In the DMPO incubates a weak band corresponding to Hb-DMPO adduct was observed (Table 6.1). However, the ESI-MS spectra of the Hb/DBNBS incubates showed no evidence of β-globin mass-adduct formation (data not shown). It is possible that in this case, DBNBS is not an efficient trap of the Cysβ93 radical. Spin scavenging by TEMPOL$^{\bullet}$ is expected to be up to 10^2-fold faster than spin trapping by DBNBS (99). Thus, DBNBS may not be able to compete with reduction of the thiyl radical using electrons from Reaction 6.7 or with scavenging by O_2.

6.6 Conclusions

This work provides strong evidence for thiyl radical formation on Cysβ93 during copper-enhanced CO/H_2O driven metHb reduction. Copper in excess of that which binds to the high affinity copper site of Hb (Figure 6.11) plays an important role in thiyl radical formation in the metHb/CO reaction since DTPA inhibits carbonylHb formation (Figure 6.4). Since heme reduction is greatly accelerated at high (mM compared to low μM) Hb concentrations, intramolecular electron transfer between Cysβ93 and the heme is not likely an efficient process. However, it must be borne in mind that the total copper concentration (3.5 μM) in incubates containing micromolar Hb was close to the K_d (2 μM) for the low-affinity copper-binding site of Hb (Figure 6.11). The experiment in

Figure 6.3 needs to be repeated at higher copper concentrations (e.g., 20 μM) to see the effects on the rate of carbonylHb formation. Nonetheless, the very slow rate of Hb reduction at micromolar protein suggests that electron coupling between the heme Fe and Cysβ93 is poor. Release of NO from Cysβ93 in deoxyHb-SNO has been proposed to involve intramolecular electron transfer from the deoxy (Fe^{II}) heme to CysSNO on Cysβ93 (160):

$$ONS\sim\sim\sim Fe^{II}O_2 \rightleftharpoons ONS\sim\sim\sim Fe^{II} + O_2 \qquad (6.8)$$

$$ONS\sim\sim\sim Fe^{II} \rightleftharpoons NO^{\bullet} + {}^{-}S\sim\sim\sim Fe^{III} \qquad (6.9)$$

In Reactions 6.8 and 6.9, the heme Fe and the S of Cysβ93 are connected by the path shown in Figure 6.6. In a proposed mechanism of NO release from deoxyHb, intramolecular electron transfer occurs between the Fe^{II} and the SNO group (Reaction 6.9). Given the present results, this mechanism of NO release from Hb-SNO is unlikely.

7.0 Conclusions and Suggestions for Future Work

7.1 Chapters 2, 3 and 4

Studies on control of S-nitrosothiol stability studies are consistent with metal-catalyzed NO release from RSNOs. Stability of RSNOs in solution is a function of the presence of trace Cu^{I} ions. We have shown that metal chelators inhibit S-nitrosation of Cysβ93 in oxyHb/CysSNO and oxyHb/GSNO incubates and our results strongly point to a mechanism involving Cu^{II}-catalysis of Cysβ93 S-nitrosation by *free* NO generated by Cu^{I}-catalysis of RSNO breakdown. These results are *inconsistent* with Hb-SNO formation *via* simple *trans*-S-nitrosation (NO^{+} transfer) and with published *trans*-S-nitrosation equilibrium and rate constants derived from experimental data where Hb-SNO formation was only inferred, not observed (66,130,131).

We have also found that in oxyHb/GSNO incubates, CuZnSOD targets NO from GSNO to Cysβ93 of oxyHb. Furthermore, we propose that erythrocyte CuZnSOD plays a vital role in vasorelaxation by targeting NO to Cysβ93 of oxyHb and preventing its scavenging by the $Fe^{II}O_2$ heme. The allosteric transition of Hb controls the products formed in CuZnSOD-catalyzed NO transfer from GSNO to Hb since NO is channeled to Cysβ93 in oxyHb incubates but scavenged by the heme in deoxyHb incubates. The critical factor in channeling would be the formation of an oxyHb-CuZnSOD encounter complex. Conversion of NO to NO_3^-, with loss of its potent vasorelaxing properties, occurs in the absence of CuZnSOD or at oxyHb concentrations way below physiological values, conditions that eliminate or disrupt oxyHb-CuZnSOD complexation.

Like protein phosphorylation, protein S-nitrosation represents a fundamental mechanism for the reversible post-translational control of protein activity and cellular function (159). Our data suggest a general mechanism for selectivity in protein S-nitrosation (Schemes 4.11-4.12 and 4.13-4.14, Chapter 4.0). Only proteins with cysteine residues that can act as donors to a NO-transferase such as CuZnSOD will be S-nitrosated. Co-localization of the donor and transferase, as occurs in RBCs for oxyHb and CuZnSOD, will promote S-nitrosation of the target, which in the present case serves to preserve the bioactivity of NO.

7.2 Chapters 5 and 6

We have found that heme nitrosylation of deoxyHb by S-nitrosogluthatione requires copper. Our data are *inconsistent* with direct reduction of GSNO by deoxyHb, but are consistent with catalysis of GSNO breakdown by trace Cu to yield *free* NO, which is subsequently scavenged by the deoxyheme. Since deoxyHb is stable in the presence of GSNO when free Cu is rigorously excluded from the system, direct reduction of GSNO by deoxyHb is unlikely to be of biological significance.

Thiyl radicals are formed on Cysβ93 during copper-enhanced CO/H_2O-driven reduction of metHb. Evidence for Cysβ93 adduct formation was obtained using the radical scavenger TEMPOL$^{\bullet}$. The key role played by copper in thiyl radical formation during the metHb/CO reaction is consistent with the mechanism proposed for its catalysis of Hb S-nitrosation reactions by RSNOs. Contrary to suggestions in the literature, intramolecular electron transfer between the heme and Cysβ93 is unlikely important in the copper-catalyzed processes discussed here. Tables 7.1 and 7.2 summarize the

products of the deoxyHb/RSNO and oxyHb/RSNO and the correspondingDEA/NO reactions examined in this thesis.

Table 7.1. Summary of products of deoxyHb/RSNO or deoxyHb/DEA/NO incubates

5 min incubate[a]		products observed					
DeoxyHb	Cyβ93/NO[b]	Heme Fe (%)[c] Soret/Visible	Cysβ93-SH (%)[d] FTIR	β-globin + NO[e] ESI-MS	RSNO (RA)[f] ESI-MS	RSH(RA)[f] ESI-MS	RSSR (RA)[f] ESI-MS
Hb/CysSNO	1	1 Fe^{II} 99 $Fe^{II}NO$	100	not observed	not observed	~15	~85
Hb/CysSNO/DTPA[g]	1	20 Fe^{II} 80 $Fe^{II}NO$	100	not observed	~20	~25	~75
Hb/GSNO	1	1 Fe^{II} 99 $Fe^{II}NO$	100	not observed	~5	~20	~80
Hb/GSNO/DTPA[g]	1	44 Fe^{II} 47 $Fe^{II}NO$ 8 Fe^{III} 1 $Fe^{III}NO$	100	not observed	~45	~65	~35
Hb/GSNO/neo[g]	1	75 Fe^{II} 25 $Fe^{II}NO$	100	not observed	~90	~30	~70
dialHb/GSNO[h]	1	67 Fe^{II} 33 $Fe^{II}NO$	100	not observed	~35	~40	~60
dialHb/GSNO/neo	1	98 Fe^{II} 2 $Fe^{II}NO$	100	not observed	~95	~25	>20
3xDEAE-Hb/GSNO[i]	2	98 Fe^{II} 2 $Fe^{II}NO$	100	not observed	~90	~80	>20
3xDEAE-Hb/GSNO/ /CuZnSOD[j]	2	57 Fe^{II} 43 $Fe^{II}NO$	100	not observed	~5	~50	~50
3xDEAE-Hb/GSNO/ $CuSO_4$[k]	2	68 Fe^{II} 32 $Fe^{II}NO$	100	not observed	~5	~35	~65
3xDEAE-Hb/DEA/NO[l]	4	50 Fe^{II} 50 $Fe^{II}NO$	100	not observed	-	-	-
Hb/GSNO (μM)[m]	1	10 Fe^{II} 90 $Fe^{II}NO$	100	not observed	~15	~30	~70
Hb/GSNO/DTPA/neo (μM)[m]	1	15 Fe^{II} 85 $Fe^{II}NO$	100	not observed	~20	~45	~55

Footnotes to Table 7.1

[a] DeoxyHb (24 mM heme) was incubated with the reagents indicated for 5 min in 200 mM sodium phosphate buffer (pH 7.2) at 25°C. The results are the averages of at least triplicate experiments

[b] Ratio of Cysβ93 to NO-donor concentration

[c] Redox and sixth ligand (where indicated) of heme Fe determined by multicomponent analysis of Soret and visible regions of the absorption spectra

[d] Cysβ93 ν(SH) band at 2577 (deoxyHb) and 2588 cm^{-1} (oxyHb) monitored by FTIR

[e] Precence of peak corresponding to NO adduct of Hb β-globin in the ESI mass spectrum

[f] Relative abundance (RA) of $(RSX + H)^+$ peak in the ESI mass spectrum of the incubate compared to a RSX standard of known concentration (X = NO, H, SR)

[g] 500 μM DTPA and 200 μM neocuproine were added where indicated

[h] Hb dialyzed *vs* EDTA as described in Chapter 5

[i] Hb passed 3 times through a DEAE column as described in Chapter 4

[j] Incubate of 15 mM (heme) 3xDEAE-Hb with 10 μM CuZnSOD monomer as described in Chapter 4

[k] Incubate of 15 mM (heme) 3xDEAE-Hb with 10 μM $CuSO_4$ as described in Chapter 4

[l] Incubate of 15 mM (heme) 3xDEAE-Hb with 3.75 mM DEA/NO as NO donor as described in Chapter 4

[m] 2 μM incubate of Hb as described in Chapter 4

Table 7.2. Summary of products of oxyHb/RSNO or oxyHb/DEA/NO incubates

5 min incubate[a]		products observed					
OxyHb	Cysβ93/NO[b]	Heme (%)[c] Soret/Visible	Cysβ93-SH (%)[d] FTIR	β-globin + NO[e] ESI-MS	RSNO (%)[f] ESI-MS	RSH(%)[f] ESI-MS	RSSR (%)[f] ESI-MS
Hb/CysSNO	1	52 $Fe^{II}O_2$ 48 Fe^{III}	not observed	observed	not observed	~95	not observed
Hb/CysSNO (+ DTPA)[g]	1	60 $Fe^{II}O_2$ 40 Fe^{III}	100	not observed	~15	~75	~25
Hb/GSNO	1	54 $Fe^{II}O_2$ 46 Fe^{III}	not observed	observed	~5	~95	not observed
Hb/GSNO/DTPA[g]	1	77 $Fe^{II}O_2$ 23 Fe^{III}	100	not observed	~25	~80	~20
Hb/GSNO/neo[g]	1	88 $Fe^{II}O_2$ 12 Fe^{III}	100	not observed	~90	~30	~70
dialHb/GSNO[h]	1	72 $Fe^{II}O_2$ 28 Fe^{III}	100	not observed	~70	~80	~20
dialHb/GSNO/neo	1	95 $Fe^{II}O_2$ 5 Fe^{III}	100	not observed	~90	~50	~50
Hb/GSNO	2	62 $Fe^{II}O_2$ 48 Fe^{III}	not observed	observed	~5	~95	not observed
3xDEAE-Hb/GSNO/ /CuZnSOD/DTPA/neo)[i,j]	2	98 $Fe^{II}O_2$ 2 Fe^{III}	100	not observed	~95	~25	>20
3xDEAE-Hb/GSNO/ /CuZnSOD[i,j]	2	53 $Fe^{II}O_2$ 42 Fe^{III}	not observed	observed	~5	~90	not observed
3xDEAE-Hb/GSNO /$CuSO_4$[k]	2	68 $Fe^{II}O_2$ 32 Fe^{III}	~80	not observed	~5	~30	~70
3xDEAE-Hb/DEA/NO[l]	4	52 $Fe^{II}O_2$ 48 Fe^{III}	100	not observed	-	-	-
Hb/GSNO (μM)[m]	1	53 $Fe^{II}O_2$ 47 Fe^{III}	100	not observed	~20	~20	~80
Hb/GSNO/DTPA/neo (μM)[m]	1	57 $Fe^{II}O_2$ 43 Fe^{III}	100	not observed	~25	~60	~40

[a-m] See footnotes to Table 7.1

7.3 Revised Model of Reactions of NO with Hb during the Respiratory Cycle

Since NO causes rapid vasorelaxation (9), Hb and CuSOD could regulate blood flow by releasing NO under low oxygen tension (56,138). Physiological low-molecular-weight RSNOs such as GSNO, are potential NO donors to oxyHb Cysβ93 *in vivo* (134,192). We propose the scheme shown on Figure 7.1 that summarizes a model involving CuZnSOD catalysis of oxyHb Cysβ93 S-nitrosation and deoxyHb Cysβ93 denitrosation. In the lungs the partial pressure of O_2 is high (~80 mmHg) and Hb reaches its maximum oxygen saturation point. The sulfur atom of oxyHb Cysβ93 loses a proton and forms a thiolate anion that reduces CuZnSOD. Then, Cu^{I}ZnSOD-catalyzed degradation of GSNO or other RSNO in the RBC releases NO, which is transferred to the Cysβ93 radical (Steps 1 and 2). In the microcirculation, the O_2 partial pressure lowers (~30 mmHg) and Cu^{II}ZnSOD is reduced by GSH. OxyHb releases O_2 becoming deoxyHb, which releases NO by a Cu^{I}ZnSOD-catalyzed mechanism (Step 3). NO is released from the RBC to exert its vasorelaxtion action and further increase tissue oxygenation. In the capillaries deoxyHb can also bind NO at the α-heme Fe^{II} (Step 4) and return to the lungs where NO is exhaled or forms RSNO (Step 5), which goes back into the cycle (Step 2).

This study suggests a possible mechanism of Hb S-nitrosation in the RBC. Further, elucidation of this mechanism as well as that of Hb-SNO denitrosation should help in the design of drugs for blood-pressure control (192), provide some insight into essential hypertension (193), and impact on the design of a new generation of blood substitutes (194,195).

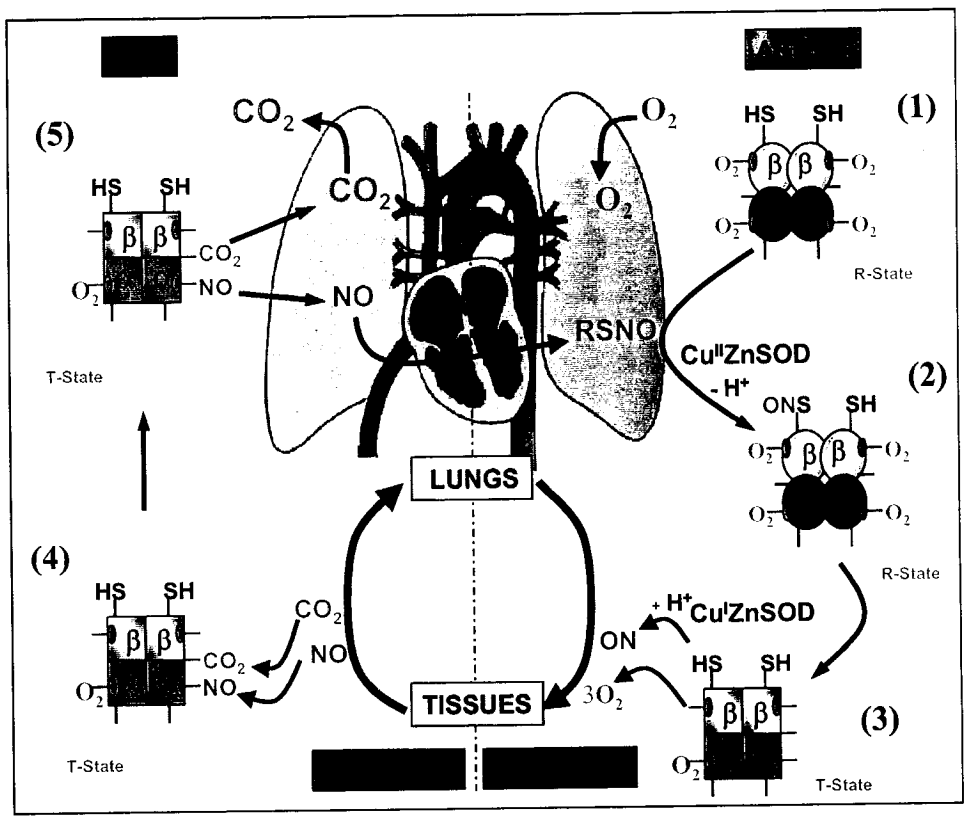

Figure 7.1. Model of CuZnSOD-catalyzed transport of NO by Hb during the respiratory cycle. This model is described in Section 7.3.

7.4 Suggestions for Future Work

(1) Study reactions of RSNOs with forms of Hb other than deoxy and oxy to investigate the effects of different heme ligands on Cysβ93 reactivity. For example, metHb, cyanometHb and carbonylHb could be studied.

(2) Compare S-nitrosation and denitrosation reactivity under various conditions for other Hbs, including human fetal, rat, bovine, and horse Hbs. Investigate CuZnSOD-catalysis for these different Hbs, which vary in the number and type of cysteine residues.

(3) Sequence by MS/MS the modified β-globin peptides from the S-nitrosation and TEMPOL-labelling reactions. Sequencing by MS can be carried out on a triple quadrupole or QTOF MS instrument.

(4) Using TEMPOL$^{\bullet}$ as a thiyl radical scavenger, investigate the mechanism of radical formation in oxyHb in the presence or absence of CuZnSOD.

(5) Examine the competition between deoxy heme and Cysβ93 for NO in Hb/GSNO/CuZnSOD incubates containing different ratios of oxyHb and deoxyHb.

(6) Examine the mechanism of Hb-SNO denitrosation in the presence of various amounts of GSH.

(7) To determine if and how NO can be transferred from the heme to Cysβ93 (196,197), the products of oxyHb should be examined.

8.0 References

1. Ignarro, L. J. (1990) *Annu. Rev. Pharmacol. Toxicol.* **30,** 535.
2. Feldman, P. L. (1993) *Chem. Eng.* Special Report (December 20), 26.
3. Butler, A. R., and Williams, D. L. H. (1993) *Chem. Soc. Rev.* **22,** 233.
4. Stamler, J. S., Singel, D. J., and Loscalzo, J. (1992) *Science* **258,** 1898.
5. Thatcher, G. R. J., and Weldon, H. (1998) *Chem. Soc. Rev.* **27,** 331.
6. Jourd'heuil, D., Gray, L., and Grisham, M. B. (2000) *Biochem. Biophys. Res. Commun.* **273**(1), 22.
7. Williams, D. L. H. (1999) *Acc. Chem. Res.* **32,** 869.
8. Singh, R. J., Hogg, N., Joseph, J., and Kalyanaraman, B. (1996) *J. Biol. Chem.* **271**(31), 18596.
9. Myers, P. R., Minor, R. L., Jr., Guerra, R., Jr., Bates, J. N., and Harrison, D. G. (1990) *Nature* **345,** 161.
10. Williams, D. L. H. (1996) *Chem. Commun.*, **10**, 1085.
11. Cotton, F. A., and Wilkinson, G. (1972) *Advance Inorganic Chemistry: a Comprehensive Text, 354-362*, Third Ed., Interscience Publishers, New York
12. Gow, A. J., and Stamler, J. S. (1998) *Nature* **391**(6663), 169.
13. Cooper, C. E. (1999) *Biochim. Biophys. Acta* **1411**(2-3), 290.
14. Tabrizi-Fard, M. A., Lee, W. I., and Fung, H. L. (1999) *Biochem. Pharmacol.* **58**(4), 671.
15. Saran, M., Michel, C., and Bors, W. (1990) *Free Radical Res. Commun.* **10,** 221.
16. Doyle, M. P., and Hoekstra, J. W. (1981) *J. Inorg. Biochem.* **14**(4), 351.
17. Arnelle, D. R., and Stamler, J. S. (1995) *Arch. Biochem. Biophys.* **318**(2), 279.

18. Arulsamy, N., Bohle, D. S., Butt, J. A., Irvine, G. J., Jordan, P. A., and Sagan, E. (1999) *J. Am. Chem. Soc.* **121,** 7115.

19. Pawloski, J. R., Swaminathan, R. V., and Stamler, J. S. (1998) *Circulation* **97**(3), 263.

20. Gergel, D. (1997) *Arch. Biochem. Biophys.* **347**(2), 282.

21. Stubauer, G., Giuffre, A., and Sarti, P. (1999) *J. Biol. Chem.* **274**(40), 28128.

22. De Oliviera, M. G., Shishido, S. M., Seabra, A. B., and Morgon, N. H. (2002) *J. Phys. Chem.* **106**(38), 8963.

23. Komiyama, T., and Fujimori, K. (1997) *Bioorg. Medicinal Chem. Lett.* **7**(2), 175.

24. Askew, S. C., Barnett, D. J., McAninly, J., and Williams, D. L. H. (1995) *J. Chem. Soc., Perkin Trans. II*, 741.

25. Palmer, R. M., Ferrige, A. G., and Moncada, S. (1987) *Nature* **327**(6122), 524.

26. Radomski, M. W., Rees, D. D., and Dutra, A. (1992) *Br. J. Pharmacol.* **107,** 745.

27. Park, J. (1996) *Biochem. Biophys. Res. Commun.* **220,** 31.

28. Clancy, R., Levartovsky, D., Leszczynska-Piziak, J., Yegudin, J., and Abramson, S. (1994) *Proc. Natl. Acad. Sci U. S. A.* **91,** 3680.

29. Lipton, S. A., Choi, Y. B., Pan, Z. H., Lei, S. Z., Chen, H. S., Sucher, N. J., Loscalzo, J., Singel, D. J., and Stamler, J. S. (1993) *Nature* **364,** 626.

30. Hausladen, A., Privalle, T., Keng, T., DeAngelo, J., and Stamler, J. S. (1996) *Cell* **86,** 719.

31. Gaston, B., Reilly, J., Drazen, J. M., Fackler, J., Ramdev, P., Arnelle, D., Mullins, M. E., Sugarbaker, D. J., Chee, C., Singel, D. J., Loscalzo, J., and Stamler, J. S. (1993) *Proc. Natl. Acad. Sci U. S. A.* **90,** 10957.

32. Davisson, R., Travis, M., Bates, J., and Lewis, S. (1996) *Circ. Res.* **79,** 256 262.

33. Rauhala, P., Parameswarannay, K. P., Sziraki, I., Lin, A. M.-Y., and Chiueh, C. C. (1996) *Synapse* **23,** 58.

34. Kluge, I., Gutteck-Amsler, U., Zollinger, M., and Do, K. Q. (1997) *J. Neuro-Chem.* **69,** 2599.

35. Kim, Y.-M., de Vera, M. E., Watkins, S. C., and Billar, T. R. (1997) *J. Biol. Chem.* **272,** 1402.

36. Minetti, M. (1995) *Biochemistry* **21,** 7177.

37. Carnhan, G. E., Lenhert, P. G., and Ravichandran, R. (1978) *Acta Christallogr.* **B34,** 2645.

38. Keefer, L. K., Flippen-Anderson, J. L., George, C., Shanklin, A. P., Dunams, T. M., Christodoulou, D., Saavedra, J. E., Sagan, E. S., and Bohle, D. S. (2001) *Nitric Oxide: Biology and Chemistry* **5**(4), 377.

39. Roy, B. (1994) *J. Org. Chem.* **59,** 7019.

40. Artz, J. D., and Thatcher, G. R. J. (1998) *Chem. Res. Toxicol.* **11**(12), 1394.

41. Hogg, N., Singh, R. J., Joseph, J., Neese, F., and Kalyanaraman, B. (1995) *Free Rad. Res.* **22**(1), 47.

42. Gibson, A., Babbedge, R., and Brave, S. R. (1992) *Br. J. Pharmacol.* **107,** 715.

43. Bannenberg, G., Xue, J., and Engman, L. (1995) *J. Pharmacol. Exp. Ther* **272,** 1238.

44. Maragos, C. M., Morley, D., Wink, D. A., Dunams, T. M., Saavedra, J. E., Hoffman, A., Bove, A. A., Isaac, L., Hrabie, J. A., and Keefer, L. K. (1991) *J. Med. Chem.* **34**(11), 3242.

45. Williams, W. J., Beantler, E., Erslev, A. J., and Rundles, R. W. (2001), pp. 11, McGraw-Hill Book Company A Blakisten Pablication, New York.

46. Nagatomo, S., Nagai, M., Tsuneshige, A., Yonetani, T., and Kitagawa, T. (1999) *Biochemistry* **38**(30), 9659.

47. Creighton, T. E. (1996) *Proteins - Structures and Molecular Properties*, II Ed. (Freeman, Ed.), New York.

48. Antonini, E., and Brunori, M. (1971) *Hemoglobin and Myoglobin in Their Reactions with Ligands.* Frontiers of Biology (Monographs, N.-H. R., Ed.), 21, North-Holland Publishing Company, Amsterdam.

49. Furchgott, R. F., and Zawadzki, J. V. (1980) *Nature* **288**(5789), 373.

50. Ignarro, L. J., Buga, G. M., Wood, K. S., Byrns, R. E., and Chaudhuri, G. (1987) *Proc. Natl. Acad. Sci. U. S. A.* **84**(24), 9265.

51. Gladwin, M. T., Shelhamer, J. H., Schechter, A. N., Pease-Fye, M. E., Waclawiw, M. A., Panza, J. A., Ognibene, F. P., and Cannon, R. O., 3rd. (2000) *Proc. Natl. Acad. Sci. U. S. A.* **97**(21), 11482.

52. Stamler, J. S., Jaraki, O., Osborne, J., Simon, D. I., Keaney, J., Vita, J., Singel, D., Valeri, C. R., and Loscalzo, J. (1992) *Proc. Natl. Acad. Sci. U. S. A.* **89**(16), 7674.

53. Marley, R., Feelisch, M., Holt, S., and Moore, K. (2000) *Free Radic. Res.* **32**(1), 1.

54. Fang, K., Ragsdale, N. V., Carey, R. M., MacDonald, T., and Gaston, B. (1998) *Biochem. Biophys. Res. Commun.* **252**(3), 535.

55. Gladwin, M. T., Ognibene, F. P., Pannell, L. K., Nichols, J. S., Pease-Fye, M. E., Shelhamer, J. H., and Schechter, A. N. (2000) *Proc. Natl. Acad. Sci. USA* **97**(18), 9943.

56. Stamler, J. S., Jia, L., Eu, J. P., McMahon, T. J., Demchenko, I. T., Bonaventura, J., Gernert, K., and Piantadosi, C. A. (1997) *Science* **276,** 2034.

57. Wolzt, M., MacAllister, R. J., Davis, D., Feelisch, M., Moncada, S., Vallance, P., and Hobbs, A. J. (1999) *J. Biol. Chem.* **274**(41), 28983.

58. Jia, L., Bonaventura, C., Bonaventura, J., and Stamler, J. S. (1996) *Nature* **380,** 221.

59. Chan, N. L., Rogers, P. H., and Arnone, A. (1998) *Biochemistry* **37**(47), 16459.

60. Gross, S. S., and Lane, P. (1999) *Proc. Natl. Acad. Sci. U. S. A.* **96**(18), 9967.

61. Yonetani, T., Tsuneshige, A., Zhou, Y., and Chen, X. (1998) *J. Biol. Chem.* **273**(32), 20323.

62. Funai, E. F., Davidson, A., Seligman, S. P., and Finlay, T. H. (1997) *Biochem. Biophys. Res. Commun.* **239**(3), 875.

63. McMahon, T. J., and Stamler, J. S. (1999) *Methods Enzymol.* **301,** 99.

64. McMahon, T. J., Exton Stone, A., Bonaventura, J., Singel, D. J., and Solomon Stamler, J. (2000) *J. Biol. Chem.* **275**(22), 16738.

65. Bonaventura, C., Ferruzzi, G., Tesh, S., and Stevens, R. D. (1999) *J. Biol. Chem.* **274**(35), 24742.

66. Patel, R. P., Hogg, N., Spencer, N. Y., Kalyanaraman, B., Matalon, S., and Darley-Usmar, V. M. (1999) *J. Biol. Chem.* **274**(22), 15487.

67. Petkau, A., Kelly, K., Chelack, W. S., Pleskach, S. D., Barefoot, C., and Meeker, B. E. (1975) *Biochem.Biophys. Res. Commun.* **67**(3), 1167.

68. Misra, H. P., and Fridovich, I. (1972) *J. Biol. Chem.* **247**(21), 6960.

69. Lavelle, F., Michelson, A. M., and Dimitrijevic, L. (1973) *Biochem. Biophys. Res. Commun.* **55**(2), 350.

70. Paschen, W., and Weser, U. (1973) *Biochim. Biophys. Acta* **327**(1), 217.

71. Gregory, E. M., Goscin, S. A., and Fridovich, I. (1974) *J. Bacteriol.* **117**(2), 456.

72. Hewitt, M. P., Mills, J. H., and Hunter, B. (1975) *Can. Vet. J.* **16**(12), 371.

73. Vance, P. G., Keele, B. B., Jr., and Rajagopalan, K. V. (1972) *J. Biol. Chem.* **247**(15), 4782.

74. Rapp, U., Adams, W. C., and Miller, R. W. (1973) *Can. J. Biochem.* **51**(2), 158.

75. Gregory, E. M., and Fridovich, I. (1973) *J. Bacteriol.* **114**(3), 1193.

76. Gregory, E. M., and Fridovich, I. (1973) *J. Bacteriol.* **114**(2), 543.

77. Peeters-Joris, C., Vandevoorde, A. M., and Baudhuin, P. (1975) *Biochem. J.* **150**(1), 31.

78. Tyler, D. D. (1975) *Biochem. J.* **147**(3), 493.

79. Villafranca, J. J., Yost, F. J., Jr., and Fridovich, I. (1974) *J. Biol. Chem.* **249**(11), 3532.

80. Wood, E., Dalgleish, D., and Bannister, W. (1971) *Eur. J. Biochem.* **18**(2), 187.

81. Bannister, J., Bannister, W., and Wood, E. (1971) *Eur. J. Biochem.* **18**(2), 178.

82. Halliwell, B. (1999) *Free Radic. Res.* **4**, 261.

83. Keele, B. B., Jr., McCord, J. M., and Fridovich, I. (1971) *J. Biol. Chem.* **246**(9), 2875.

84. Forman, H. J., and Fridovich, I. (1973) *Arch. Biochem. Biophys.* **158**(1), 396.

85. Jourd'heuil, D., Laroux, F. S., Miles, A. M., Wink, D. A., and Grisham, M. B. (1999) *Arch. Biochem. Biophys.* **361,** 323.

86. Bare, G. H., Alben, J. O., and Bromberg, P. A. (1975) *Biochemistry* **14**(8), 1578.

87. Alben, J. O., Bare, G. H., and Bromberg, P. A. (1974) *Nature* **252,** 736.

88. Shaanan, J. (1983) *J. Mol. Biol.* **171,** 31.

89. Heidner, E. J., Lander, R. C., and Perutz, M. F. (1976) *J. Mol. Biol.* **104,** 707.

90. Dong, A., and Caughey, W. S. (1994) in *Methods Enzymol.* **232**, 139.

91. Dong, A. C., Huang, P., and Caughey, W. S. (1992) *Biochemistry* **31**(1), 182.

92. Perkins, M. J. (1980) in *Spin Trapping* (Gold, V., and Bethell, D., eds) Vol. 17, pp. 1, Academic Press, Toronto.

93. Carloni, A. A.; Eberson, L. P.; Greci, L.; Stipa, P. (1997) *J. Chem. Soc. Perkin Trans.* **2**, 877.

94. Moore, G. R., and Pettigrew, G. W. (1990), *Cytochromes c. Evolutionary, Structural, and Physicochemical Aspects*, pp. 309, Springer-Verlag, Berlin.

95. Janzen, E. G., Towner, R. A., Krygsman, P. H., Lai, E. K., Poyer, J. L., Brueggemann, G., and McCay, P. B. (1990) *Free Radic. Res. Commun.* **9**(3-6), 353.

96. Iwahashi, H., Parker, C. E., Mason, R. P., and Tomer, K. B. (1990) *Rapid Commun. Mass Spectrom.* **4**(9), 352.

97. Filosa, A. (2001) PhD Thesis, *Department of Chemistry and Biochemistry*, pp. 167, Concordia University, Montreal.

98. Barr, D. P., Gunther, M. R., Deterding, L. J., Tomer, K. B., and Mason, R. P. (1996) *J. Biol. Chem.* **271**(26), 15498.

99. Wright, J. P., and English, A. M. (2003) *J. Am. Chem. Soc.* **125**(28), 8655.

100. Tomasi, A., and Iannone, A. (1993) *ESR Spin-Trapping Artifacts in Biological Systems*, Vol. 13, pp. 353, Plenum Press, New York.

101. Butler, A. R., and Rhodes, P. (1997) *Anal. Chem.* **249,** 1.

102. Xu, L., Eu. J.P. Meissner, G., and Stamler, J. S. (1998) *Science* **279,** 235.

103. Tao, L., Murphy, M. E., and English, A. M. (2002) *Biochemistry* **41**(19), 6185.

104. Bainbrigge, N., Butler, A. R., and Gobitz, C. H. (1997) *J. Chem. Perkin Trans.* **2,** 351.

105. Dicks, A. P., Beloso, P. H., and Williams, D. L. H. (1997) *J. Chem. Soc., Perkin Trans.* **2,** 1429.

106. Toubin, C., Yeung, D. Y., English, A. M., and Peslherbe, G. H. (2002) *J. Am. Chem. Soc.* **124**(50), 14816.

107. McAninly, J., Williams, D. L. H., Askew, S. C., Butler, A. R., and Russell, C. (1993) *J. Chem. Soc., Commun.*, 1758.

108. Pietraforte, D., Mallozzi, C., Scorza, G., and Minetti, M. (1995) *Biochemistry* **34**(21), 7177.

109. Coleman, D. L., and Blout, E. R. (1968) *J. Am. Chem. Soc.* **90**(9), 2405.

110. Strickland, E. H. (1974) *Critical Reviews in Biochemistry,* pp. 113, CRC Press, Inc., Cleveland.

111. Schmid, F.X. (1997) *Protein Structure* (Creighton, T.E., ed.), 2nd edn, pp. 261, Oxford University Press, Oxford.

112. Riddles, P. W., Blakeley, R. L., and Zerner, B. (1983) *Methods Enzymol.* **91,** 49.

113. Ramamurthi, A., and Lewis, R. S. (1997) *Chem. Res. Toxicol.* **10**(4), 408.

114. Antholine, W. E., Taketa, F., Wang, J. T., Manoharan, P. T., and Rifkind, J. M. (1985) *J. Inorg. Biochem.* **25**(2), 95.

115. Wang, P. G., Xian, M., Tang, X., Wu, X., Wen, Z., Cai, T., and Janczuk, A. J. (2002) *Chem. Rev.* **102**(4), 1091.

116. Wang, K., Zhang, W., Xian, M., Hou, Y. C., Chen, X. C., Cheng, J. P., and Wang, P. G. (2000) *Curr. Med. Chem.* 7(8), 821.

117. Noble, D. R., and Williams, D. L. (2002) *J. Chem. Perkin Trans.* **2,** 1834.

118. Megson, I. L. (2000) *Drugs of the Future* **25**(7), 701.

119. Hou, Y. C., Janczuk, A., and Wang, P. G. (1999) *Curr. Pharm. Des.* **5**(6), 417.

120. Singh, S. P., Wishnok, J. S., Keshive, M., Deen, W. M., and Tannenbaum, S. R. (1996) *Proc. Natl. Acad. Sci. U. S. A.* **93**(25), 14428.

121. Gladwin, M. T., Schechter, A. N., Shelhamer, J. H., Pannell, L. K., Conway, D. A., Hrinczenko, B. W., Nichols, J. S., Pease-Fye, M. E., Noguchi, C. T., Rodgers, G. P., and Ognibene, F. P. (1999) *J. Clin. Invest.* **104**(7), 937.

122. Kandori, K. (1998) *J. Am. Chem. Soc.* **120,** 5828.

123. Sampath, V., Zhao, X. J., and Caughey, W. S. (1994) *Biochem. Biophys. Res. Commun.* **198**(1), 281.

124. Spencer, N. Y., Zeng, H., Patel, R. P., and Hogg, N. (2000) *J. Biol. Chem.* **275**(47), 36562.

125. Di Iorio, E. E. (1981) in *Methods Enzymol.* **76**, 57.

126. Aleryani, S., Milo, E., Rose, Y., and Kostka, P. (1998) *J. Biol. Chem.* **273,** 6041.

127. Gow, A. J., Luchsinger, B. P., Pawloski, J. R., Singel, D. J., and Stamler, J. S. (1999) *Proc. Natl. Acad. Sci. U. S. A.* **96**(16), 9027.

128. Noble, D. R., and Williams, D. L. (2000) *Nitric Oxide* **4**(4), 392.

129. Bishop, C., and Surgenor, D. M. (1964) *Red Blood Cell*, Academic Press, New York.

130. Rossi, R., Lusini, L., Giannerini, F., Giustarini, D., Lungarella, G., and Di Simplicio, P. (1997) *Anal. Biochem.* **254**(2), 215.

131. Hogg, N. (1999) *Anal. Biochem.* **272**(2), 257.

132. Iizuka, T., and Kotani, M. (1969) *Biochim. Biophys. Acta* **194**(2), 351.

133. Vitello, L. B., Erman, J. E., Miller, M. A., Mauro, J. M., and Kraut, J. (1992) *Biochemistry* **31**(46), 11524.

134. Romeo, A. A., Filosa, A., Capobianco, J. A., and English, A. M. (2001) *J. Am. Chem. Soc.* **123**, 1782.

135. Lane, P., and Gross, S. (2002) *Nature Medicine* **8**(7), 657.

136. McMahon, T. J., Moon, R. E., Luschinger, B. P., Carraway, M. S., Stone, A. E., Stolp, B. W., Gow, A. J., Pawloski, J. R., Watke, P., Singel, D. J., Piantadosi, C. A., and Stamler, J. S. (2002) *Nat. Med.* **8**(7), 711.

137. Tsikas, D., Sandmann, J., Luessen, P., Savva, A., Rossa, S., Stichtenoth, D. O., and Frolich, J. C. (2001) *Biochim. Biophys. Acta* **1546**(2), 422.

138. Romeo, A. A., Capobianco, J. A., and English, A., M. (2002) *J. Biol. Chem.* **227**(27), 24135.

139. Lei, Y., and Anson, F. C. (1995) *Inorg. Chem.* **34**, 1083.

140. Gartner, A., and Weser, U. (1983) *FEBS Lett.* **155**(1), 15.

141. Dershwitz, M., and Novak, R. F. (1982) *J. Biol. Chem.* **257**(1), 75.

142. Forman, H. J., Evans, H. J., Hill, R. L., and Fridovich, I. (1973) *Biochemistry* **12**(5), 823.

143. Gladwin, M. T., Wang, X., Reiter, C. D., Yang, B. K., Vivas, E. X., Bonaventura, C., and Schechter, A. N. (2002) *J. Biol. Chem.* **277**(31), 27818.

144. Jourd'heuil, D., Hallen, K., Feelisch, M., and Grisham, M. B. (2000) *Free Radic. Biol. Med.* **28**(3), 409.

145. Deem, S., Gladwin, M. T., Berg, J. T., Kerr, M. E., and Swenson, E. R. (2001) *Am J Respir Crit Care Med* **163**(5), 1164.

146. Scorza, G., Pietraforte, D., and Minetti, M. (1997) *Free Radic. Biol. Med.* **22**(4), 633.

147. Van Assendelft, O. W., and Zijlstra, W. G. (1975) *Anal. Biochem.* **69**(1), 43.

148. Antonini, E., Wyman, J., Brunori, M., Taylor, F. J., Rossi Farinelli, A., and Caputo, A. (1964) *J. Biol. Chem.* **239**, 907.

149. McCord, J. M., and Fridovich, I. (1969) *J. Biol. Chem.* **244**(22), 6049.

150. Marklund, S., and Marklund, G. (1974) *Eur. J. Biochem.* **47**(3), 469.

151. Kurobe, N., Suzuki, F., Okajima, K., and Kato, K. (1990) *Clinica Chimica Acta* **187**, 11.

152. Liu, S. X., Fabisiak, J. P., Tyurin, V. A., Borisenko, G. G., Pitt, B. R., Lazo, J. S., and Kagan, V. E. (2000) *Chem. Res. Toxicol.* **13**(9), 922.

153. Dihl, H., and Smith, G. F. (1972) *The Copper Reagents: Cuproine, Neocuproine, Bathocuproine*, Second Ed. (Schilt, A. A. a. M. L., Ed.), The G. Frederick Smith Chemical Company

154. Barra, D., Martini, F., Bannister, J. V., Schinina, M. E., Rotilio, G., Bannister, W. H., and Bossa, F. (1980) *FEBS Lett.* **120,** 53.

155. Hagel, L. (1989) *Gel filtration. In Protein Purification. Principles, high resolution methods, and applications,* (Janson, J. C., and Rydén, L., Eds.), VCH Publishers Inc., Weinheim, Cambridge, New York

156. Mengwei, Y. (2003) *Concordia University, Department of Chemistry and Biochemistry* (unpublished observations).

157. Rossi, R., Barra, D., Bellelli, A., Boumis, G., Canofeni, S., Di Simplicio, P., Lusini, L., Pascarella, S., and Amiconi, G. (1998) *J. Biol. Chem.* **273**(30), 19198.

158. Griffith, O. W. (1999) *Free Rad. Biol. & Med.* **27**(9/10), 922.

159. Hoffmann, J., Haendeler, J., Zeiher, A. M., and Dimmeler, S. (2001) *J. Biol. Chem.* **276**(44), 41383.

160. Pezacki, J. P., Ship, N. J., and Kluger, R. (2001) *J. Am. Chem. Soc.* **123,** 4615.

161. Pawloski, J. R., Hess, D. T., and Stamler, J. S. (2001) *Nature* **409**(6820), 622.

162. Mauk, A. G., and Gray, H. B. (1979) *Biochem. Biophys. Res. Commun.* **86**(1), 206.

163. James, B. R., and Williams, R. J. P. (1961) *J. Chem. Soc.* , 2007.

164. Sheu, F. S., Zhu, W., and Fung, P. C. (2000) *Biophys. J.* **78**(3), 1216.

165. Williams, W. J., Beantler, E., Erslev, A. J., and Rundles, R. W. (1972) *Hematology*, McGraw-Hill Book Company, A Blakisten Publication, New York.

166. Abbyad, P., Tromp, J., Lam, J., and Salin, E. (2001) *J. Anal. At. Spectrom.* **16,** 464.

167. Dong, A., Huang, P., and Caughey, W. S. (1990) *Biochemistry* **29**(13), 3303.

168. Mahalingam, T. R., Vijayalakshmi, S., Prabhu, R. K., Thiruvengadasami, A., Wilber, A., Mathews, C. K., and Shanmugasundaram, K. R. (1997) *Biol. Trace Elem. Res.* **57**(3), 223.

169. Upmacis, R. K., Hajjar, D. P., Chait, B. T., and Mirza, U. A. (1997) *J. Am. Chem. Soc.* **119**, 10424.

170. Eich, R. F., Li, T., Lemon, D. D., Doherty, D. H., Curry, S. R., Aitken, J. F., Mathews, A. J., Johnson, K. A., Smith, R. D., Phillips, G. N., Jr., and Olson, J. S. (1996) *Biochemistry* **35**(22), 6976.

171. Kuma, F. (1981) *J. Biol. Chem.* **256**(11), 5518.

172. Bonaventura, C., Godette, G., Tesh, S., Holm, D. E., Bonaventura, J., Crumbliss, A. L., Pearce, L. L., and Peterson, J. (1999) *J. Biol. Chem.* **274**(9), 5499.

173. Bickar, D., Bovaventura, C., and Bonaventura, J. (1984) *J. Biol. Chem.* **259**(17), 10777.

174. Nazhat, N. B., Saadalla-Nazhat, R. A., Fairburn, K., Jones, P., Blake, D. R., Nielsen, B. R., Symons, M. C., and Winyard, P. G. (1999) *Biochim. Biophys. Acta* **1427**(2), 276.

175. Deterding, L. J., Barr, D. P., Mason, R. P., and Tomer, K. B. (1998) *J. Biol. Chem.* **273**(21), 12863.

176. Ichimori, K., Arroyo, C. M., and Nakazawa, H. (1996) *Methods Enzymol.*, **268**, 203.

177. Pietraforte, D., and Minetti, M. (1997) *Biochem. J.* **321**(3), 743.

178. Katoch, R., Trivedi, G. K., and Phadke, R. S. (1999) *Steroids* **64**(12), 849.

179. Kroll, C., and Borchert, H. H. (1999) *Eur. J. Pharm. Sci.* **8**(1), 5.

180. Iwahashi, H., Parker, C. E., Mason, R. P., and Tomer, K. B. (1992) *Anal. Chem.* **64**(19), 2244.

181. Witting, P. K., Douglas, D. J., and Mauk, A. G. (2000) *J. Biol. Chem.* **275**(27), 20391.

182. Houston, C. T., and Reilly, J. P. (1999) *Anal. Chem.* **71**(16), 3397.

183. Kurnikov, I. V. (1999), PhD Thesis, *Department of Chemistry*, University of Pittsburgh, Pittsburgh.

184. Curry, W. B., Grabe, M. D., Kurnikov, I. V., Skourtis, S. S., Beratan, D. N., Regan, J. J., Aquino, A. J., Beroza, P., and Onuchic, J. N. (1995) *J. Bioenerg. Biomembr.* **27**(3), 285.

185. Nocek, J. M., Zhou, J. S., De Forest, S., Priyadarshy, S., Beratan, D. N., Onuchic, J. N., and Hoffman, B. M. (1996) *Chem. Rev.* **96**(7), 2459.

186. Yang, T., Horejsh, D. R., Mahan, K. J., Zaluzec, E. J., Watson, T. J., and Gage, D. A. (1996) *Anal. Biochem.* **242**(1), 55.

187. Siuzdak, G. (1996) *Mass Spectrometry for Biotechnology*, Academic Press, San Diego.

188. Antholine, W. E., Basosi, R., Hyde, J. S., and Taketa, F. (1984) *J. Inorg. Biochem.* **21**, 125.

189. Balagopalakrishna, C., Abugo, O. O., Horsky, J., Manoharan, P. T., Nagababu, E., and Rifkind, J. M. (1998) *Biochemistry* **37**(38), 13194.

190. Maples, K. R., Eyer, P., and Mason, R. P. (1990) *Mol. Pharmacol.* **37**(2), 311.

191. Augusto, O., Lopes de Menezes, S., Linares, E., Romeoro, N., Radi, R., and Denicola, A. (2002) *Biochemistry* **41**(48), 14323.

192. Liu, X., Miller, M. J., Joshi, M. S., Sadowska-Krowicka, H., Clark, D. A., and Lancaster, J. R., Jr. (1998) *J. Biol. Chem.* **273**(30), 18709.

193. Wessel, D. L., Adatia, I., Giglia, T. M., Thompson, J. E., and Kulik, T. J. (1993) *Circulation* **88**(5 Pt 1), 2128.

194. Rioux, F., Harvey, N., Moisan, S., Lariviere, R., Lebel, M., Grose, J. H., and Burhop, K. (1999) *Can. J. Physiol. Pharmacol.* 77(3), 188.

195. Kohno, M., Yokokawa, K., Minami, M., Yasunari, K., Maeda, K., Kano, H., Hanehira, T., and Yoshikawa, J. (1999) *Metabolism* **48**(10), 1256.

196. Gladwin, M. T., Lancaster, J. J. R., Freeman, B. A., and Schechter, A. N. (2003) *Nature Medicine* **9**(5), 496.

197. Stamler, J. S., Hess, D. T., and Singel, D. J. (2003) *Nature Medicine* **9**(5), 481.